THE SECOND LAW IN QUANTUM PURE STATE THERMODYNAMICS: MAKING HEAT FLOW FROM COLD TO HOT & OTHER INTERESTING THINGS

by

PHILLIP CHARLES LOTSHAW

A DISSERTATION

Presented to the Department of Chemistry and Biochemistry
and the Graduate School of the University of Oregon
in partial fulfillment of the requirements
for the degree of
Doctor of Philosophy

June 2020

DISSERTATION APPROVAL PAGE

Student: Phillip Charles Lotshaw

Title: The Second Law in Quantum Pure State Thermodynamics: Making Heat Flow from Cold to Hot & Other Interesting Things

This dissertation has been accepted and approved in partial fulfillment of the requirements for the Doctor of Philosophy degree in the Department of Chemistry and Biochemistry by:

Andrew Marcus	Chair
Michael Kellman	Advisor
Marina Guenza	Core Member
Daniel Steck	Institutional Representative

and

Kate Mondloch	Interim Vice Provost and Dean of the Graduate School

Original approval signatures are on file with the University of Oregon Graduate School.

Degree awarded June 2020

DISSERTATION ABSTRACT

Phillip Charles Lotshaw

Doctor of Philosophy

Department of Chemistry and Biochemistry

June 2020

Title: The Second Law in Quantum Pure State Thermodynamics: Making Heat Flow from Cold to Hot & Other Interesting Things

Recent theoretical and experimental work on the foundations of statistical mechanics and thermodynamics has shown that quantum pure states typically evolve to thermal equilibrium. We focus on formulating the second law of thermodynamics for these states. The standard quantum von Neumann quantum entropy is constant during equilibration, $S^{vN} = 0$, in apparent conflict with the entropy increase of the second law, $\Delta S_{univ} > 0$. We explore a recently developed entropy S^{Q}_{univ} for a pure state and test its behavior in simulations of a model system and environment evolving in time with heat flow to equilibrium. We find that the entropy approaches the correct classical value in a type of classical limit with weak coupling. With stronger coupling, we find a new source of quantum "excess entropy production," which has its origin in the quantum spreading of the wavepacket. Are there quantum thermodynamic effects related to this new source of entropy? To test this, we developed a model for a small variable temperature quantum oscillator bath. We performed simulations where two small baths are linked by a system, with unequal couplings to the baths. The model evolves to a novel type of equilibrium state with unequal temperatures in

the baths, with heat flow from cold to hot along the path to equilibrium. We give an account of this behavior in terms of the second law with the quantum entropy S^Q_{univ}. The new formulation of the second law thus appears well-founded and fruitful, with surprising new quantum thermodynamic effects that may still be awaiting discovery, for example in molecules or systems far from equilibrium.

This dissertation includes previously published and unpublished co-authored material.

CURRICULUM VITAE

NAME OF AUTHOR: Phillip Charles Lotshaw

GRADUATE AND UNDERGRADUATE SCHOOLS ATTENDED:
University of Oregon, Eugene, OR, USA
Willamette University, Salem, OR, USA

DEGREES AWARDED:
Doctor of Philosophy, Physical Chemistry, 2020, University of Oregon
Bachelor of Arts, Physics, 2012, Willamette University

AREAS OF SPECIAL INTEREST:
Quantum statistical mechanics
Thermodynamics
Quantum dynamics

PROFESSIONAL EXPERIENCE:

Head Teaching Assistant, General Chemistry Laboratory, 2017-2018

Graduate Education Mentor, Science Literacy Program, 2016-2017

GRANTS, AWARDS AND HONORS:

Graduate Student Teaching Excellence Award, Department of Chemistry and Biochemistry, 2018

PUBLICATIONS:

P. C. Lotshaw and M. E. Kellman, Phys. Rev. E **100**, 042105 (2019).

P. C. Lotshaw and M. E. Kellman, J. Phys. Chem. A **123**, 831 (2019).

G. L. Barnes, P. C. Lotshaw, and M. E. Kellman, ArXiv e-prints (2018), arXiv:1511.06176v3 [quant-ph].

ACKNOWLEDGEMENTS

I abundantly thank my advisor Michael Kellman for his many years of support and dedication to helping me grow as a scientist. I appreciate Andy Marcus, Marina Guenza, and Dan Steck for serving on my committee and providing helpful feedback and encouragement on my research. I thank Jeff Cina for many interesting and friendly conversations about science about life. Rob Yelle gave patient and much appreciated technical assistance with computations and Craig Rasmussen helped with MPI parallel programming. I thank Benjamín Alemán for encouragement and helping me become a better writer. Dietrich Belitz, John Toner and David Perry contributed to stimulating discussions and Steve Hsu brought important references to our attention. I thank George Barnes for contributing the original version of the computer code that was expanded on in this dissertation. In addition to my Ph.D. research I also benefitted greatly from learning to become a better teacher, with special thanks to Elly Vandegrift, Julie Mueller, Nicola Barber, Deborah Exton, and Tom Greenbowe.

This work was supported by the U.S. Department of Energy Basic Energy Sciences program under Contract DE-FG02-05ER15634. This work used the Extreme Science and Engineering Discovery Environment (XSEDE), which is supported by National Science Foundation grant number ACI-1548562. This work used the XSEDE supercomputer Stampede2 at the Texas Advanced Computing Center through the University of Oregon Campus Champion Allocation TG-TRA170043. This work benefited greatly from access to the University of Oregon high performance computers ACISS and Talapas.

Dedicated to my family.

TABLE OF CONTENTS

Chapter Page

Chapter Page

APPENDICES

LIST OF FIGURES

Figure Page

LIST OF TABLES

Table Page

CHAPTER I

INTRODUCTION

Much contemporary research has focused on the idea that thermodynamics and statistical mechanics can be understood as a result of entanglement between a system and environment that are collectively in a quantum pure state. However, it has not been entirely clear how to formulate the **second law of thermodynamics** in this context: the quantum von Neumann entropy S^{vN} of the pure state is zero, in conflict with the second law $\Delta S_{univ} > 0$. My work explores a recently developed **"quantum entropy of the universe"** S^{Q}_{univ} to formulate the second law for a system-environment pure state [1–3]. The system-environment pure state is taken as an isolated total system or "universe" in formulating the second law, but this is not meant as a model for the actual cosmological universe. The second law with S^{Q}_{univ} gives a unified account of classical thermodynamics along with new specifically **quantum thermodynamic effects** related to finite size and strong coupling, with a new source of **quantum "excess entropy production"** that can be much greater than the classical entropy production for certain states. This culminates in the discovery of a system of two small quantum baths that evolves to a novel **equilibrium state with different temperatures in the baths**, with **heat flow from cold to hot** along the path to equilibrium [4, 5]. S^{Q}_{univ} is maximized in the asymmetric temperature equilibrium, in accord with the second law, with excess entropy production playing a pivotal role. The new formulation of the second law contributes to the larger field of contemporary work on quantum thermodynamics [6–38] and points the way to future studies of novel quantum thermodynamic effects related to excess entropy production.

Modern research into quantum "typicality" [11–18] and the eigenstate thermalization hypothesis [19–27] has begun to formulate a new theoretical **quantum foundation of statistical mechanics and thermodynamics** that begins with a quantum system-environment pure state which evolves in time with entanglement to thermal equilibrium. The claim of these approaches is that pure state thermalization behavior should be expected in "typical" situations with sufficiently complex dynamics and that this is the fundamental reason we observe thermodynamic behavior in the real world. To give a full account of quantum thermodynamic behavior it is necessary to formulate the second law of thermodynamics for a pure state evolving in time, including its relation to classical thermodynamics and potentially new types of quantum thermodynamic behavior.

In classical thermodynamics, the **second law** is a very important universal statement about what types of physical processes are possible: apart from transient fluctuations, all real processes increase the entropy of the universe until it reaches a maximum at equilibrium,

$$\Delta S_{univ} > 0. \tag{1.1}$$

This poses a problem in quantum thermodynamics. The standard quantum von Neumann entropy has the constant value of zero for a pure state of an isolated system and environment; it cannot increase in accord with the second law. To address this problem I will explore a recently developed [1] **quantum pure state entropy** S^Q_{univ} to formulate the second law.

I am concerned with three goals in formulating the second law with S^Q_{univ}. The first goal is to demonstrate that S^Q_{univ} obtains the **correct classical limit** and to explore its behavior outside this limit. The second goal is to look for **new types of**

quantum thermodynamic effects associated with small size and strong coupling, both of which are important aspects of quantum systems that aren't considered in classical statistical mechanics and thermodynamics. The third goal is to give a **second-law account of new quantum effects** in terms of S^Q_{univ}.

The first step therefore is to test the behavior of S^Q_{univ} in comparison with the classical thermodynamic entropy. S^Q_{univ} was defined in Ref. [1] and tested in simulations with a simple but somewhat crude model. I improve on the work of Ref. [1] by devising a much more realistic model for a pure state of a system and environment in a heat flow process. For this process $\boldsymbol{\Delta S^Q_{univ}}$ **approaches the classical entropy change in a type of classical limit** with a large bath and weak coupling. Stronger coupling gives **"excess quantum entropy production"** $\Delta S^x > 0$ from quantum spreading of the wavepacket, with ΔS^Q_{univ} greater than expected from classical heat flow alone. Thus S^Q_{univ} obtains the correct classical limit, while outside this limit there is excess entropy production ΔS^x in quantum time evolution. This fulfills the first goal outlined above.

The next step is to study **new types of quantum thermodynamic behavior** in pure states with quantum properties that differ from what's assumed in classical thermodynamics: First, small size quantum environments have a non-standard, **size-dependent temperature-energy relationship**. Second, and perhaps most interesting, finite size and strong coupling combine in a system of two asymmetrically coupled small quantum baths that evolves in time to a classically forbidden type of equilibrium state with different temperatures in the baths, with **heat flow from cold to hot** along the path to equilibrium. Thus quantum properties are associated with new types of quantum thermodynamic behavior, fulfilling the second goal outlined above.

The final step is to give a second-law account of the novel quantum thermodynamic behavior. I find that S^Q_{univ} is maximized at the asymmetric temperature equilibrium, very unlike the classical S_{univ}, with ΔS^x playing a pivotal role. Thus the third goal is fulfilled, showing $\boldsymbol{S^Q_{univ}}$ **gives a second-law account of novel quantum thermodynamic behavior**.

I briefly comment at the end on some ideas for what might come next from S^Q_{univ} in the second law. This includes **ideas for experimental studies** of the theoretical effects studied in this dissertation, ideas for **different new types of quantum thermodynamic effects**, and for studies of **non-thermal behavior**. It seems hopeful that there are more novel effects to discover, with significance for the foundations of thermodynamics and potential technological applications.

This dissertation is organized as follows: Chapter II gives background information on classical and pure state quantum thermodynamics and statistical mechanics, leading to the definition of the quantum entropy from Ref. [1]. Chapter III studies the quantum entropy in comparison with classical relations, adapted from Ref. [2]. Chapter IV studies the relation between "excess entropy production," strong quantum coupling, and spreading of the wavepacket in quantum dynamics, adapted from Ref. [3]. Chapter V analyzes thermodynamic behavior with a small quantum variable temperature bath, with interesting finite-size temperature effects, adapted from Ref. [4]. Chapter VI studies a two-bath quantum system where strong coupling and small size combine to give a non-standard equilibrium state with an asymmetric temperature distribution, with heat flow from cold to hot along the path to equilibrium, adapted from Ref. [5]. Chapter VII concludes with a summary of the results and ideas for future research.

This dissertation includes previously published and unpublished material co-authored by Michael E. Kellman [1–5]. Michael Kellman and I both contributed to developing the models and theories, analyzing results, and writing the chapters and appendices of this dissertation. I performed all computer calculations in this dissertation.

CHAPTER II

BACKGROUND: CLASSICAL THERMODYNAMICS AND STATISTICAL MECHANICS, QUANTUM PURE STATE THERMODYNAMICS, AND THE SECOND LAW

The emerging field of pure state quantum thermodynamics seeks to answer two basic types of questions as mentioned in the introduction: What is the quantum origin of classical thermodynamic behavior? Are new types of quantum thermodynamic behavior possible? In this chapter, I will briefly review contemporary approaches to understanding the first question, as background for the work in the remainder of this dissertation and as a starting point to looking for new types of quantum thermodynamic behavior. The chapter will begin with a condensed review of the essential ideas from classical thermodynamics and statistical mechanics, leading into the modern approaches to quantum pure state thermodynamics and the recently proposed quantum formulation of the second law with the entropy S^Q_{univ} from Ref. [1]. This background will be the starting point for the new explorations with S^Q_{univ} and the second law in the remainder of this dissertation.

The review in this chapter is intended for readers familiar with thermodynamics, statistical mechanics, and quantum mechanics, as a way to briefly highlight the essential features of the theory leading to the formulation of the quantum thermodynamic entropy S^Q_{univ}. Readers may wish to skip to the definition of S^Q_{univ} in Section 2.6, or to the new work of this dissertation starting in Chapter III, referring to this background as needed.

The chapter is organized as follows: Section 2.1 very briefly reviews the second law of thermodynamics. Section 2.2 and 2.3 review the classical formalism of

statistical mechanics as a basis for thermodynamics and the second law. Sections 2.4 and 2.5 introduce the basic ideas and rationales for quantum pure state thermodynamics. Section 2.6 introduces the recently developed [1] entropy S^Q_{univ} to formulate the second law in pure state quantum thermodynamics and motivates the new research in the next chapter.

2.1. The second law in classical thermodynamics

Classical thermodynamics is founded in a few elementary laws that give universal restrictions on the types of processes that are possible in macroscopic systems. The second law states that all real spontaneous processes increase the entropy of the universe until it reaches a maximum at equilibrium,

$$\Delta S_{univ} > 0. \tag{2.1}$$

The second law has many consequences, all focused around the idea that natural dynamics maximize the total entropy of universe. A major consequence is that thermodynamic process are *irreversible*: Low entropy states evolve to high entropy states and do not go back. For example, heat flows from hot to cold and not the other way around. Thus it is often said that the second law defines the "arrow of time." This is indispensable in describing the real world.

The laws of thermodynamics were developed phenomenologically from experimental evidence in the 19th century. In the 19th and 20th centuries, there was a lot of interest in trying to explain the phenomenology of thermodynamics with a more fundamental microscopic theory. This led to the development of classical statistical mechanics, which I briefly review in the next two sections. I'll then discuss contemporary work developing a more fundamental theory of quantum pure state

thermodynamics, leading to the second law with the new quantum entropy S^Q_{univ} that is studied throughout the remainder of this dissertation.

2.2. Classical and semi-classical statistical mechanics

Classical statistical mechanics is based on the idea that the mechanical motions of enormous numbers of tiny molecules gives rise to the laws and relations of thermodynamics. Thermodynamic processes involving a system $\mathcal{S}$ and its large environment $\mathcal{E}$ are too complex to analyze directly with mechanics, so instead a simplified statistical approach is taken. The fundamental assumption of statistical mechanics is that a single $\mathcal{SE}$ in nature, which in classical theory is in a single unknown state any instant in time, can be analyzed without knowing its true state by using a statistical ensemble of all the possible microscopic $\mathcal{SE}$ states with associated probabilities. This approach is very successful in formulating thermodynamics and describing thermodynamic properties of real $\mathcal{SE}$ total systems in nature. The next section will discuss classical theoretical rationales for why the fundamental assumption is so successful in describing real systems, leading into the contemporary rationales in quantum theory later in the chapter. The remainder of this section describes the basic formalism of classical and semi-classical statistical mechanics. I will focus on heat flow in semi-classical statistical mechanics, with quantum energy levels but not quantum states evolving in time, although many of the same relations hold also in classical statistical mechanics in phase space with appropriate modifications.

The system $\mathcal{S}$ and environment $\mathcal{E}$ are taken together as constituting an isolated total system or "universe." This is not meant to imply that the total system is the

actual cosmological universe, it's just a term to indicate that any interactions with other exterior systems are negligible and need not be considered.

Fig. 2.1 shows a schematic energy level diagram for a standard $\mathcal{SE}$ universe. The environment $\mathcal{E}$ is a large, effectively infinite many body system with a density ρ of microscopic states that increases exponentially with energy $E_{\mathcal{E}}$ at a rate determined by the temperature T,

$$\rho(E_{\mathcal{E}}) \sim e^{E_{\mathcal{E}}/k_B T}, \tag{2.2}$$

where k_B is the Boltzmann constant; I will often adopt reduced units where $k_B = 1$, so that T has units of energy. The exponential scaling of ρ is an approximate generic feature for large environments. The set of microscopic environment states will be denoted $\{\epsilon\}$ with energies E_ϵ. The system $\mathcal{S}$ in the figure has a few microscopic states $\{s\}$ with energies E_s. This is characteristic of typical microscopic systems such as the vibrational energy levels in a molecule.

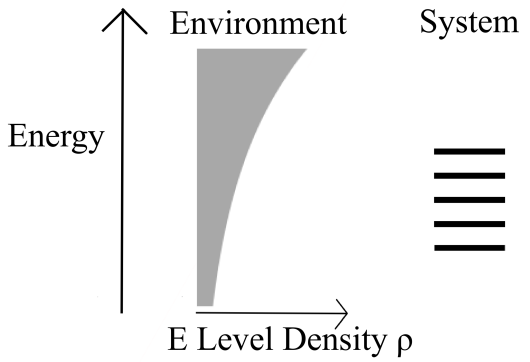

FIGURE 2.1. Schematic energy level diagram for a system-environment "universe" in statistical mechanics.

The state of an $\mathcal{SE}$ universe is described by the *microcanonical ensemble*, beginning with a total energy E and sometimes other constraints for the specific $\mathcal{SE}$ in consideration. To formulate the microcanonical ensemble, the first step is to count the number W of microscopic system-environment states s, ϵ in the *microcanonical energy shell* $E - \delta E/2 \leq E_s + E_\epsilon \leq E + \delta E/2$ that satisfy all the constraints. The width of the energy shell δE tends to zero in the classical limit where energy is an exact constant of motion. In semi-classical statistical mechanics, δE is taken as small enough that the energy $E_\mathcal{S} + E_\mathcal{E}$ is effectively fixed but large enough that there are many s, ϵ quantum energy levels in the energy shell. The final step is to assume that all of the s, ϵ states in the energy shell can be treated as equally probable,

$$p_{s,\epsilon} = \frac{1}{W}. \tag{2.3}$$

Properties of $\mathcal{S}$ and $\mathcal{E}$ are then taken as averages over the s, ϵ states, for example the system energy is taken as the average

$$E_\mathcal{S} = \langle E_s \rangle = \sum_{s,\epsilon} E_s p_{s,\epsilon}. \tag{2.4}$$

It's important to note that in classical and semi-classical theory a true $\mathcal{SE}$ is always in a single state s, ϵ, which is much different than the microcanonical ensemble of all s, ϵ states described above. There are different rationales for why it is reasonable to use the microcanonical probabilities of Eq. 2.3 for describing real $\mathcal{SE}$ universes in nature, these are described in the next section. The remainder of this section will focus on showing how the microcanonical ensemble is used in a practical example of heat flow, as is fundamental to the later work in this dissertation.

The left of Fig. 2.2 shows an example of an $\mathcal{SE}$ microcanonical ensemble before $\mathcal{S}$ and $\mathcal{E}$ have interacted, where they each have individually fixed energies as a constraint. In this example there are W_0 states s, ϵ where $\mathcal{S}$ is in its ground state $s = 0$ shown in red and $\mathcal{E}$ has equal probabilities for all the states ϵ under the red bar, with the microcanonical shell width δE.

The right of Fig. 2.2 shows $\mathcal{S}$ and $\mathcal{E}$ after they've interacted, exchanged energy, and gone to thermal equilibrium. The equilibrium microcanonical ensemble contains W_{eq} different s, ϵ state pairs at the same total $\mathcal{SE}$ energy E, shown by the matching colors of $\mathcal{S}$ levels and bands of $\mathcal{E}$ states in the microcanonical energy shell. Now all the $\mathcal{S}$ levels are accessible thanks to heat flow from $\mathcal{E}$. The colors in the figure show how to match the $\mathcal{SE}$ states s, ϵ at the same total energy E but are otherwise arbitrary.

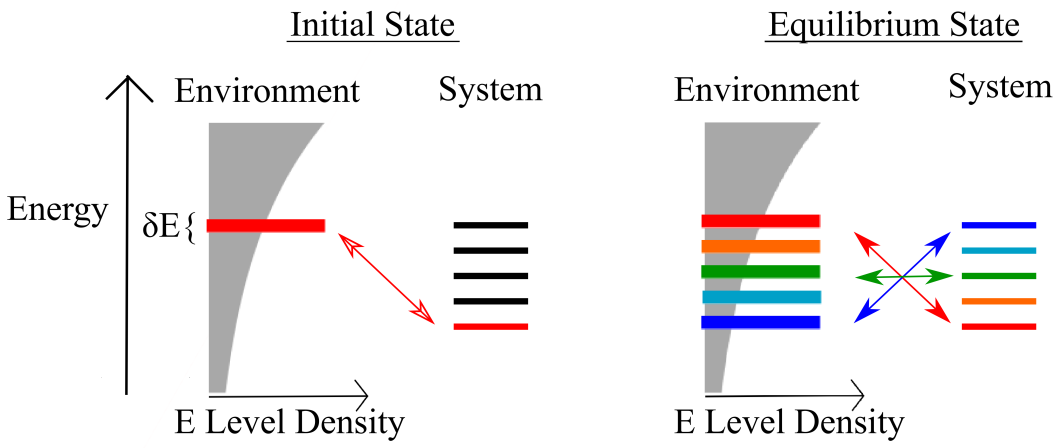

FIGURE 2.2. Thermalization in the microcanonical ensemble. The initial microcanonical ensemble on the left describes the system $\mathcal{S}$ and environment $\mathcal{E}$ before they've interacted, where $\mathcal{S}$ and $\mathcal{E}$ have separate fixed energies in the energy shell of width δE, shown by the red system level and the red band of environment levels. The equilibrium microcanonical ensemble on the right describes $\mathcal{S}$ and $\mathcal{E}$ after they've interacted and exchanged heat. All the $\mathcal{SE}$ states at the same total energy are accessible, shown by matching the similarly colored $\mathcal{S}$ levels and bands of $\mathcal{E}$ levels.

The second law for this equilibration process is formulated beginning with the Boltzmann entropy for the microcanonical ensemble

$$S_{univ} = -\sum_{s,\epsilon} p_{s,\epsilon} \ln p_{s,\epsilon} = \ln W, \tag{2.5}$$

where the sum runs over all s, ϵ in the microcanonical ensemble with probabilities from Eq. 2.3. For the example process in Fig. 2.2

$$\Delta S_{univ} = \ln \frac{W_{eq}}{W_0} > 0, \tag{2.6}$$

since more states are accessible at equilibrium $W_{eq} > W_0$. Thus the microcanonical Boltzmann entropy increases in accord with the second law. In general, thermodynamic processes always include the removal of a constraint, such as the initial constraint on the $\mathcal{S}$ and $\mathcal{E}$ energies in Fig. 2.2, and this always gives access to more microcanonical states with $\Delta S_{univ} > 0$. The second law reflects the tendency for $\mathcal{SE}$ universes to explore greater numbers of microscopic states during spontaneous thermodynamic processes.

A final note is that it is very often desirable to describe the system $\mathcal{S}$ alone, without needing to go into detail about $\mathcal{E}$. To do this, probabilities p_s for the $\mathcal{S}$ states s can be calculated by summing $p_{s,\epsilon}$ over all the $\mathcal{E}$ states ϵ,

$$p_s = \sum_{\epsilon} p_{s,\epsilon}. \tag{2.7}$$

For a standard equilibrium state as in the right of Fig. 2.2, the $\mathcal{S}$ probabilities are given by the *canonical ensemble* or *Boltzmann distribution*

$$p_s = \frac{e^{-E_s/kT}}{Z}, \tag{2.8}$$

where $Z = \sum_s e^{-E_s/kT}$ is a normalizing factor called the partition function. The canonical ensemble Eq. 2.8 can be derived using the density of environment states from Eq. 2.2; in essence, there are exponentially more $\mathcal{E}$ states at high energy that pair with the low energy $\mathcal{S}$ states as seen in Fig. 2.2, and since all the $\mathcal{SE}$ states s, ϵ are equally likely, this makes the low-energy $\mathcal{S}$ states exponentially more likely in the canonical ensemble Eq. 2.8.

This concludes the basic mathematical approach to statistical mechanics, which has proven very successful in describing thermodynamic properties of natural systems. The approach is based on assuming equal probabilities for all the microscopic states s, ϵ of the $\mathcal{SE}$ universe in Eq. 2.3. To streamline the presentation so far, the equal probability assumption has not yet been justified. The next section considers the basic approaches to justifying this assumption in classical statistical mechanics, leading to the contemporary approaches in quantum theory described in the remaining sections.

2.3. Theoretical motivations for the microcanonical ensemble

Statistical mechanics is based on the fundamental assumption that real systems can be modeled with the equiprobable microcanonical ensemble distribution over all possible s, ϵ states as in Eq. 2.3. This works well in practice for modeling states at thermal equilibrium. However, it's not so obvious why it should work so well—in classical and semi-classical theory, real systems are in single microscopic s, ϵ states, which are conceptually much different than the microcanonical ensemble distribution over all s, ϵ. In this section, I'll briefly discuss some of the main approaches to rationalizing the success of the microcanonical ensemble in classical and semi-classical statistical mechanics. The approaches differ in how they relate true system properties to the probabilities in the microcanonical ensemble. The approaches here will be

related later to contemporary approaches in quantum pure state statistical mechanics in Section 2.5, where there will be more to say about the fundamental nature of the probabilities.

The most common approach to rationalizing the microcanonical ensemble is the ergodic hypothesis [20], which conjectures that a real $\mathcal{SE}$ total system in a single s, ϵ at any point in time will wander through all the s, ϵ equally over time. Then the equal probabilities $p_{s,\epsilon}$ of Eq. 2.3 can be viewed as time averages over the dynamics. In this view real systems evolve to equilibrium when they are ergodic or "close enough" to ergodic to justify the approximate use of Eq. 2.3. However, it's been difficult to prove ergodicity generally; only a few very simple systems such as billiards in a box are known to give exact ergodic behavior. Furthermore, the ergodic hypothesis is usually studied in the context of an infinite time average, while the time intervals over which we observe real systems are finite and may be much less than the time intervals needed for approximate ergodic behavior. In total the ergodic hypothesis gives a sensible connection between $\mathcal{SE}$ dynamics and the microcanonical probabilities, but there doesn't seem to be a general proof of exactly which systems and circumstances it applies to.

Another approach is based on the notion of typicality [39, 40], that the overwhelming majority of microscopic s, ϵ states have many of the same properties as the microcanonical average. An example is seen in the microscopic states of a gas in a box—almost all the microscopic states of the gas molecules have an approximately uniform total density in the box. The uniform density is also given as the average property in the microcanonical ensemble, since the microcanonical ensemble average is an average almost entirely over typical states with uniform density. Furthermore, a small collection of gas molecules will be distributed according

to the Boltzmann distribution, since this is the typical distribution for a subsystem within the microcanonical ensemble. In this view the microcanonical probabilities of Eq. 2.3 are a convenient way to calculate the properties of typical states, rather than a statement about time-averaged dynamics, as with the ergodic hypothesis. To relate the typicality idea to real systems, one needs to assume that real systems are in typical states, perhaps with small fluctuations in accord with the fluctuations within the microcanonical ensemble. It is certainly true that many real systems are in typical states, but real systems can also be in highly atypical (non-equilibrium) states, so not every state can be assumed typical. Thus the typicality approach gives some useful insight into why statistical mechanics works when states are typical or undergo small fluctuations about typical states, but it introduces a new question of how and when states actually become typical.

A better approach seems to come from combining the statistical idea of typicality with the dynamical idea of the ergodic hypothesis: States thermalize because their dynamics cause them to evolve into the relatively large set of typical states, where their properties can be calculated from the microcanonical ensemble. This certainly seems to be true in experience, where dynamics of real systems do cause them to evolve to equilibrium states with typical properties, but this lacks a general proof.

A final approach is based in information theory [41], which views the equal probabilities of Eq. 2.3 as a best-guess result of statistical inference given a limited amount of subjective information about the energy E and other constraints on $\mathcal{SE}$. This gives a statistical rationale for using equal probabilities in the microcanonical ensemble based on our subjective knowledge, but it doesn't directly consider how the $\mathcal{SE}$ dynamics actually gives this result, which is independent of our subjective knowledge.

In total, the above considerations give some evidence for why a real system can be modeled using equal probabilities for all the states in the microcanonical ensemble, but still there is controversy over the foundations as represented in the variety of different types of approaches discussed above. Much of the controversy is over the meaning of the probabilities—whether they reflect true dynamical time-averaged properties, or a convenient way of getting at typical state properties, or subjective guesses based on limited information. One of the goals of contemporary work in quantum pure state thermodynamics is to show that the probabilities in statistical mechanics can instead be understood as a consequence of the basic quantum description of nature. The next section introduces the basic setup, followed by the theoretical motivations in Section 2.5.

2.4. Quantum pure state statistical mechanics

Quantum pure state thermodynamics considers a pure state $|\Psi_{\mathcal{SE}}\rangle$ to describe the system-environment $\mathcal{SE}$ universe, with an aim of showing that much of statistical mechanics can be understood as a consequence of the quantum properties of the state, without any need to assume the microcanonical ensemble. Instead, the Boltzmann distribution for the system in Eq. 2.8 and related results can be understood to arise from system-environment entanglement in $|\Psi_{\mathcal{SE}}\rangle$. In this sense the quantum pure state mimics the microcanonical ensemble, since both give the same statistical mechanics for the system $\mathcal{S}$. This is the basis for formulating statistical mechanics solely in terms of a quantum pure state $|\Psi_{\mathcal{SE}}\rangle$. This section will sketch how to understand this thermal behavior with a pure state $|\Psi_{\mathcal{SE}}\rangle$; the next section will discuss the theoretical motivations for this behavior.

The setup begins with a quantum pure state for the $\mathcal{SE}$ universe

$$|\Psi_{\mathcal{SE}}\rangle = \sum_{s,\epsilon} c_{s,\epsilon}|s\rangle|\epsilon\rangle, \tag{2.9}$$

expressed in the Hilbert space spanned by basis vectors $\{|s\rangle|\epsilon\rangle\}$ from the tensor product basis of zero-order system energy eigenstates states $\{|s\rangle\}$ and zero-order environment energy eigenstates states $\{|\epsilon\rangle\}$. The pure state Eq. 2.9 is the most basic type of quantum state for an isolated "universe," when there aren't any significant interactions with further exterior systems, in essence the same type of situation considered in classical microcanonical statistical mechanics. There are other mixed-state approaches to quantum thermodynamics that are appropriate in other situations, I'll comment on these briefly at the end of the section.

The connection to statistical mechanical ensembles is made through the fundamental probabilistic properties of the quantum state. The probability of measuring any system-environment basis state $|s\rangle|\epsilon\rangle$ is given by the wavefunction as

$$p_{s,\epsilon} = |\langle s|\langle\epsilon|\Psi_{\mathcal{SE}}\rangle|^2 = |c_{s,\epsilon}|^2, \tag{2.10}$$

with $c_{s,\epsilon}$ the expansion coefficients of $|\Psi_{\mathcal{SE}}\rangle$ in the $\{|s\rangle|\epsilon\rangle\}$ basis in Eq. 2.9. The quantum $p_{s,\epsilon}$ will generally not be equal for different s, ϵ, as they are in the microcanonical ensemble with Eq. 2.3. Nonetheless, the quantum $p_{s,\epsilon}$ can give the same predictions as the microcanonical ensemble for many properties of interest that depend on averages over many $p_{s,\epsilon}$, for example in determining the average system energy, etc.

Fig. 2.3 shows a very simple schematic example of thermalization envisioned with a pure state, analogous to the microcanonical thermalization of Fig. 2.2. The pure state begins in a separable superposition

$$|\Psi_{\mathcal{SE}}(t=0)\rangle = |\psi_{\mathcal{S}}\rangle|\varphi_{\mathcal{E}}\rangle \tag{2.11}$$

where $|\psi_{\mathcal{S}}\rangle$ and $|\varphi_{\mathcal{E}}\rangle$ are system and environment states respectively. In the example state on the left of Fig. 2.3, the system is in the ground state $|\psi_{\mathcal{S}}\rangle = |0\rangle$ shown in red. The environment is in a superposition state $|\varphi_{\mathcal{E}}\rangle = \sum_\epsilon c_\epsilon|\epsilon\rangle$ with probabilities $p_\epsilon = |c_\epsilon|^2$ that are focused around a central energy, shown in a simple way by the red bump (a state could naturally have a much more complex probability distribution than in this simple example). This is a quantum analog of the initial microcanonical state on the left of Fig. 2.2.

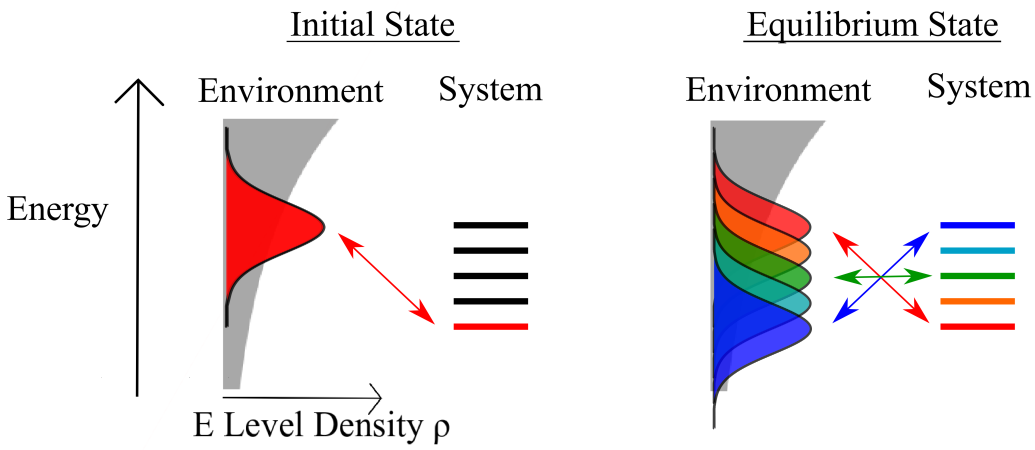

FIGURE 2.3. Schematic thermalization process with a quantum pure state $|\Psi_{\mathcal{SE}}\rangle$.

The initial state of Eq. 2.11 is expected to have thermodynamic behavior where it evolves in time to thermal equilibrium. The time-dependent behavior follows the Schrödinger equation

$$|\Psi_{\mathcal{SE}}(t)\rangle = e^{-i\hat{H}t/\hbar}|\Psi_{\mathcal{SE}}(0)\rangle, \tag{2.12}$$

where $\hbar$ is the reduced Planck's constant and $\hat{H}$ is the Hamiltonian energy operator

$$\hat{H} = \hat{H}_{\mathcal{S}} + \hat{H}_{\mathcal{E}} + \hat{H}_{\mathcal{SE}}, \tag{2.13}$$

with $\hat{H}_{\mathcal{S}}$ and $\hat{H}_{\mathcal{E}}$ the Hamiltonians of the isolated system and environment and $\hat{H}_{\mathcal{SE}}$ their interaction. The time-evolved state $|\Psi_{\mathcal{SE}}(t)\rangle$ has the generic form of Eq. 2.9, where generally all the $c_{s,\epsilon} \neq 0$, so that all the $|s\rangle|\epsilon\rangle$ basis states have non-zero probability in Eq. 2.10.

The right of Fig. 2.3 shows a very simple schematic example of the initial state after time evolution to thermal equilibrium (the theoretical motivations for this type of time-evolution behavior will be presented in the next section). At equilibrium, all the system levels $|s\rangle$ are accessed and paired with corresponding entangled environment superpositions $|\varphi_{\mathcal{E}}^{(s)}\rangle$ that are shifted in energy based on the energy transfer to the system. The pairs of entangled $|s\rangle$ and $|\varphi_{\mathcal{E}}^{(s)}\rangle$ are shown with matching colors in the figure. The total state can be expressed as

$$|\Psi_{\mathcal{SE}}(t)\rangle = \sum_s c_s|s\rangle|\varphi_{\mathcal{E}}^{(s)}\rangle, \tag{2.14}$$

where in comparison with Eq. 2.9 this has $|\varphi_{\mathcal{E}}^{(s)}\rangle = \sum_\epsilon (c_{s,\epsilon}/c_s)|\epsilon\rangle$ as the state of the environment that goes with the system state $|s\rangle$. The equilibrium quantum state is analogous to the equilibrium microcanonical ensemble on the right of Fig. 2.2.

The state in Eq. 2.14 is said to be *entangled* when the $|\varphi_{\mathcal{E}}^{(s)}\rangle$ are different for different $|s\rangle$ states, as seen in the example of Fig. 2.3. An entangled state cannot be separated into separate system and environment states as in Eq. 2.11, instead it can

only be expressed as a sum of entangled system-environment pairs such as $|s\rangle|\varphi_{\mathcal{E}}^{(s)}\rangle$. For the thermalization process, we expect the different interactions among the $|s\rangle|\epsilon\rangle$ basis states will cause entanglement where the environment states are approximately distinct from one another for $s \neq s'$,

$$\langle\varphi_{\mathcal{E}}^{(s)}|\varphi_{\mathcal{E}}^{(s')}\rangle \approx 0. \tag{2.15}$$

The entanglement describes quantum correlations between $\mathcal{S}$ and $\mathcal{E}$ that are very interesting in their own right [42, 43], and will be important here in formulating thermal behavior.

The thermal behavior of $|\Psi_{\mathcal{SE}}(t)\rangle$ is formulated in terms of the system behavior in comparison with the standard thermal Boltzmann distribution of Eq. 2.8. When the system behavior is given by the Boltzmann distribution, then all the standard relations from statistical mechanics apply to the system.

The system behavior is given by the system reduced density operator $\hat{\rho}_{\mathcal{S}}(t)$, as follows. First, the total state $|\Psi_{\mathcal{SE}}\rangle$ is represented in terms of the density operator for the universe state $\hat{\rho}_{\mathcal{SE}}(t) = |\Psi_{\mathcal{SE}}(t)\rangle\langle\Psi_{\mathcal{SE}}(t)|$. This is an alternate way of describing the total state that encodes all the same physical information as $|\Psi_{\mathcal{SE}}(t)\rangle$. The system reduced density operator is then calculated by taking the partial trace over the environment of $\hat{\rho}_{\mathcal{SE}}(t)$,

$$\hat{\rho}_{\mathcal{S}}(t) = \mathrm{Tr}_{\mathcal{E}}\hat{\rho}_{\mathcal{SE}}(t) = \sum_{\epsilon}\langle\epsilon|\Psi_{\mathcal{SE}}(t)\rangle\langle\Psi_{\mathcal{SE}}(t)|\epsilon\rangle. \tag{2.16}$$

In essence, this is summing contributions from all the different environment states $|\epsilon\rangle$ to get the average behavior of the system. With some algebra and using the identity on the environment Hilbert space $\hat{1}_{\mathcal{E}} = \sum_{\epsilon}|\epsilon\rangle\langle\epsilon|$ this gives

$$\hat{\rho}_{\mathcal{S}}(t) = \sum_{s,s'} c_s c_{s'}^* \langle \varphi_{\mathcal{E}}^{(s')} | \varphi_{\mathcal{E}}^{(s)} \rangle |s\rangle\langle s'| \approx \sum_s |c_s|^2 |s\rangle\langle s|, \tag{2.17}$$

where the last approximate equality uses the entanglement relation between the environment states Eq. 2.15.

The system is said to be in a mixed state on the right of Eq. 2.17, since it cannot be expressed in terms of a pure state density operator $\hat{\rho}_{\mathcal{S}}(t) \neq |\psi_{\mathcal{S}}(t)\rangle\langle\psi_{\mathcal{S}}(t)|$. This is due to entanglement with $\mathcal{E}$, with $\langle \varphi_{\mathcal{E}}^{(s)} | \varphi_{\mathcal{E}}^{(s')} \rangle \approx 0$. Instead, the system behaves like a probabilistic mixture or ensemble of pure state $\sum_s p_s |s\rangle\langle s|$, with probabilities $p_s = |c_s|^2$ and without quantum coherence between the different $|s\rangle$. It is very important to note that these ensemble-like predictions for $\mathcal{S}$ are deduced entirely from the quantum state $|\Psi_{\mathcal{SE}}\rangle$ rather than from ensemble assumptions as in classical and semi-classical microcanonical statistical mechanics. When the quantum system predictions agree with the classical Boltzmann distribution we will have a sensible way to understand statistical mechanics from $|\Psi_{\mathcal{SE}}\rangle$ without the microcanonical ensemble.

Thermalization of the system is assessed by comparing $\hat{\rho}_{\mathcal{S}}(t)$ with the system density operator for the thermal Boltzmann distribution

$$\hat{\rho}_{\mathcal{S}}^{\text{Boltzmann}} = \frac{e^{-\hat{H}_{\mathcal{S}}/k_B T}}{Z} = \sum_s \frac{e^{-E_s/k_B T}}{Z} |s\rangle\langle s|, \tag{2.18}$$

where $Z = \sum_s e^{-E_s/k_B T}$ is the partition function. The Boltzmann distribution operator $\hat{\rho}_{\mathcal{S}}^{\text{Boltzmann}}$ gives the same Boltzmann probabilities as the classical Boltzmann distribution of Eq. 2.8, with $p_s = \langle s|\hat{\rho}_{\mathcal{S}}^{\text{Boltzmann}}|s\rangle = \exp(-E_s/k_B T)/Z$. The system is said to have evolved to thermal equilibrium when it evolves to a state

$$\hat{\rho}_{\mathcal{S}}(t) \approx \hat{\rho}_{\mathcal{S}}^{\text{Boltzmann}} \tag{2.19}$$

and stays close to $\hat{\rho}_{\mathcal{S}}^{\text{Boltzmann}}$ for most subsequent times t. Then all of the system relations from the standard Boltzmann distribution apply to the system $\mathcal{S}$ in the total state $|\Psi_{\mathcal{SE}}(t)\rangle$, where they appear as a result of quantum state dynamics with entanglement of $\mathcal{S}$ and $\mathcal{E}$.

In this section I have sketched how thermodynamics and statistical mechanics can be formulated solely in terms of quantum pure states evolving in time, without the microcanonical ensemble. This relies on time evolution with system-environment entanglement such that the system alone is described by a reduced density operator in accord with the standard Boltzmann distribution, as in Eq. 2.18 and 2.19. This time-evolution behavior has not yet been justified theoretically; the next section will discuss the two contemporary theoretical arguments for why this type of behavior should be expected. But first, to close this section I will briefly comment on alternate approaches to formulating quantum thermodynamics that begin with mixed states, as is appropriate in alternate situations.

It's notable that a different type of approach in contemporary work on quantum thermodynamics begins with a mixed state [28, 32, 44, 45] instead of a pure state as was the starting point here in Eq. 2.9. In these studies, the environment is often treated as a mixed state Boltzmann distribution, representing a local component $\mathcal{E}$ of a total larger environment $\mathcal{E}'$ at temperature T. The larger $\mathcal{E}'$ gives entanglement with $\mathcal{E}$ leading to the Boltzmann mixed state for $\mathcal{E}$, then usually $\mathcal{E}'$ is ignored in the subsequent analysis of $\mathcal{SE}$ thermodynamic behavior. This is the same starting point one would get by assuming a microcanonical ensemble type description for the total $\mathcal{SEE}'$ system, so that $\mathcal{E}$ begins in the Boltzmann distribution. Thus these approaches can give a useful way to analyze thermodynamic behavior of $\mathcal{S}$ interacting with a local $\mathcal{E}$ in a thermal distribution, but they cannot give a new foundation for how

to understand statistical mechanics as a result of quantum dynamics without the microcanonical ensemble.

By comparison, the approach here with pure states focuses on deducing statistical mechanics directly from quantum mechanics, without any initial assumption of standard statistical mechanical behavior in the microcanonical ensemble. This approach is suited to formulating a new foundation for quantum statistical mechanics, where the classical assumption of the microcanonical ensemble is replaced by a more basic quantum state description. This also gives a way forward to analyzing non-microcanonical types of behavior in quantum pure states, with potential for new types of quantum thermodynamic effects that deviate from microcanonical predictions (see Chapter VI).

Having sketched the quantum pure state approach to formulating statistical mechanics with $|\Psi_{\mathcal{SE}}\rangle$ evolving in time to equilibrium, I'll now discuss contemporary theoretical approaches to motivating this equilibration behavior.

2.5. Theoretical motivations for quantum pure state thermodynamics

Two basic theories have been given as potential explanations for why quantum pure states $|\Psi_{\mathcal{SE}}(t)\rangle$ should evolve to equilibrium states with the system in the Boltzmann distribution as in Eq. 2.18, as discussed in the previous section. In both of these theories, the important conceptual difference compared to classical theory is that the system Boltzmann distribution is deduced from the fundamental quantum probabilities associated with the state $|\Psi_{\mathcal{SE}}\rangle$ instead of by assuming probabilities in the classical microcanonical ensemble. One of these theories is called "quantum typicality" [11–18]. It is based on statistical arguments about the types of states that are possible in the Hilbert space, essentially a quantum version of the classical

typicality argument of Section 2.3. The other theory is called the "eigenstate thermalization hypothesis" or ETH [19–27], it gives a dynamical argument for thermalization, essentially a quantum version of the classical ergodic hypothesis of Section 2.3. I'll briefly review these two approaches here, beginning with typicality.

The quantum typicality approach gives a statistical argument for why to expect system thermalization, based on the observation that thermalization is a property of almost all states $|\Psi_{\mathcal{SE}}^{random}\rangle$ chosen at random from the system-environment Hilbert space [12, 14]. For the purposes of this dissertation, this can be viewed as the statement that for a system $\mathcal{S}$ weakly interacting with a temperature bath $\mathcal{E}$, almost all randomly selected states $|\Psi_{\mathcal{SE}}^{random}\rangle$ in the Hilbert space are such that the system reduced density operator follows the Boltzmann distribution,

$$\hat{\rho}_{\mathcal{S}}^{\text{random}} = \text{Tr}_{\mathcal{E}}|\Psi_{\mathcal{SE}}^{random}\rangle\langle\Psi_{\mathcal{SE}}^{random}| \approx \frac{e^{-\hat{H}_{\mathcal{S}}/kT}}{Z}, \tag{2.20}$$

in accord with Eq. 2.18. The majority of randomly selected states have the thermal property of Eq. 2.20 so it is said that these states are "typical." Precise mathematical statements of typicality and related results can be found in Refs. [11–18].

The quantum typicality approach follows the same type of reasoning as the classical typicality approach discussed in Section 2.3: since most possible states are thermal, it seems plausible that real states will also be thermal. If a state isn't initially thermal, it's plausible that it will evolve to spend most of its later times in thermal states, since there are many more thermal states than non-thermal states. However, apart from plausibility based on the relative abundance of typical thermal states, it isn't clear when or why atypical non-thermal states should evolve into typical thermal states. An acute counterexample can be found in integrable systems with non-trivial constants of motion that never evolve to thermal equilibrium [20].

Although integrability is not expected in complex systems, it is still unclear whether and when complex pure state universes will evolve from atypical states to spend most later time in typical states. What initial conditions, Hamiltonians, and timescales are needed for an atypical non-equilibrium state to evolve to equilibrium? Some partial answers to how quantum time evolution can take an initial non-equilibrium atypical state to spend most later time in typical thermal equilibrium states can be found in Refs. [10, 11, 13, 16–18], but this remains a very important and open question in the quantum formulation of statistical mechanics through typicality.

A second approach to quantum pure state thermodynamics is called the "eigenstate thermalization hypothesis" or ETH, which is based on a dynamical argument about ergodic-like quantum behavior that is embedded into eigenstates of complex $\mathcal{SE}$ total systems [19–27]. The approach is often based on reasoning about the quantum dynamics of classically chaotic systems, where couplings can be modeled as random matrices [20] that couple all the $|s\rangle|\epsilon\rangle$ states, somewhat similar to the classical ergodic hypothesis where a real system explores all the s, ϵ states over time as discussed in Section 2.3. With these effectively random couplings the eigenstates $|\xi\rangle$ mix many nearby $|s\rangle|\epsilon\rangle$ zero-order states, so that thermalization is embedded into each eigenstate. For the purposes of this dissertation, this can be seen as the statement that for each eigenstate $|\xi\rangle$ of a system $\mathcal{S}$ weakly interacting with a temperature bath $\mathcal{E}$, tracing over the environment to get the system reduced density matrix $\hat{\rho}_{\mathcal{S}}^{(\xi)}$ gives the thermal Boltzmann distribution

$$\hat{\rho}_{\mathcal{S}}^{(\xi)} = \mathrm{Tr}_{\mathcal{E}}|\xi\rangle\langle\xi| \approx \frac{e^{-\hat{H}_S/kT}}{Z}. \tag{2.21}$$

The ETH condition on thermalization in the eigenstates Eq. 2.21 guarantees that if an $\mathcal{SE}$ universe reaches a steady state, this state will be thermal, as can be shown following a similar argument to Deutsch [21, 22].

The main merit of the ETH approach is that it shows explicitly how a non-thermal initial state can evolve into a thermal state and stay thermal for most time, based on the structure of the eigenstates. The main weakness of ETH is that it is unclear which Hamiltonians have the hypothesized thermal eigenstate structure of Eq. 2.21. To address this question, a number of studies have examined the behavior of eigenstates in different types of models with random [20–22, 25–27] or structured [19, 23] interaction Hamiltonians. These studies have shown some compelling evidence for ETH in certain types of models, but it's desirable to have a more general formulation that doesn't need to be checked with each new model on a case-by-case basis. It's also unclear whether there can be ETH-like situations where the eigenstates encode unexpected types of *non-standard* quantum thermodynamic behavior that differ from the standard thermal behavior of Eq. 2.21. If so, this could be an important component in the foundations of quantum thermodynamics.

Both the quantum typicality and ETH approaches to quantum thermodynamics provide some evidence for why to expect the approach to thermal equilibrium for quantum pure states, as sketched in Section 2.4. However, both of these approaches are still in development, with important unanswered questions that need to be addressed before either or both can be viewed as the general foundation for thermodynamics and statistical mechanics. Thus thermalization appears to be plausible but cannot be assumed; it must be tested for each type of $\mathcal{SE}$ state and Hamiltonian. In this dissertation I will therefore assess the thermodynamic behavior in each type of model I use. It's also unclear if or when there can be new types

of quantum thermodynamic behavior. Chapter VI and Ref. [5] show an example where this is the case, with implications for the future development of the theoretical foundations of quantum thermodynamics.

2.6. The second law and the entropy S^Q_{univ} in quantum pure state thermodynamics

So far this chapter has developed the basic ideas of quantum pure state thermodynamics, based on a quantum pure state evolving in time with entanglement to equilibrium, with the system in the thermal Boltzmann distribution. However, there is an important gap in the description so far when compared with standard thermodynamics. There has not been a formulation of the second law of thermodynamics for a quantum pure state evolving to equilibrium. This section recapitulates the recent idea of Ref. [1] to formulate the second law in quantum thermodynamics using a quantum entropy definition S^Q_{univ} for a pure state $|\Psi_{\mathcal{SE}}\rangle$. This will be the starting point for the new work in this dissertation, beginning in the next chapter, which expands on the work of Ref. [1] to explore the behavior of S^Q_{univ} in relation to classical thermodynamics and new types of specifically quantum thermodynamic behavior.

The second law as described in Section 2.1 is based on an entropy for an isolated system or universe that increases during a spontaneous process. In classical thermodynamics, this is formulated with the Boltzmann entropy $S = k_B \ln W$ of Eq. 2.5, based on the assumption of the microcanonical ensemble. The approach with quantum pure states replaces the microcanonical ensemble with a more basic quantum state $|\Psi_{\mathcal{SE}}\rangle$ as described in Sections 2.4-2.5. Thus a new approach to formulating the second law is needed. There are definitions for entropy in quantum mechanics,

however the notion of an entropy for an isolated state that increases in a spontaneous process is problematic. In quantum mechanics, entropy is usually defined as the *von Neumann entropy* S^{vN}. For a state described by a density operator $\hat{\rho}$, the von Neumann entropy is defined as

$$S^{vN} = -\mathrm{Tr}\hat{\rho}\ln\hat{\rho}, \tag{2.22}$$

where Tr is the trace. To evaluate Eq. 2.22, the density operator is expressed in diagonal form in terms of its eigenvectors $|\psi_i\rangle$ and eigenvalues λ_i

$$\hat{\rho} = \sum_i \lambda_i |\psi_i\rangle\langle\psi_i|, \tag{2.23}$$

where λ_i is the probability that a measurement in the eigen basis will yield the state $|\psi_i\rangle$. The von Neumann entropy S^{vN} of Eq. 2.22 is then given in terms of the probabilities λ_i as

$$S^{vN} = -\sum_i \lambda_i \ln\lambda_i, \tag{2.24}$$

where the sum runs over all i with $\lambda_i \neq 0$.

The von Neumann entropy is problematic for defining a thermodynamic entropy for a pure state such as $|\Psi_{\mathcal{SE}}\rangle$. For a pure quantum state $|\Psi(t)\rangle$, the density operator can always be expressed in diagonal form as

$$\hat{\rho}^{\mathrm{pure}}(t) = |\Psi(t)\rangle\langle\Psi(t)|. \tag{2.25}$$

There is one non-zero eigenvalue $\lambda = 1$ and the von Neumann entropy is

$$S^{vN,\text{pure}} = 1 \ln 1 = 0. \tag{2.26}$$

Thus the von Neumann entropy of a pure state cannot increase past zero. In terms of the system-environment thermalization of the pure state $|\Psi_{\mathcal{SE}}(t)\rangle$ of Section 2.4, $S^{vN}(t)$ does not increase during the approach to thermal equilibrium, so it cannot be used to express the second law in the standard form of Eq. 2.1. There are some situations where it is entirely appropriate to use the von Neumann entropy, as described in the next paragraph, but ultimately a new method of formulating the second law is needed, as described soon after.

It should be noted that the von Neumann entropy is very useful in certain other situations in thermodynamics and for characterizing entanglement. In pure state thermodynamics, the system $\mathcal{S}$ becomes entangled with the environment $\mathcal{E}$, so that the system alone is described by the thermal Boltzmann distribution of Eq. 2.18. For the $\mathcal{S}$ thermal state, the von Neumann entropy takes the classical value based on the Boltzmann factors $\lambda_s = \exp(-E_s/k_BT)/Z$,

$$S^{vN}_{\mathcal{S}} = S^{\text{Boltzmann}}_{\mathcal{S}}. \tag{2.27}$$

Thus $S^{vN}_{\mathcal{S}}$ gives the standard entropy for the system $\mathcal{S}$ at thermal equilibrium. However, this does not help with formulating the second law, which depends on the entropy of the total $\mathcal{SE}$ universe. This varying behavior of S^{vN} for $\mathcal{S}$ and $\mathcal{SE}$ is related to the role of S^{vN} as a measure of entanglement. The pure state is not entangled with anything, so it has a single non-zero eigenvalue $\lambda = 1$ and $S^{vN} = 0$. Entangled states have more than one non-zero eigenvalue, with $S^{vN} > 0$. S^{vN} increases with more entanglement, reaching its maximum value for a maximally entangled state where all

the λ_i are equal. Thus S^{vN} gives a useful way of characterizing entanglement and it gives the standard thermodynamic entropy for an entangled quantum system in the Boltzmann distribution, but it can't formulate the second law as in Eq. 2.1 for a pure state $|\Psi_{\mathcal{SE}}\rangle$. How should the second law be formulated in quantum pure state thermodynamics?

Ref. [1] argued that a new definition of quantum thermodynamic entropy should be used to formulate the second law for a quantum pure state $|\Psi_{\mathcal{SE}}\rangle$. To define the entropy, first the state was expressed in a reference basis $\{|\alpha\rangle\}$ of the total $\mathcal{SE}$ Hilbert space,

$$|\Psi_{\mathcal{SE}}\rangle = \sum_{\alpha} c_\alpha |\alpha\rangle. \tag{2.28}$$

The entropy was then defined with a standard Shannon entropy expression using the probabilities p_α in the reference basis

$$p_\alpha = |c_\alpha|^2 \tag{2.29}$$

to give the quantum entropy

$$S^Q_{univ} = -\sum_{\alpha} p_\alpha \ln p_\alpha. \tag{2.30}$$

The quantum entropy differs from the von Neumann entropy S^{vN} in the choice of basis to evaluate the probabilities, for S^{vN} it is the basis of eigenstates $\{|\psi_i\rangle\}$ of the density operator with probabilities λ_i, whereas with S^Q_{univ} it is the as yet unspecified reference basis $\{|\alpha\rangle\}$ with probabilities p_α. The entropy takes different values depending on the choice of the reference basis $\{|\alpha\rangle\}$. One of the main goals of Ref. [1] was to

provide a rationale for a choice of reference basis to give a thermodynamic entropy S^Q_{univ} consistent with the second law.

Ref. [1] developed the reference basis in the context of modeling heat flow between a system and environment, with the idea that the reference basis should correspond to the physical process. In this process, the average $\mathcal{S}$ zero-order energy $\langle \hat{H}_\mathcal{S} \rangle$ is changing with heat flow from $\mathcal{E}$. The change in $\langle \hat{H}_\mathcal{S} \rangle$ is due to changes in the probabilities of measuring different system zero-order energy levels $|s\rangle$ as the system evolves from a non-equilibrium state to the equilibrium Boltzmann thermal state of Eq. 2.18. Thus it was argued that the reference basis reflecting the physical process should contain the system basis of zero-order energy eigenstates $|s\rangle$ of the isolated system. After specifying the system basis, it is necessary to specify a basis for the environment. The probabilities for the environment zero-order energy levels $|\epsilon\rangle$ change along with the $|s\rangle$ during heat flow, such that in the standard situation with weak coupling $\langle \hat{H}_{\mathcal{SE}} \rangle \approx 0$ the total zero-order energy is approximately constant $\langle \hat{H}_\mathcal{S} \rangle + \langle \hat{H}_\mathcal{E} \rangle \approx E$. Thus it was argued that the environment basis representing the physical process should be the basis of zero-order environment energy eigenstates $|\epsilon\rangle$. With this choice the total $\mathcal{SE}$ reference basis is

$$\{|\alpha\rangle\} = \{|s\rangle|\epsilon\rangle\}, \tag{2.31}$$

so that the quantum entropy is defined as

$$S^Q_{univ} = -\sum_{s,\epsilon} p_{s,\epsilon} \ln p_{s,\epsilon}. \tag{2.32}$$

Note the expression for S^Q_{univ} in Eq. 2.32 is the same expression used in classical statistical mechanics for the Boltzmann microcanonical entropy in Eq. 2.5, except

that in S^Q_{univ} the probabilities $p_{s,\epsilon}$ are taken directly from the wavefunction instead of being assumed equal as they were with the microcanonical ensemble. Thus the quantum entropy S^Q_{univ} can be thought of as generalizing the Boltzmann entropy by replacing the assumed probabilities of the microcanonical ensemble with the true probabilities $p_{s,\epsilon}$ from the quantum state, very much in the spirit of the quantum approach to formulating all of statistical mechanics in terms of fundamental quantum probabilities. There will be more to say about the theoretical justification for the $|s\rangle|\epsilon\rangle$ reference basis in Chapter IV, where it will be shown that this choice uniquely leads to a natural separation of S^Q_{univ} into system and environment parts S_{sys} and S_{env} that each agree with their standard values from thermodynamics, giving further support for S^Q_{univ} as an appropriate generalization of S_{univ} in quantum thermodynamics.

Ref. [1] computationally tested the behavior of S^Q_{univ} in Eq. 2.32 in a very simple model of $\mathcal{SE}$ heat flow between a system $\mathcal{S}$ of a few evenly spaced levels and an environment $\mathcal{E}$ with similarly-spaced highly-degenerate levels, with a degeneracy pattern designed to give it a temperature T. ΔS^Q_{univ} was compared with the free energy change of the system $-\Delta F_{sys}$ in terms of the very important classical microcanonical relationship $\Delta S_{univ} = -\Delta F_{sys}/T$. The observed ΔS^Q_{univ} was close to but slightly larger than $-\Delta F_{sys}/T$, so that ΔS^Q_{univ} was in good approximate agreement with this important standard thermodynamic relation.

Several other authors have defined similar types of quantum pure state entropies in different approaches to formulating the second law in quantum pure state thermodynamics [10, 29, 30] and also to characterize the information content of a pure state [31, 46]; for a more thorough discussion of these entropies see Ref. [1]. However, none of these approaches had the virtue of Ref. [1] in testing the behavior of the pure state entropy in comparison with the very important relationship to the

system free energy change in $-\Delta F_{sys}/T$. The approximate agreement between these quantities in Ref. [1] motivates this dissertation research to further explore S^Q_{univ} of Eq. 2.32 as a meaningful thermodynamic entropy for formulating the second law in quantum pure state thermodynamics.

Despite the success of Ref. [1] in demonstrating approximate agreement between ΔS^Q_{univ} and the classically related $-\Delta F_{sys}/T$, the model of Ref. [1] had some unrealistic features compared to what's expected in the real world, and the small discrepancy between ΔS^Q_{univ} and $-\Delta F_{sys}/T$ was unexplored. The goal of the next chapter is to remedy these shortcomings of Ref. [1], to give a more realistic and systematic account of S^Q_{univ} in comparison with classical microcanonical behavior in the free energy relation. After arriving at a good quantum account of classical second law behavior, later chapters will then develop a route to exploring and understanding new types of specifically quantum thermodynamic behavior.

CHAPTER III

QUANTUM MICROCANONICAL ENTROPY, BOLTZMANN'S EQUATION, AND THE SECOND LAW

This chapter includes previously published material co-authored by Michael E. Kellman [2]. Michael Kellman and I both contributed to developing the model and theory, analyzing the results, and writing the manuscript. I performed the computations.

3.1. Introduction

Classical statistical mechanics is perhaps most often founded on the idea of the microcanonical ensemble and a suitable notion of entropy, such that the second law can be stated in the classic formulation of Clausius that the entropy increases in a spontaneous process: $\Delta S_{univ} > 0$. In quantum thermodynamics and statistical mechanics, this raises a fundamental question. If the "universe" (defined as any closed interacting and entangling system-environment composite entity) is taken to be in a pure state, by that fact the quantum von Neumann entropy is identically equal to zero. Then what, if anything, fills the role of S_{univ}? We have explored an approach to this question in a recent paper [1] in which we defined and computationally tested in a system-environment universe a new quantum entropy S^{Q}_{univ} that is distinctly different from the von Neumann entropy. This new entropy is briefly recapitulated here in Section 3.5 before the presentation of computational results; for a deeper discussion, the reader should see Ref. [1]. We regard our focus on a new approach to

quantum entropy to be part of a broad examination of the foundations of quantum thermodynamics and statistical mechanics; a partial listing of contributions can be found in Refs. [6–8, 10–19, 28–32, 36, 37].

We were able to recover reasonable thermodynamic behavior, with $\Delta S^{Q}_{univ} > 0$ and a notion of a quantum microcanonical ensemble, with S^{Q}_{univ} related to the classical Boltzmann relation

$$S = k \ln W. \tag{3.1}$$

In classical thermodynamics and statistical mechanics, there is also the very important relationship between the free energy change of the system at fixed T, V and the entropy change of the *universe*:

$$-\frac{1}{T}\,\Delta F_{sys} = \Delta S_{univ} \tag{3.2}$$

This equality holds when the free energy change of the system is a surrogate for the entropy change of the universe in the second law, specifically, at fixed T and V. This is the meaning of the use of the free energy F as a thermodynamic potential. In Ref. [1] we tested the relationship corresponding to Eq. 3.2 for S^{Q}_{univ} and found approximate equality:

$$-\frac{1}{T}\,\Delta F_{sys} \approx \Delta S^{Q}_{univ}. \tag{3.3}$$

Despite the apparent success indicated by the numerical result expressed in Eq. 3.3 in reproducing classical thermodynamic relations, with the approach in Ref. [1] we are left with some real questions. First of all, Eq. 3.3 does not hold exactly. Generally, in Ref. [1] we found *excess entropy production*, i.e. ΔS^{Q}_{univ} greater than

would be expected from the system free energy change ΔF_{sys}. It is not clear that the classical expression Eq. 3.2, which is based on the microcanonical ensemble, will hold generally in our quantum approach, even as an approximation. The newly defined S^Q_{univ} also has a much different formal basis than the Boltzmann equation Eq. 3.1 and the conceptual constructs that go with the microcanonical ensemble. These considerations raise the question of whether a microcanonical limit inheres in the quantum approach and simulations. Furthermore, Ref. [1] was built for purposes of computational simplicity on some not totally satisfactory properties of the system, the bath, and the initial state. Ref. [1] used as an environment a rather artificial temperature bath consisting of harmonically spaced levels with high degeneracy, chosen to match the evenly spaced levels of a restricted harmonic system. This artificial "non-continuous harmonic bath" limits the system to a similar harmonic structure, clearly a very serious limitation. A further consequence is that this basis automatically leads to an exact microcanonical zero-order energy. In contrast, classical statistical mechanics is usually based on an idea of a microcanonical energy shell of finite width. In time-dependent quantum dynamics, the notion of a fixed energy shell becomes especially problematic. On the other hand, there are other special assumptions in Ref. [1] that could bias our computations toward the microcanonical limit Eq. 3.2. In particular, the initial bath states in the simulations of Ref. [1] were chosen in a way that in retrospect could artificially bias the results toward microcanonical behavior. Thus, both system and bath were artificially restricted by comparison with what one would like to model in the real world.

In this chapter we seek to remedy these features, devising a bath that allows for an approximation to a true continuum of levels, and adopting a more general procedure for picking the initial state. We investigate this in numerical quantum simulations,

and find that in the limit of small coupling, we are able to successfully recover sensible microcanonical behavior. As an interesting counterpoint, we find away from the microcanonical limit that the excess entropy production is a ubiquitous feature of time-dependent quantum states that may be a fruitful subject for future exploration of quantum thermodynamics and statistical mechanics of entangled system and environment.

The outline of the chapter is as follows. In Section 3.2 we describe the system-environment "universe" including the interaction of the system with environment heat bath. Section 3.3 concerns thermalization and the development of a "thermal basis set." Section 3.4 presents our initial state selection. Section 3.5 presents the key notion of the new quantum entropy S^{Q}_{univ} and its relation to free energy and "excess entropy production." The final sections present results of simulations, the approach to microcanonical behavior and the phenomenon of excess entropy production, and a final discussion.

3.2. Model quantum universe

In this section we describe a model system-environment universe, the Hamiltonian of the system, of the environment functioning as a realistic temperature bath, and the interaction between them. The setup is similar to Refs. [1, 6] except that we make significant modifications to the environment temperature bath used in those papers, seeking to make it considerably more realistic.

We model a quantum system and quantum environment, taken together as a pure state "quantum universe" $|\Psi\rangle$. The total Hamiltonian of the universe $\hat{H}$ is the sum of the Hamiltonians of the isolated system $\hat{H}_{\mathcal{S}}$ and environment $\hat{H}_{\mathcal{E}}$ along with an interaction $\hat{H}_{\mathcal{SE}}$,

$$\hat{H} = \hat{H}_{\mathcal{S}} + \hat{H}_{\mathcal{E}} + \hat{H}_{\mathcal{SE}}. \tag{3.4}$$

We choose to work in the zero-order energy eigenbasis of the system and environment so that $\hat{H}_{\mathcal{S}}$ and $\hat{H}_{\mathcal{E}}$ are given in diagonal form. The system zero-order eigenstates will be denoted by Roman letters $|n\rangle$ and the environment states by Greek letters $|\epsilon\rangle$.

3.2.1. Model system

For the system we choose a degenerate pair of linearly coupled harmonic oscillators, a simple model of vibrational motion in ABA triatomic molecules. In the system energy basis the Hamiltonian is

$$\hat{H}_{\mathcal{S}} = N\omega_0 + \kappa n, \tag{3.5}$$

For a given total number of oscillator quanta N for the two-oscillator system, the quantum number n takes values $0, .., N$. We choose various N in the simulations of this paper. We work in reduced units so that $E_n = n$. Details on the system Hamiltonian are available in Refs. [1, 6] and references therein.

3.2.2. Model environment temperature bath

In Refs. [1, 6], following the work of Gemmer et al. [37], we defined an environment in such a way that it had properties appropriate to a temperature bath, in accord with standard relations between thermodynamic temperature and quantum level patterns in statistical mechanics. While the environment defined in Refs. [1, 6] behaves properly as a temperature bath, it nonetheless has serious limitations of physical realism. It consists of a set of harmonically spaced discrete energy levels,

with high degeneracy of each level. This "harmonic bath" degeneracy pattern was designed to match the energy levels of the system, which was a set of discrete harmonic oscillator levels. This was done for reasons of computational simplicity and tractability, but it means that we were ignoring bath levels not in resonance with the system levels, unlike a realistic physical temperature bath. Moreover, the harmonic bath is inadequate in dealing with anything other than a harmonic system, since its structure makes it unable to simulate anharmonic systems interacting with an environment. In this paper we seek to rectify these shortcomings by constructing a more realistic, "continuous bath" environment.

We model the quantum environment in analogy to a classical statistical description of an environment. In classical statistical mechanics, the entropy S of an isolated system is given by Boltzmann's equation

$$S = k_B \ln W(E), \tag{3.6}$$

with $W(E)$ the volume of phase space in the energy shell $[E, E + \delta E]$, or in the case of quantized energy levels the number of states within the shell. The temperature is then determined by the definition

$$T \equiv \left(\frac{\partial S}{\partial E} \right)^{-1}. \tag{3.7}$$

For conditions in which other thermodynamic variables besides E are held fixed, and assuming that the isolated system is large so that its temperature can be treated as constant under small changes in energy, the solution to Eqs. 3.6 and 3.7 is

$$W(E) \sim e^{E/k_B T}, \tag{3.8}$$

i.e. the number of states grows exponentially with energy. One can then partition out a small subsystem of the total isolated system and assume that the remainder, called "the environment," has practically the same density of states as the total system because of its relatively large size. Based on the postulate of equal *a priori* probabilities of all states of the isolated system, this leads to the classical canonical ensemble for the subsystem, with Boltzmann probability $p_n \sim e^{-E_n/k_BT}$. See for example a nicely intuitive presentation of Einstein [47].

The exponential scaling of $W(E)$ in Eq. 3.8 is an important universal feature of large environment heat baths [47–49] that is directly connected to the universality of the Boltzmann distribution for a subsystem interacting with a heat bath, as shown in Fig. 2.2 and Eq. 2.8. The exponential scaling is valid in limited energy ranges of approximately constant temperature, e.g. in limited energy ranges accessed under heat flow to a small subsystem. A detailed discussion of how Eq. 3.8 can be derived from explicit environment models, including examples with gas and spin environments, can be found in Ref. [50]; note however that the exponential scaling is much more general than these gas and spin examples, it must apply just as well for other explicit environment heat baths such as the oscillator baths often used in modeling open quantum systems. Here we will simply use the exponential scaling in $W(E)$ to define a generic type of model environment that has this essential feature of any true environment heat bath, without going into explicit detail about structure within the environment.

We will now devise our model quantum environment based on the scaling $W \sim e^{E/k_BT}$ derived above. We consider environment states in a total energy range $[E_{env}^{\min}, E_{env}^{\max}]$ that is large relative to the system energy range. The scaling of W_{env} with energy gives the relation

$$W_{env} = \int_{E_{env}^{\min}}^{E_{env}^{\max}} \frac{dW_{env}}{dE} dE = A\left(e^{E_{env}^{\max}/k_BT} - e^{E_{env}^{\min}/k_BT}\right), \tag{3.9}$$

where A is a parameter. To set the energies of the individual quantum states, we begin by inverting the left and right sides of Eq. 3.9 to get

$$E_{env}^{\max} = \ln\left(\frac{W_{env}}{A} + e^{E_{env}^{\min}/k_BT}\right) k_BT. \tag{3.10}$$

Using Eq. 3.10 we can now calculate the maximum energy of the environment $E_{env}^{\max}$ for any number of states W_{env}. For example, if $W_{env} = 1$ then the maximum energy is

$$E_1 \equiv E_{env}^{\max(W_{env}=1)} = \ln\left(\frac{1}{A} + e^{E_{env}^{\min}/k_BT}\right) k_BT, \tag{3.11}$$

which is consistent with an environment containing a single quantum state of energy E_1 in the interval $[E_{env}^{\min}, E_1]$. Considering two environment states $W_{env} = 2$ gives a maximum energy E_2, which is consistent with an environment containing two states of energies E_1 and E_2 in the interval $[E_{env}^{\min}, E_2]$. Continuing in this way, the energy E_ϵ of the ϵth environment state is

$$E_\epsilon = \ln\left(\frac{\epsilon}{A} + e^{E_{env}^{\min}/k_BT}\right) k_BT, \tag{3.12}$$

with all of the ϵ states of energies $E_1, ..., E_\epsilon$ being contained in the interval $[E_{env}^{\min}, E_\epsilon]$. The total set of environment energy levels is calculated by setting $\epsilon = 1, 2, ..., W_{env}$ in Eq. 3.12 with fixed parameters $W_{env}, T, E_{env}^{\min}$, and $E_{env}^{\max}$, and with A given in terms of these parameters by rearranging the left and right sides of the integrated total number of states in Eq. 3.9. The individual quantum energy levels E_ϵ become logarithmically

closer together as the quantum number ϵ increases, leading to a total number of states that increases exponentially with energy according to Eqs. 3.8 and 3.9. An example of the resulting environment level pattern is shown schematically in Fig. 3.1.

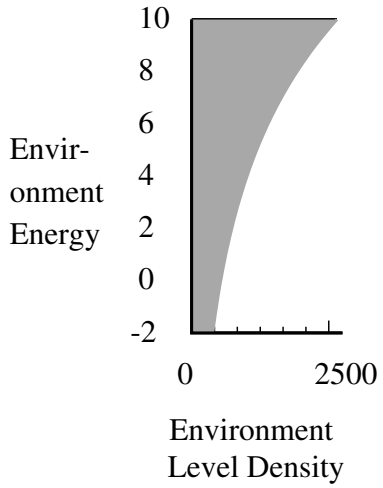

FIGURE 3.1. Model fixed temperature environment level density increases exponentially with energy. This example has W_{env} =14 085 states, $E_{env}^{\min} = -2$, $E_{env}^{\max} = 10$, and $T = 6.22$ energy units (See Section 3.2.2.)

Throughout this paper we work in units where the Boltzmann constant is $k_B = 1$, and choose $T = 6.22$ energy units of the system. Smaller values of T lead to faster relative increases in the number of states with energy, since T is in the denominator of the exponential in Eq. 3.8, and larger T give a smaller relative increase in density. This intermediate value of T (in our basis) is convenient for computations because it produces a level density that increases only modestly from the top to the bottom of the basis. Other parameters are indicated in the figure captions.

A similar model quantum temperature bath has recently been presented in Ref. [35]. We note that we are able to achieve good thermal behavior with a significantly smaller bath energy range and a generic system-environment coupling, in contrast to Ref. [35] with a coupling dependent on the bath energy. These advantages

stem from important considerations of modeling the total universe, namely the further modification of the system and environment to an appropriate "thermal" basis set, described in Section 3.3, and the method of varying the initial bath state together with the initial system state, described in Section 3.4.

3.2.3. System-environment coupling

The interaction between a real quantum system and environment is generally very complicated, and we do not wish to presume any particular structure to such an interaction in our model. Following previous work [1, 6, 37], we therefore model the interaction Hamiltonian $\hat{H}_{\mathcal{SE}}$ as a random matrix with off-diagonal elements chosen from a Gaussian distribution of mean 0 and standard deviation k. We have also tried a different type of uniformly distributed random coupling with matrix elements $\pm k$ of equal magnitude but random signs, finding very similar results to those we report here with the Gaussian random coupling, so our results don't seem to depend strongly on the random magnitudes in the coupling (later in Chapter V we will also study a more structured type of coupling for a different type of environment). The specific values of k used in this paper can be found in the figures and their captions, and a rationale for varying k will be introduced later in Section 3.6.2.2. In all cases we choose k to be much less than the system level spacing, corresponding to weak coupling. Larger values of k beyond the weak coupling limit could be an interesting subject of future research, but are beyond our scope here.

3.2.4. Time evolution and simulations

To determine the time-dependent behavior of the universe pure state $|\Psi\rangle$, we first numerically diagonalize the universe Hamiltonian $\hat{H}$ and then transform the

initial state into the energy eigenbasis. A series of time steps are calculated from the initial state using $|\Psi(t)\rangle = e^{-i\hat{H}t/\hbar}|\Psi(0)\rangle$, and at each time step the state $|\Psi(t)\rangle$ is transformed back into the zero-order basis to examine the dynamical behavior. There is no compounding numerical error over time since each subsequent time step does not depend on the previous step.

At each time step, the statistics of the system are determined by calculating the reduced density operator of the system $\hat{\rho}_{\mathcal{S}}$, obtained by taking the partial trace over the environment of the universe density operator $\hat{\rho} = |\Psi\rangle\langle\Psi|$,

$$\hat{\rho}_{\mathcal{S}} = \mathrm{Tr}_{\mathcal{E}}\hat{\rho} = \sum_{\epsilon}\langle\epsilon|\Psi\rangle\langle\Psi|\epsilon\rangle. \tag{3.13}$$

3.3. Thermalization and "thermal basis set"

The obvious universe basis set to use would seem to be the system-environment tensor product basis $\{|n\rangle\}\otimes\{|\epsilon\rangle\}$ with zero-order energy levels given by $E_{univ} = E_n + E_\epsilon$. However, we have found that it is very useful to truncate this basis to a smaller subset, called the "thermal basis set," for the following reasons. At equilibrium, we expect the system embedded in the bath to be described by a Boltzmann distribution at the designed temperature T. We will use this as an important check that our model displays reasonable thermodynamic behavior. Initially we did simulations (details of the method in Sections 3.2.4 and 3.4) using the tensor product basis, a schematic of which is shown in Fig. 3.2. However, we found when using the tensor product basis that the system would not thermalize to a proper Boltzmann distribution, indicating unrealistic thermodynamic behavior. We now explain the reasons for this, and the remedy that we have devised.

Fig. 3.2 shows the tensor product basis, as well as the truncated "thermal" basis that we eventually adopted. In the figure, the basis is visually separated into sub-basis set "columns" $|n\rangle \otimes \{|\epsilon\rangle\}$ for each state $n = 0, 1, 2$ of a three level system paired with all the environment states $\epsilon = 1, ..., W_{env}$ as shown in Fig. 3.1. It can be seen that the tensor product basis contains two qualitatively distinct types of regions. In the central region of states with $0 \leq E_{univ} \leq 10$, tensor product states are present containing each of the system states, so the system can transition between all of its energy levels by exchanging heat with the environment. The exchange of heat providing access to all of the system states is what produces the Boltzmann distribution in statistical mechanics. In general, this "thermal" part of the basis occupies the energy range

$$E_{sys}^{max} + E_{env}^{\min} \leq E_{univ} \leq E_{sys}^{min} + E_{env}^{\max}. \tag{3.14}$$

Consider now the outer regions $E_{univ} < 0$ and $E_{univ} > 10$ (respectively $E_{univ} < E_{sys}^{max} + E_{env}^{\min}$ and $E_{univ} > E_{sys}^{min} + E_{env}^{\max}$). Above $E_{univ} = 10$ the system cannot transition to its $n = 0$ state in the $n = 0$ column of Fig. 3.2 since there are no universe states with energy greater than 10 in that column. This means that the environment has so much energy that it cannot absorb heat from the system, which does not make sense for a large environment at finite temperature like we are trying to model. The result is that in the computations, system probabilities get stuck in high energy system states and are unable to thermalize to a Boltzmann distribution. Similarly, in the region below $E_{univ} = 0$ the system cannot transition to its $n = 2$ state in the $n = 2$ column of Fig. 3.2 since there are no universe states with energy less than 0 in that column. To allow thermalization, we therefore delete these physically unsuitable regions $E_{univ} < 0$ and $E_{univ} > 10$ from all columns of the basis, leaving

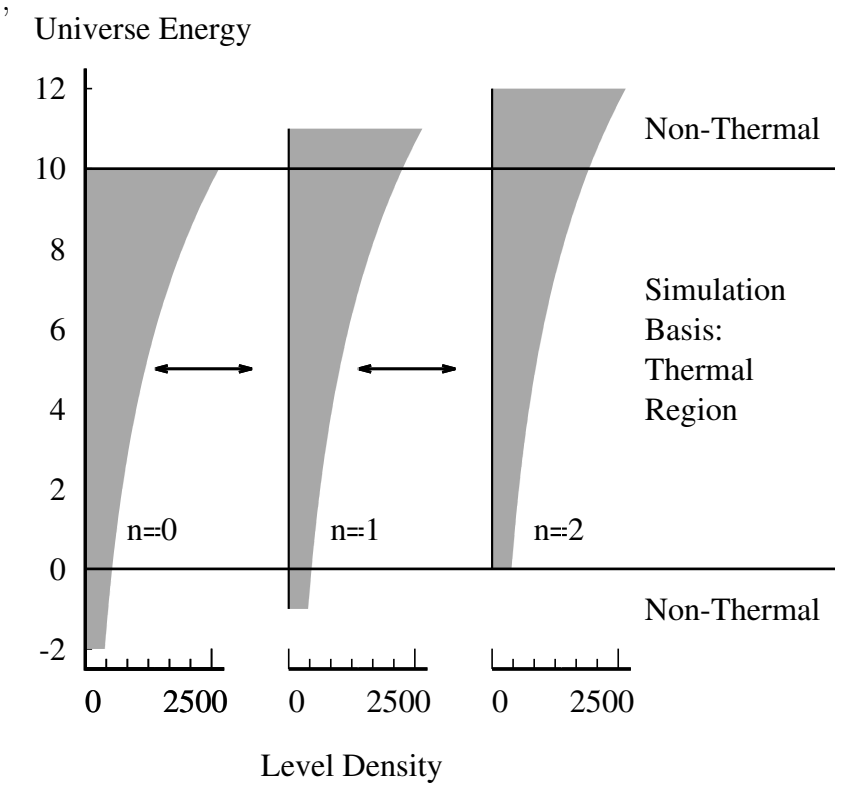

FIGURE 3.2. Energy level density diagram for the full tensor product universe basis, visually separated into components by the system level n. We use only the "thermal" region of the $\mathcal{SE}$ tensor basis, as described in the text.

the region $0 \leq E_{univ} \leq 10$ in our calculations, as indicated by the horizontal lines in Fig. 3.2. We call this truncated basis the "thermal basis set."

The claim that the thermal basis leads to proper thermalization in our calculations, while the full tensor product basis does not, leads to an interesting question. Presumably, nature "uses" the full tensor product basis, not the truncated thermal basis. How then does nature avoid the problem with thermalization that we have encountered in our calculations? A reasonable answer seems to be that in the real natural environment, the range of E_{env} is so large compared to that of E_{sys} that the considerations presented here do not have any practical effect, i.e. thermalization is not a problem. In fact, we have seen in simulations that using a

larger environment energy range does alleviate the thermalization problem. However, making the environment bigger also entails additional computational time, which can make it impractical for our purposes. Another factor may be that in thermodynamic systems in nature, the coupling between system and environment is weak compared with what we consider in this paper. In our calculations, the thermal basis truncation is necessary for thermalization, but also an advantage computationally. This may be useful for future simulations of larger systems.

3.4. Initial state fabrication, measurement, and time evolution

We want to perform simulations that could relate to experiments that might actually be carried out in the laboratory on a small system-environment universe. We will be working in the thermal basis of Section 3.3. We imagine preparation in a laboratory environment of an unentangled system state whose subsequent time evolution we want to observe. Consider an $\mathcal{SE}$ universe that is already at equilibrium in an entangled state $|\Psi^{eq}\rangle$. To prepare a desired system state, suppose we then perform a measurement of the energy of the system, obtaining one of the zero-order system energy eigenvalues. In a conventional description of measurement, we have a new $\mathcal{SE}$ state $|\Psi(t=0)\rangle$ that is the normalized projection of $|\Psi^{eq}\rangle$ onto the system state $|n\rangle$ that was the result of the measurement,

$$|\Psi^{eq}\rangle \to N|n\rangle\langle n|\Psi^{eq}\rangle \equiv |\Psi(0)\rangle, \tag{3.15}$$

where N is a normalizing constant. We can now time-evolve this state and watch its evolution, by hypothesis to a new equilibrium state, with associated quantum entropy production ΔS^{Q}_{univ}.

This process of measurement, time evolution, and re-equilibration is what we will model in our simulations. The procedure we use is illustrated with a particular example in Fig. 3.3. To begin, we need the initial equilibrium state $|\Psi^{eq}\rangle$ that will be measured as in the scheme above. However, *a priori* we do not know how to write down such a complex entangled state. We therefore "synthesize" this state as follows. We start with an "artificial" pre-equilibrated state, an example is shown in the top left of Fig. 3.3, and let this time evolve to equilibrium. The artificial state is chosen to be a separable pure state of the system and environment, $|\Psi_{artificial}\rangle = |sys\rangle|env\rangle$. We choose the system to be in a zero-order eigenstate $|sys\rangle = |n'\rangle$. After choosing $|n'\rangle$, we give probability amplitudes with random phases to all the environment states $|\epsilon\rangle$ that are paired with $|n'\rangle$ in the thermal basis, described previously in Section 3.3. The probability amplitude magnitudes are chosen so that the environment state $|env\rangle$ has a Gaussian probability distribution centered at an energy $E_{env} = E_{univ} - E_{n'}$ that depends on the system level n' and the system + environment energy E_{univ}. We choose $E_{univ} = 5$ so that the peak of the universe state $|\Psi_{artificial}\rangle$ is in the center of the thermal basis energy range $0 \leq E_{univ} \leq 10$ from Section 3.3.

The state $|\Psi_{artificial}\rangle$ is then time evolved, again in the thermal basis following the method of Section 3.2.4 until it reaches an equilibrium state $|\Psi^{eq}_{artificial}\rangle$ with steady F_{sys}, S^{Q}_{univ}, and zero-order system probabilities $\rho^{n,n}_{\mathcal{S}}$ that fluctuate about a Boltzmann distribution. The state $|\Psi^{eq}_{artificial}\rangle$ is then what we take as our starting equilibrated $\mathcal{SE}$ state. The subscript *"artificial"* is meant not to diminish the quality of this equilibrated state, but simply to indicate its origin. An example of the state $|\Psi^{eq}_{artificial}\rangle$ is shown in the top right of Fig. 3.3, where the probability contributions for the state are separated into three components for the three system levels $n = 0, 1, 2$.

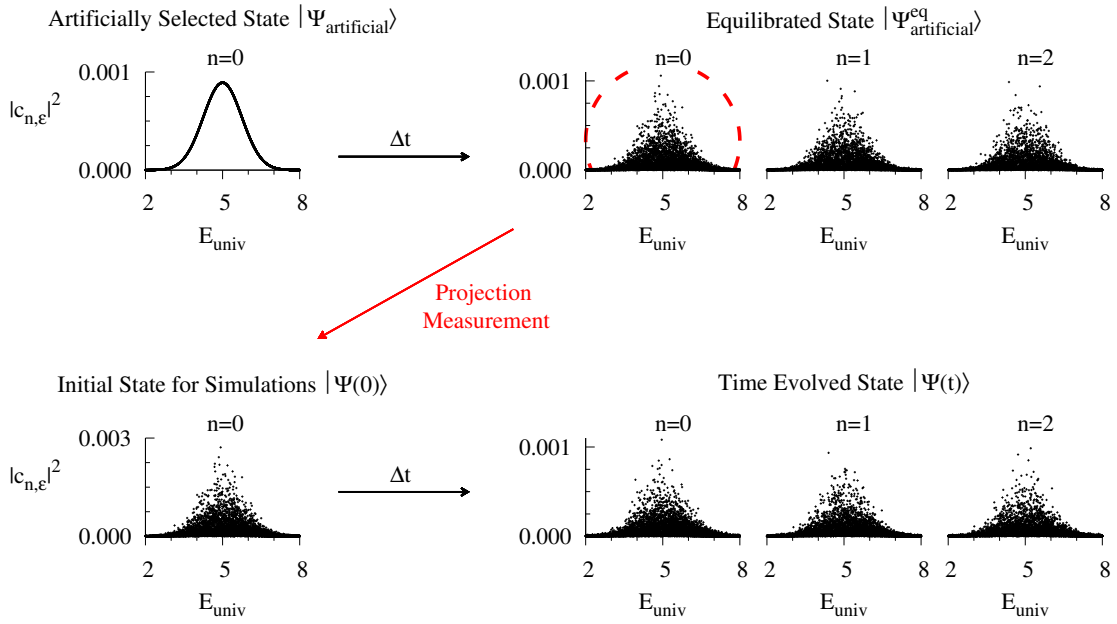

FIGURE 3.3. Schematic of the model measurement procedure used to generate the initial states $|\Psi(0)\rangle$ used in the computations. Details are in the text.

To mimic a measurement of the zero-order energy state of the system with a definite outcome, we then project the equilibrated state $|\Psi^{eq}_{artificial}(t)\rangle$ onto one of the system zero-order eigenstates $|n\rangle$ following Eq. 3.15, "collapsing the wave function" to get our initial state $|\Psi(0)\rangle$. In Fig. 3.3 an example of a projective measurement to the $n = 0$ level is shown. The projection takes the $n = 0$ component of the state $|\Psi^{eq}_{artificial}\rangle$, circled with a red dashed line; multiplies the state coefficients by a normalizing constant N; then uses this normalized state as the initial state for the simulations $|\Psi(0)\rangle$ as shown in the bottom left corner of Fig. 3.3.

The initial states $|\Psi(0)\rangle$ "synthesized" through this model of quantum measurement have qualitative properties that are suitable for studying quantum state thermalization. First, the majority of the state probability is concentrated in a small range around the central energy $E_{univ} = 5$, somewhat similar to a microcanonical

energy shell that contains all of the classical state probability. Thus, we might expect microcanonical-like thermodynamic behavior from the state. At the same time, the state also has decaying tails with some small probability at high and low energies, as expected for realistic quantum states with energy uncertainty. In sum, we believe that the state probabilities are distributed over different energies in a reasonable way. Second, the state has significant variations in probability between basis states, with the exact distribution being determined by dynamics within the $\mathcal{SE}$ universe leading up to the measurement. These variations would be expected in real states, as opposed for example to the highly ordered probability distribution of the artificial state. We conclude that the initial state $|\Psi(0)\rangle$ has reasonable properties for a quantum state that could be made in a lab and that might be expected to behave in a microcanonical-like way.

We will time evolve these states and present results in Section 3.6 on thermodynamic behavior of the system and of the entropy S^Q_{univ}. But first, we will recapitulate the theoretical foundation for S^Q_{univ} in Section 3.5.

3.5. Quantum entropy of the universe, free energy, and excess entropy production

In this Section, we briefly recapitulate the idea of the quantum entropy of the universe S^Q_{univ} developed in Ref. [1]. Then, we introduce the idea of excess entropy production beyond the microcanonical entropy, from comparison of the behavior of S^Q_{univ} to classical results for the behavior of the system free energy and microcanonical entropy.

The basic idea is to define a type of entropy for a pure quantum state that will increase suitably during spontaneous processes. This will necessarily be different

from the standard von Neumann entropy. In Ref. [1] we defined an entropy S^Q_{univ} and conventional system properties E_{sys}, S_{sys}, and free energy F_{sys} and computed their dynamical behavior for a model system-environment universe. In particular, we tested the behavior of these entities against the fundamental thermodynamic relation Eq. 3.2. Briefly, as developed in detail in Ref. [1], we define the quantum entropy S^Q_{univ} for a pure $\mathcal{SE}$ state as the standard Shannon entropy defined with respect to the zero-order energy basis $\{|\alpha\rangle\} = \{|s\rangle|\epsilon\rangle\}$ of the $\mathcal{SE}$ complex:

$$|\Psi_{\mathcal{SE}}(t)\rangle = \sum_\alpha c_\alpha(t)|\alpha\rangle. \tag{3.16}$$

Taking

$$p_\alpha(t) = |c_\alpha(t)|^2 \tag{3.17}$$

we define the "entropy of the universe" as

$$S^Q_{univ} = -\sum_\alpha p_\alpha \ln p_\alpha \tag{3.18}$$

Our procedure in the following is to calculate $-T\Delta S^Q_{univ}$, and compare this with a separate calculation of ΔF_{sys}. To the extent that these two quantities are equal, we will obtain a recovery of standard thermodynamics ideas and results. The general method gives ΔS_{sys} for various initial states as the change in the von Neumann entropy $\Delta S^{vN}_{\mathcal{S}} = -\Delta \mathrm{Tr}\hat{\rho}_{\mathcal{S}} \ln \hat{\rho}_{\mathcal{S}}$ calculated from the reduced density matrix of the system, and the temperature T. Accordingly, for the thermalization process, we calculate the free energy change

$$\Delta F_{sys} = \Delta\langle E_{\mathcal{S}}\rangle - T\Delta S^{vN}_{\mathcal{S}}. \tag{3.19}$$

The ΔF_{sys} thus defined takes its standard value, i.e. $F_{sys}(0) = E_n$ for an initial system level n and $F_{sys} = -kT \ln Z$ at equilibrium, since at equilibrium the system density operator is well described as small fluctuations about a dephased Boltzmann distribution $\hat{\rho}_{\mathcal{S}} = \exp(-\hat{H}_{\mathcal{S}}/T)/Z$. Thus, ΔF_{sys} is equivalent to the microcanonical entropy change expected classically in Eq. 3.2, and is used as a measure of classical behavior for the new entropy S^{Q}_{univ}.

Entropies with varying similarity to Eq. 3.18 have been considered in different contexts by von Neumann [9, 10] and recently by Han and Wu [30] in connection with a "quantum H-theorem"; and also by Kak [31] and Stotland et al. [46] in the context of quantum information theory. Closest to our approach are Refs. [30, 31]; note should also be made of the work of Esposito et al. [28] and Reeb and Wolf [32] on irreversible entropy production by a system in a heat bath. The definition of S^{Q}_{univ} in Eq. 3.18 is proposed in a frankly empirical spirit, with its justification and validity meant to be judged by its fruitfulness in describing physical phenomena. This seems to be in keeping with the historical line of development of the idea of entropy in thermodynamics, and later in statistical mechanics.

In Ref. [1] we tested ΔS^{Q}_{univ} against the equality Eq. 3.2 by computing the relevant system property ΔF_{sys} using the reduced density operator of the system. We found that the two sides of Eq. 3.2 were nearly, but not exactly equal in the simulations. The computation of ΔF_{sys} gave results generally in accord with the microcanonical expectation Eq. 3.2. However, the computed ΔS_{univ} was slightly greater than what would be expected from the microcanonical ensemble—there was *excess entropy production*. In this paper, in accord with the discussion following Eq. 3.19, this will be defined as

$$\Delta S^x \equiv \Delta S^Q_{univ} + \frac{1}{T}\,\Delta F_{sys} \tag{3.20}$$

keeping in mind that it is expected that $\Delta F_{sys} < 0$. Then excess entropy production corresponds to the observation that

$$\Delta S^Q_{univ} > -\frac{1}{T}\Delta F_{sys} \tag{3.21}$$

The excess entropy production can then be entirely ascribed to the environment, as follows. The entropy change ΔS^Q_{univ} can be decomposed according to the discussion of Nielsen and Chuang [51], such that on average the fluctuating ΔS^Q_{univ} is equal to the system von Neumann entropy change ΔS^{vN}_{sys} plus a suitably defined environment entropy change contribution ΔS_{env}. Putting this into Eq. 3.20 and using the inequality from Eq. 3.21 gives

$$\Delta S^x = \Delta S_{env} + \frac{\Delta\langle E_S\rangle}{T} > 0. \tag{3.22}$$

The entropy change of the environment is then greater than the amount predicted by heat flow, $\Delta S_{env} > -\Delta\langle E_S\rangle/T$, and this environment contribution is the entire source of the excess entropy production. The excess entropy production was ascribed in Ref. [1] to energy uncertainty in the time-dependent state of the evolving system-environment entangled universe state. We will have occasion here to sharpen this perspective considerably in Section 3.6. For now, it is enough to say that in the microcanonical limit, ΔS^Q_{univ} gives the classical result $-\frac{1}{T}\Delta F_{sys} = \Delta S_{univ}$ with excess entropy production zero, while the interesting deviations $\Delta S^x > 0$ related to energy uncertainty are observed outside of this limit.

3.6. Results

In this section we evaluate the quantitative results of our simulations with respect to obtaining proper thermalization, and then evaluate the central results on behavior of the entropy production ΔS^Q_{univ} with respect to the free energy of the system, microcanonical behavior, and excess entropy production.

3.6.1. Boltzmann thermal equilibration in the thermal basis set.

In Section 3.3 we discussed the necessity to define the "thermal basis set" to get proper Boltzmann thermal equilibration. Here we describe our actual computational success with the thermal basis in finding good numerical agreement between the equilibrium system distribution and the Boltzmann distribution expected at our designed temperature T. Fig. 3.4 shows three-level and eight-level systems as examples of the system equilibrium behavior. For reasons of computational tractability, we later use primarily the two and three level systems in the results described later in Section 3.6.2, but here also show the eight level system that extends to higher energies in order to verify the expected curvature of the Boltzmann distribution.

For the eight level system with energy range $0 \leq E_{sys} \leq 7$, we expanded the environment energy range to $-7 \leq E_{env} \leq 10$. This gives a tensor product basis with $-7 \leq E_{univ} \leq 17$ which we then truncate above and below (following Eq. 3.14) to a thermal basis set of states in the energy range $0 \leq E_{univ} \leq 10$. The resulting thermal basis covers the same total universe energy range as in Fig. 3.2 but has eight total system levels instead of three. Using the thermal basis, both the eight and three level

systems have equilibrium probability distributions $\rho_{\mathcal{S}}^{n,n}$ in Fig. 3.4 that are very close to the expected Boltzmann distribution, indicating good thermalization.

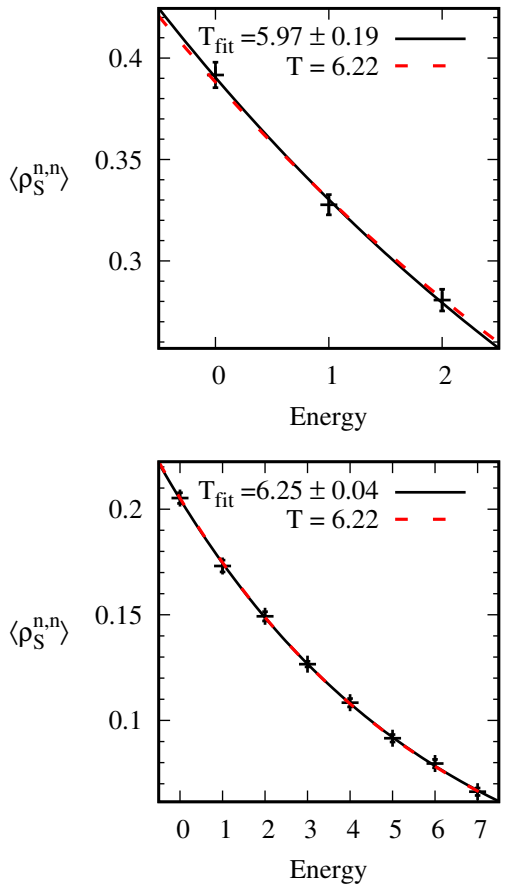

FIGURE 3.4. Mean system probabilities $\rho_{\mathcal{S}}^{n,n}$ at equilibrium are well fit by a Boltzmann distribution with T_{fit} approximately the designed temperature $T = 6.22$ energy units. (See Section 3.2.2.) The reported error in T_{fit} is the asymptotic standard error of the nonlinear least squares fit.

We now describe how we found the probabilities of Fig. 3.4 numerically. Since even at equilibrium the system undergoes significant fluctuations over time in a finite model of both system and bath, we time average the diagonal elements of the reduced density operator $\rho_{\mathcal{S}}^{n,n}(t)$ in Eq. 3.13 to determine a mean equilibrium distribution $\langle \rho_{\mathcal{S}}^{n,n} \rangle$ and then fit with a normalized exponential distribution $\langle \rho_{\mathcal{S}}^{n,n} \rangle \sim$

$\exp(-E_n/k_B T_{fit})$ to determine a best fit temperature. The system reduced density operator was averaged over 100 time steps at equilibrium that were spread over a time range significantly longer than the system relaxation time in order to average out short-lived fluctuations at equilibrium.

The time averaged system-level probabilities $\langle \rho_S^{n,n} \rangle$ were always within one standard deviation from the expected Boltzmann probability at the designed temperature T, consistent with the idea of the system fluctuating about the Boltzmann distribution at equilibrium. However, despite this success we have noticed that there usually appears to be a very small remnant of the initial system state in the final equilibrium distribution, in that its average probability (not including the standard deviation) is often $\sim 10^{-3}$ higher than expected. For example, this can be seen in the top panel of Fig. 3.4, where the initial state $n = 0$ probability is slightly above the red, dotted Boltzmann curve at the designed temperature $T = 6.22$. This very small effect appears to be due to the finite size of our model and can be minimized by increasing the number of states in the calculation at the cost of additional computational resources. Overall we found good fitted temperatures for the three level system calculations reported here, with T_{fit} good to within 5% of the analytical temperature in 9 out of 10 time windows we examined. For the two-level system, the T_{fit} were good to within 11% of T in 7 out of 8 time windows, with the inferior agreement reflecting the extreme sensitivity of T_{fit} to the level probabilities when there are only two system levels. Even so, the average system probabilities were always within one standard deviation from the expected Boltzmann probability, consistent with expected Boltzmann behavior. We conclude that the model universe with the thermal basis set is giving good thermalization behavior. This is certainly reflected in the visual appearance of the figures.

3.6.2. Free energy, excess entropy production, and microcanonical behavior.

3.6.2.1. Free energy and excess entropy production

Having established that thermalization is obtained with the thermal basis set, we test the fundamental relation $-\Delta F_{sys}/T = \Delta S_{univ}$ of Eq. 3.2, now with the quantum entropy ΔS^{Q}_{univ} on the right hand side. The top panel of Fig. 3.5 shows ΔF_{sys} and ΔS^{Q}_{univ} for each initial state n of a three level system that is strongly coupled with a small environment (size and coupling are specified in the figure). The changes in entropy are significantly larger than the changes in free energy, with the difference indicating excess entropy production $\Delta S^{x} > 0$ as defined in Eq. 3.20. For every initial state we have tested in which the system thermalized to a canonical distribution at equilibrium, there is some excess entropy production $\Delta S^{x} > 0$. This evidently stands somewhat at odds with the standard relation Eq. 3.2 for macroscopic systems in the microcanonical ensemble. The phenomenon of excess entropy production is understandable in a small quantum system, for reasons that we will discuss briefly below. But it raises the question of whether a microcanonical limit holds in the quantum thermodynamic modeling, and how such a limit is approached in a real system. We therefore investigate numerically the existence of this microcanonical limit, when finite quantum effects become negligible. If the quantum S^{Q}_{univ} is found to agree in this limit, then excess quantum entropy production may be seen as both a new aspect of thermodynamics at the finite, quantum scale, as well as intelligible departure from classical microcanonical behavior.

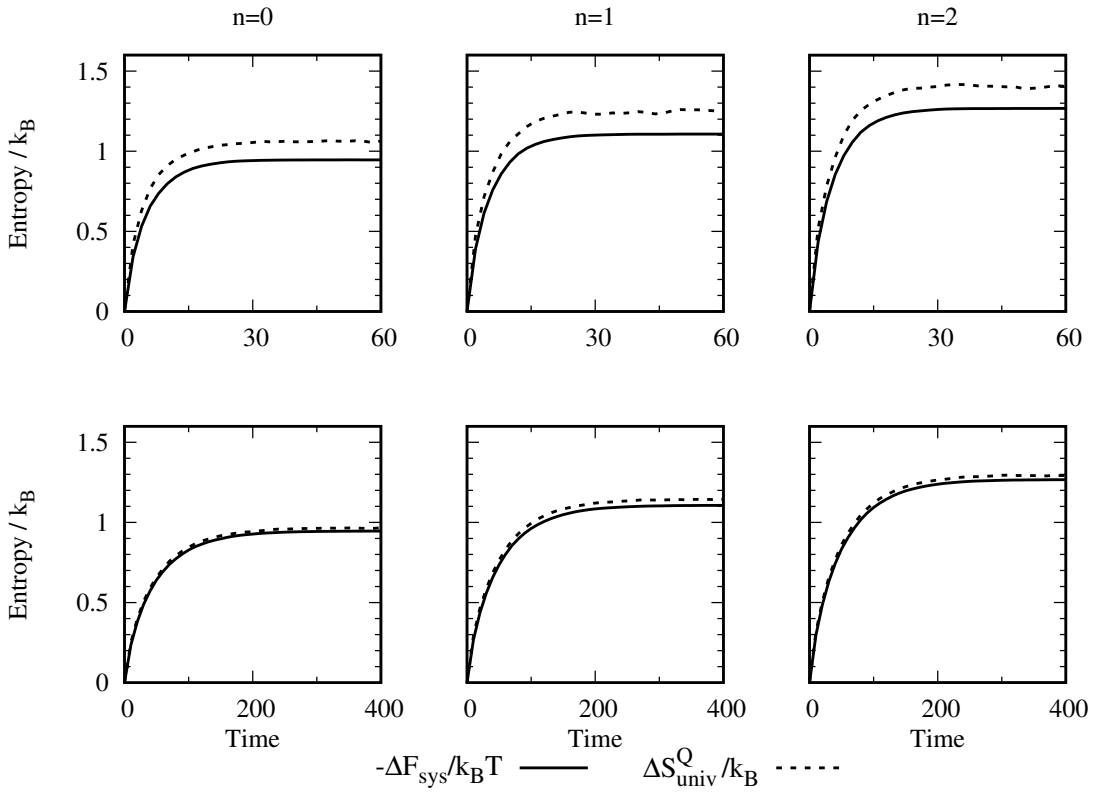

FIGURE 3.5. Top row : Strong $\mathcal{SE}$ coupling $k = 3.6 \times 10^{-3}$ to a small $W_{env} = 9\ 390$ environment generates significant excess entropy production $\Delta S^Q_{univ} > -\Delta F_{sys}/T$ for all initial states n of a three level system. Bottom row: The coupling k and number of states W_{env} have been decreased and increased respectively by a factor of nine, greatly reducing ΔS^x as the calculations head toward the macroscopic limit $\rho \to \infty, k \to 0$.

3.6.2.2. Approach to microcanonical behavior

Standard thermodynamics generally assumes an infinitely large environment and small or negligible system-environment interaction, which in our model corresponds to the limit $\rho \to \infty, k \to 0$, where ρ is the number of universe states per unit energy. Here we ask whether the standard thermodynamic relation Eq. 3.2 between entropy and free energy will hold in this limit. In the bottom row of Fig. 3.5 we show the behavior of ΔS^x with a significantly increased ρ and decreased k relative to the top row. We find a much smaller ΔS^x, i.e. a ΔS^Q_{univ} that is much closer to the microcanonical entropy change.

To more thoroughly investigate the macroscopic limit $\rho \to \infty, k \to 0$, we show the behavior of ΔS^x in Fig. 3.6 for two sets of calculations as the macroscopic limit $\rho \to \infty, k \to 0$ is approached. In each set of calculations we fix the product $k\rho = const.$ because numerically we find that this allows us to approach the desired limit while maintaining a canonical thermal distribution in the system density operator $\hat{\rho}_{\mathcal{S}}$ at equilibrium. In the figure each of the $\langle \Delta S^x \rangle$ is averaged over 22-100 different projected initial states to account for variations in the initial environment state, with each state averaged over 20-50 time steps at equilibrium to account for time-dependent fluctuations (fewer initial states and time steps were used in the averages for the largest universes to minimize computational time, however these also show the smallest error bars towards the lower left of the figure, indicating that they don't vary much.) The numerical data points in the plot are suggestive of approach to the microcanonical limit, but not conclusive, given the lack of data near the origin. We therefore adopt the strategy of fitting the results with an empirical curve, chosen to have a conceptual connection to excess entropy production, the better to probe the $k \to 0, \rho \to \infty$ limit. We will first give the form for this empirical curve, and note

its excellent performance; then discuss the physical grounds for adopting this curve; and finally discuss the implications for the idea of the microcanonical ensemble.

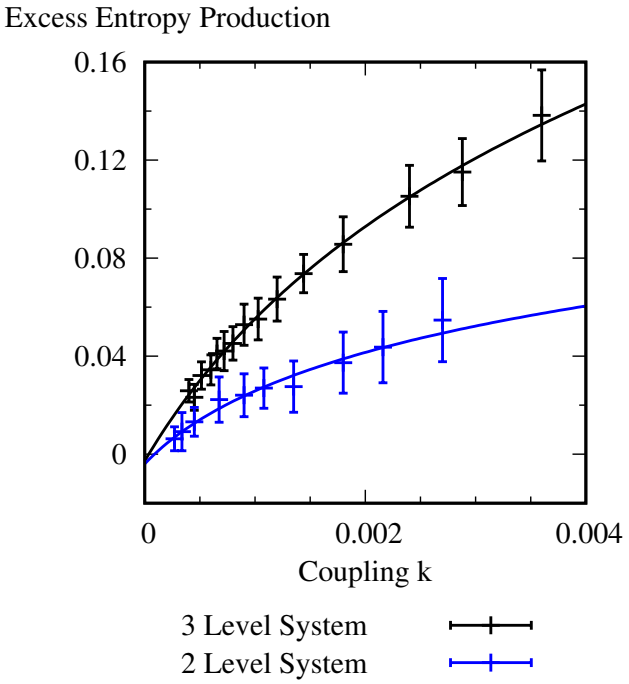

FIGURE 3.6. Excess entropy production $\langle \Delta S^x / k_B \rangle$ varying k with a fixed product $k\rho$, at equilibrium, averaged over different initial states and time steps to smooth fluctuations, details in the text. Extrapolating the fitting function Eq. 3.24 to the macroscopic limit $k \to 0, \rho \to \infty$ gives the classical result $\langle \Delta S^x \rangle = 0$ to within the asymptotic standard error of the fit parameter c, see Table 3.1.

The empirical formula has three fitting parameters a, b, c:

$$\Delta S^x / k_B \approx a \ln (1 + k/b) + c. \tag{3.23}$$

The log function gives the overall form of the curve, and goes to zero (as the data should) in the supposed microcanonical limit where the scaled coupling strength $k/b \to 0$. The parameter a is an overall empirical scale factor for the curve. The parameter c gives any residual deviation from microcanonical behavior in the limit of

	a	b	c
3 Level System	$(1.1 \pm 0.2) \times 10^{-1}$	$(1.4 \pm 0.5) \times 10^{-3}$	$(-3 \pm 4) \times 10^{-3}$
2 Level System	$(3 \pm 1) \times 10^{-2}$	$(7 \pm 5) \times 10^{-4}$	$(-4 \pm 4) \times 10^{-3}$

TABLE 3.1. Non-linear least squares fit parameters and asymptotic standard errors for the empirical excess entropy production curves of the two model systems in Fig. 3.6. The y-intercept parameter c is zero to within one standard error, indicating that extrapolating the fit to the macroscopic limit $k \to 0, \rho \to \infty$ gives the standard microcanonical result $\Delta S^x = 0$.

zero coupling $k \to 0$. The meaning and justification of the empirical formula (3.24) will be considered further below. We here note that this simple relation gives a very good fit to the numerical results in Fig. 3.6. The fit parameters a, b, c and other results concerning the fit are shown in Table 3.1. The parameter c determines the best fit estimate of ΔS^x in the macroscopic limit $k \to 0, \rho \to \infty$, and as seen in Table 3.1 it is zero to within the error of the fit. This indicates that empirically the best fit curve indeed shows approach to a numerical microcanonical limit where $\Delta S^Q_{univ} = -\Delta F_{sys}/T$, with no excess entropy production.

The black fitting curve for the three level system in Fig. 3.6 is suggestive of what may happen in the limit $k \to 0$, but due to the computational demands of diagonalizing the Hamiltonian for an increasing number of states as ρ increases, our calculations remain fairly far from the $k \to 0, \rho \to \infty$ limit. We therefore would like to be able to show that the same curve holds at smaller k in calculations we can complete with a smaller system (and correspondingly larger ρ and hence environment size). Fig. 3.6 shows in blue a series of calculations using a two level system, with fixed $k\rho = const.$ as before. The simulation results are well fit by a function of the same form throughout the region of smaller k accessible in these calculations, again with an intercept parameter $c = 0$ to within the error of the fit. In sum, both lines of computational evidence support the idea that the empirical formula of Eq. 3.24

approaches the desired microcanonical behavior Eq. 3.2 in the limit of small k, large ρ.

3.7. The empirical formula and sources of excess entropy production

Having established the success of the simulation data and the analysis with the fitting curve Eq. 3.24 in achieving the hoped-for microcanonical limit, we turn to a consideration of where the empirical curve comes from and why it is reasonable. Excess entropy production can be understood as resulting from two significant differences that arise in considering the evolution of time-dependent quantum states and the assumptions of the classical microcanonical ensemble: (1) the absence of a strict quantum microcanonical energy shell, with the presence of quantum mechanical spreading of the time-dependent state; and (2) non-microcanonical variations in probability among states in the quantum probability distribution. We consider these differences and their effect on the quantum entropy in turn. The first consideration will give rise to the parameter $1/b$ that determines the shape of the log function in the fitting curve; the second to the parameter a that acts as a scale factor. Then c reflects any residual deviation from microcanonical behavior in the empirical fit.

First, the classical microcanonical ensemble is based on a fixed energy shell $[E, E + \delta E]$ containing a total number of states $W = \rho\delta E$, where ρ is the density of states. The entropy change is independent of the energy width δE since the latter is fixed in $\Delta S_{univ} = k_B \ln W_{eq}/W_0 = k_B \ln \rho_{eq}/\rho_0$. On the other hand, a time-dependent quantum state can spread out across basis states of varying energy due to interactions among non-resonant zero-order energy levels. In our calculations the $\mathcal{SE}$ interaction causes the environment to access off-resonant levels in the dynamics, similar to how an atom in a definite excited state will emit photons with a variable-

energy Lorentzian lineshape into the environment. The quantum state can be thought of as having an "effective energy width" δE_{eff} that can change, generally increasing during the equilibration process. This spreading in the energy width is for practical purposes irreversible in our model, since recurrences in the dynamics happen only on extremely long timescales. As a simple model for this effect, we suppose the effective energy shell width to increase in proportion to the system-environment coupling k, $\delta E_{eq} = \delta E_0(1 + k/b)$, where b is an unknown parameter. This effect by itself entails excess entropy production $\Delta S^x \sim \ln(1 + k/b)$ beyond the microcanonical value, accounting for part of the form of the empirical formula.

A second consideration is crucial as well, and gives rise to the scale factor a, which empirically is much less than 1.0 in the fit. The microcanonical ensemble assumes equal probabilities $p_\alpha = 1/W$ for all states in the ensemble, which is essential in going strictly from an entropy in terms of the probabilities of the microscopic states to Boltzmann's relation of proportionality $\sim \ln W$. On the other hand, the quantum spreading to basis states outside the initial energy interval results in probabilities that are much less than those within the bulk of the distribution. This is seen clearly in the projected initial state in Fig. 3.3, where the rapidly decaying tails of the distribution have much lower probability than states near the center of the distribution. As this initial projected state evolves in time, the tails spread and grow a bit as some probability shifts away from the bulk of the distribution at $E \sim 5$ to higher and lower E for the equilibrium time evolved state in Fig. 3.3, increasing the effective width of the quantum energy shell and generating excess entropy production. But since the probabilities associated with the spreading are smaller than those in the bulk of the distribution, their entropy contribution will be smaller as well. This can be modeled

through the inclusion of the additional prefactor $a \ll 1$ that reflects the discounted excess entropy production from these states, so that $\Delta S^x \sim a \ln(1 + k/b)$.

Finally, as indicated above, the additive constant c reflects any residual deviation of the excess entropy production from zero in the supposed microcanonical limit, so that our complete empirical formula is

$$\Delta S^x / k_B \approx a \ln (1 + k/b) + c. \tag{3.24}$$

3.8. Discussion and conclusions

In Ref. [1] we began to explore a quantum "entropy of the universe" S^Q_{univ} of a pure system-environment quantum state, devised to extend the classical statement of the second law $\Delta S_{univ} \geq 0$ to quantum entangled systems. The theoretical rationale for S^Q_{univ} was carefully developed in Ref. [1], and approximate agreement with the standard classical thermodynamic relation of Eq. 3.2 was obtained, but the procedure there was limited by severe assumptions about the temperature bath and system state preparation. In the present paper, we have developed innovations that make for a much more realistic model. We have used these refinements to investigate in systematic computations the idea of microcanonical behavior in the quantum system, and point the way to future developments beyond the microcanonical paradigm.

Specifically, we have introduced three innovations. First, in Ref. [1] the environment temperature bath consisted of states with harmonic spacing equal to those of a likewise harmonic system of levels. Thus, the bath of Ref. [1] did not resemble a near-continuous spectrum of a realistic bath, nor was the whole approach capable of dealing with anything other than a harmonic system, obviously a severe limitation. In the present work, we have devised a discrete level approach to a model

for a near-continuous bath, eliminating the previous limitations. Second, we have amended the system-environment basis set to a "thermal basis" from the obvious choice of the tensor product basis. The motivation for this was the finding that the tensor product basis has trouble achieving thermal equilibrium in the simulations, for reasons closely connected to the structure of that basis. Truncating the tensor product basis in a rational way to give the "thermal basis" gives far superior results for thermalization. In addition, since the thermal basis is a truncation of the tensor product basis, it also sets a path to a much more efficient basis for larger quantum thermodynamic systems. Third, we have devised a more realistic initial state than that of Ref. [1]. We have done this by modeling a process of measurement of a given system-environment state, which then serves as the starting point for the numerical simulation of the approach to equilibrium.

Within this formal and computational setting, we have shown that when a system-environment pure state $|\Psi_{\mathcal{SE}}\rangle$ evolves to give a thermal distribution, it is possible to get behavior of S^Q_{univ} in agreement with its classical free energy correspondent according to the equation $\Delta F_{sys} = -T\Delta S^Q_{univ}$ in the microcanonical limit, involving both the system-environment coupling and the environment density of states. On the other hand, away from that limit, there is excess entropy production, a phenomenon that may be of future interest in the quantum thermodynamics of small systems away from the classical limit. The excess entropy production fits an empirical formula with a basis in time-energy uncertainty, with unequal spreading among basis states, especially outside the energy shell.

In summary, the present paper builds on the earlier Ref. [1], which proposed a new quantum entropy S^Q_{univ} of a system-environment universe. Here, we introduced developments of the basic idea of Ref. [1] that give a much more careful assessment

of the question of quantum microcanonicality, including the entropy-free energy relationship of Eq. 3.2. Our work is in concordance with and extends the line of work on evolution of quantum pure states to a condition of thermal equilibrium. One feature brought out here is the phenomenon of excess entropy production away from the microcanonical limit. This could be an interesting phenomenon in future exploration of quantum thermalization. On the other hand, the entropy S^Q_{univ} might be of even more interest when there is non-thermalizing behavior in far-from equilibrium systems.

3.9. Connection to later work

This chapter has demonstrated that S^Q_{univ} can serve as a quantum generalization of the classical entropy S_{univ} in the second law, since S^Q_{univ} follows the standard thermodynamic microcanonical result $\Delta S^Q_{univ} = -\Delta F_{sys}/T$ with a realistic model of a system-environment quantum pure state $|\Psi_{\mathcal{SE}}\rangle$. To obtain this result, it was necessary to take the model to a type of classical "microcanonical" or "macroscopic" limit of a large bath and weak coupling, where standard thermodynamic behavior prevails. "Excess entropy production" ΔS^x was observed outside of this limit, with $S^Q_{univ} > -\Delta F_{sys}/T$, but this was left largely unexplored apart from an empirical fit curve analysis. From this analysis it is unclear how to analytically formulate ΔS^x and whether it is related to novel types of quantum thermodynamic effects. The remainder of this dissertation will be focused largely on addressing these questions. The next chapter will give a much more systematic account of excess entropy production, corroborating and extending the ideas of this chapter to analyze situations of extreme ΔS^x and give an analytical account of the behavior for a specific class of states. The

remaining chapters will then develop a model to look for new types of quantum thermodynamic behavior, with ΔS^x playing a critical role.

CHAPTER IV

SYSTEMATIC ANALYSIS OF EXCESS ENTROPY PRODUCTION

This chapter includes previously unpublished material co-authored by Michael E. Kellman [3]. Michael Kellman and I both contributed to developing the model and theory, analyzing the results, and writing the manuscript. I performed the computations.

4.1. Introduction

Recent years have seen a renewal of interest in the foundations of quantum statistical mechanics, for both theoretical reasons and practical interests in new technologies. A prominent line of research has investigated thermodynamic behavior in pure state systems. Arguments based on the "eigenstate thermalization hypothesis" [20] and "typicality" [12] in entangled systems stake a persuasive claim that thermalization is a property of entanglement in pure states of complex systems. Nonetheless, we have called attention to an apparent gap in the quantum thermodynamics of pure states. The classical second law states that the "entropy of the universe" is always increasing

$$\Delta S_{univ} > 0 \tag{4.1}$$

and that the following relation between free energy and entropy change holds:

$$-\frac{1}{T}\,\Delta F_{sys} = \Delta S_{univ}. \tag{4.2}$$

However, these relations seem to be missing in quantum thermodynamics of a pure state, because the standard von Neumann quantum entropy is zero for such a state. In Chapter III and Ref. [2] we defined a S_{univ} for a pure system-environment ($\mathcal{SE}$) state, compared with ΔF_{sys}, and found that we could recover the microcanonical limit Eq. 4.2 for equilibration and thermalization. This followed an earlier presentation [1] of similar ideas which involved a heat bath with less realistic features. Others have introduced somewhat related definitions of the entropy of a pure state, both for analyzing pure state thermodynamics [10, 29, 30] and characterizing the information content of pure states [31, 46]. Cosmologists and black hole physicists speak of a "thermodynamic entropy" of a quantum system that is different from the standard entanglement or von Neumann entropy.

Our S_{univ} is a realization of a quantum thermodynamic entropy explicitly suited for a system-environment or $\mathcal{SE}$ total system or "universe." The focus in this chapter is *excess entropy production*, i.e. thermodynamic entropy ΔS^x beyond what is implied in the classical relation (4.2). This is a quantum phenomenon that was noted in Chapter III and Refs. [1, 2], in the course of exploring the attainment of the classical microcanonical limit in which Eq. 4.2 holds. In the present chapter, the goal is a deeper systematic account of the excess entropy production. A unified understanding is obtained of the quantitative behavior of ΔS^x between extreme limits of zero (i.e. classical) and maximal, massive excess entropy. We anticipate that this understanding will be useful for analysis of highly unusual, nonclassical situations in quantum thermodynamics of complex systems.

4.2. Basis set and quantum thermodynamic entropy

We consider the formal definition of the quantum entropy of the pure state and consider its rationale. The definition of S^Q will depend on a choice of basis set. Our choice is the zero-order (ZO) $\mathcal{SE}$ energy basis. In this and the following sections we argue that this choice, and only this choice, will allow recovery of classical microcanonical results, including the Boltzmann distribution, the canonical ensemble, the identity in Eq. 4.2 in the limit of weak coupling, and the standard microcanonical relation $\Delta S_{env} = Q/T$ between entropy change of the environment and heat flow.

To define the entropy we need to choose a "reference basis" $\{|\alpha\rangle\}$. In this basis a pure state is expressed as

$$|\Psi_{\mathcal{SE}}(t)\rangle = \sum_{\alpha} c_\alpha(t)|\alpha\rangle. \tag{4.3}$$

Then taking

$$p_\alpha(t) = |c_\alpha(t)|^2 \tag{4.4}$$

we define the quantum entropy

$$S^Q_{univ} = S^{\{\alpha\}}_{univ} = -\sum_{\alpha} p_\alpha \ln p_\alpha \tag{4.5}$$

with respect to the reference basis $\{|\alpha\rangle\}$. This expression for the entropy has an evident relation to the Shannon information entropy. In the quantum context it has been discussed as the "conditional information entropy" by Stotland et al. [46].

This entropy depends on the choice of reference basis. We choose the zero-order energy basis

$$\{|\alpha\rangle\} = \{|s\rangle|\epsilon\rangle\} \tag{4.6}$$

of the $\mathcal{SE}$ complex. Let the state of the universe be expanded in terms of the zero-order system-environment bases $\{|s\rangle\}$ and $\{|\epsilon\rangle\}$:

$$|\Psi\rangle = \sum_{s,\epsilon} c_{s,\epsilon}|s\rangle|\epsilon\rangle \tag{4.7}$$

with $\{|s\rangle\}$ and $\{|\epsilon\rangle\}$ the ZO basis sets of system and environment. Eqs. 4.3-4.7 comprise the essence of our quantum entropy.

What is the rationale for this? We will be simulating a quantum total system $\mathcal{SE}$ in which energy flows between a system $\mathcal{S}$ and an environment $\mathcal{E}$—a process of heat flow. In statistical mechanics we typically have in mind the measurement of an $\mathcal{S}$ energy level, e.g. the energy of a Brownian particle in a gravitational field. This justifies the choice of the zero-order system basis. Then, if we are concerned with thermalizing energy flow, the most natural further observation would be of the zero-order energy of $\mathcal{E}$ to give a total zero order energy of $\mathcal{SE}$. This naturally leads to the basis of ZO energy states $\{|\alpha\rangle\} = \{|s\rangle|\epsilon\rangle\}$. However, we might not be so interested in measuring the $\mathcal{E}$ energy—that would be the usual case in the analogy to the Brownian particle. There are further grounds to favor the $\mathcal{SE}$ ZO basis. We are naturally interested in constructs that relate to the microcanonical ensemble for a fixed total energy. Since we are interested in observing the $\mathcal{S}$ zero-order energy, the only way of getting a total energy would then seem to be as the sum $E = E_{\mathcal{S}} + E_{\mathcal{E}}$, i.e. the sum of zero order energies. Having singled out the $\mathcal{S}$ states and the energy sum E, the obvious basis is then the ZO $\mathcal{SE}$ basis. This justification seems compelling,

but we will introduce further arguments based on the idea of a division of the entropy S^Q into system and environment components, to which we turn next.

4.3. S^Q_{univ} as a sum of system and environment terms

In this section we show how the quantum entropy can be divided into a sum of system and environment components. The system component comes from the reduced density matrix; the environment component is an averaged sum of contributions, weighted by system probabilities. We begin with the general expression for the Shannon entropy of a bipartite system

$$S = -\sum_{i,\lambda} p_{i,\lambda} \ln p_{i,\lambda}. \tag{4.8}$$

We will split this into separate parts for i and λ, following Neilson and Chuang [51]. To begin, define the total probability for i as

$$p_i = \sum_{\lambda} p_{i,\lambda}. \tag{4.9}$$

Define the conditional probability for λ when the first index is i as

$$p_{\lambda|i} = \frac{p_{i,\lambda}}{p_i}. \tag{4.10}$$

Using the newly defined probabilities and the normalization $\sum_\lambda p_{\lambda|i} = 1$ the entropy becomes [51]

$$S = -\sum_{i,\lambda} p_i p_{\lambda|i} \ln p_i p_{\lambda|i} = -\sum_i p_i \ln p_i + \sum_i p_i \left(-\sum_\lambda p_{\lambda|i} \ln p_{\lambda|i} \right)$$

$$= S_i + \langle S_\lambda \rangle_{\{i\}}. \tag{4.11}$$

Eq. 4.11 gives the general decomposition of the Shannon entropy of a bipartite system into separate parts for the two systems. The entropy S_i is a standard Shannon entropy for the first system. The second system has a conditional entropy $\langle S_\lambda \rangle_{\{i\}}$ that is averaged with respect to the probabilities p_i for the first system.

Now consider the quantum entropy Eq. 4.5 with $\{|\alpha\rangle\} = \{|s\rangle|\epsilon\rangle\}$ as the reference basis of system-environment zero-order states and $p_\alpha = p_{s,\epsilon} = |c_{s,\epsilon}|^2$. The entropy can be separated into system and environment parts, in parallel with Eq. 4.11

$$S^Q_{univ} = S^Q_{sys} + \langle S^Q_{env} \rangle_{\{s\}}. \tag{4.12}$$

The system entropy

$$S^Q_{sys} = -\sum_s p_s \ln p_s \tag{4.13}$$

uses system probabilities that can be calculated from the reduced density matrix with diagonal elements $p_s = \sum_\epsilon p_{s,\epsilon} = \langle s|\hat{\rho}_{\mathcal{S}}|s\rangle$. S^Q_{sys} agrees with the standard quantum von Neumann entropy of the system when $\hat{\rho}_{\mathcal{S}}$ is dephased in the system zero-order energy basis $\{|s\rangle\}$, as in the Boltzmann thermal state and our initial states. The environment entropy is then

$$\langle S^Q_{env} \rangle_{\{s\}} = \sum_s p_s \left(-\sum_\epsilon p_{\epsilon|s} \ln p_{\epsilon|s} \right). \tag{4.14}$$

with $p_{\epsilon|s} = p_{s,\epsilon}/p_s$. The subscript $\{s\}$ in Eq. 4.14 denotes that the system probabilities p_s are calculated in the $\{|s\rangle\}$ basis in defining the conditional entropy $\langle S^Q_{env} \rangle_{\{s\}}$.

Eqs. 4.12-4.14 give our method for calculating the total entropy S^Q_{univ} in terms of system S^Q_{sys} and environment $\langle S^Q_{env}\rangle_{\{s\}}$ parts that is used throughout this paper.

4.4. Excess entropy production in the environment

We have shown how to decompose the total entropy change ΔS^Q_{univ} into separate parts ΔS^Q_{sys} and $\Delta\langle S^Q_{env}\rangle_{\{s\}}$ for the system and environment. Now we give a heuristic argument for how to relate these to their classical microcanonical counterparts ΔS^{micro}_{sys} and $\Delta\langle S^{micro}_{env}\rangle_{sys}$. We will find that excess entropy production is a component of the environment entropy change beyond the classical Q/T. We will find later in Section 4.6 that this correlates to analytical results with the Lorentzian superposition states in our numerical simulations.

First consider the classical entropy change during system-environment thermalization. The system and environment begin in isolation, corresponding to a microcanonical ensemble of $W_0 = \rho_0 \delta E$ states with entropy $S^{micro}_{univ,0} = \ln W_0$, where ρ_0 is the initial density of states and δE is the width of the microcanonical energy shell. The system and environment then exchange heat, evolving to fill a larger set of $W_f = \rho_f \delta E$ states. The microcanonical entropy change is

$$\ln \frac{\rho_f}{\rho_0} = \Delta S^{micro}_{univ} = \Delta S^{micro}_{sys} + \Delta\langle S^{micro}_{env}\rangle_{sys} \tag{4.15}$$

where the last equality uses Eq. 4.11. The environment entropy change in Eq. 4.15 is given by the standard relation between the heat Q and temperature T,

$$\Delta\langle S^{micro}_{env}\rangle_{sys} = Q/T, \tag{4.16}$$

as shown in detail in Appendix A. We now show how these quantities can be related to their quantum counterparts.

As anticipated in our previous work [2], and developed analytically for time-dependent states in Section 4.6, the quantum entropy change can be analyzed in terms of a microcanonical-like relation

$$S^Q_{univ} \sim \ln W_{\rm eff} \tag{4.17}$$

with an effective number of states $W_{\rm eff} = \rho\delta E$, and a variable effective energy width δE (we will have a bit more to say about the relation to Ref. [2] in Section 4.6.2). The width generally increases because of quantum state spreading during the dynamical equilibration process. This results in a greater width for the final equilibrium state than the initial state $\delta E_f > \delta E_0$. Then the total entropy change is

$$\Delta S^Q_{univ} \approx \ln \frac{\rho_f}{\rho_0} + \ln \frac{\delta E_f}{\delta E_0} \tag{4.18}$$

The term $\ln \rho_f/\rho_0$ is the classical system-environment entropy change from Eq. 4.15. The second term is the excess entropy production due to the quantum spreading of the energy shell:

$$\Delta S^x = \ln \frac{\delta E_f}{\delta E_0}. \tag{4.19}$$

We now use this system-environment decomposition of the entropy Eq. 4.12 to show that ΔS^x is contained entirely within the environment. Note that the quantum and classical entropy changes of the system are the same $\Delta S^Q_{sys} = \Delta S^{micro}_{sys}$ since in both cases the system thermalizes to a Boltzmann distribution. Then expressing

ΔS^Q_{univ} on the left of Eq. 4.18 in terms of system and environment parts we have that the quantum entropy change of the environment is

$$\Delta\langle S^Q_{env}\rangle_{\{s\}} \approx \Delta\langle S^{micro}_{env}\rangle_{sys} + \ln\frac{\delta E_f}{\delta E_0} = \frac{Q}{T} + \Delta S^x \tag{4.20}$$

with the approximation indicated because this is a heuristic argument, in keeping with Eq. 4.18. The quantum entropy change of the environment is thus generally greater than the classical Q/T, with excess entropy production related to the increase in the width of the quantum energy shell.

With this analysis at hand, we return to the question of the justification for the $\mathcal{SE}$ ZO reference basis in defining S^Q_{univ} in Eqs. 4.3-4.6 of Section 4.2. Our decomposition of S^Q_{univ} into system and environment parts gives standard results in the classical limit for a fixed microcanonical shell: $\Delta S^Q_{sys} = \Delta S^{micro}_{sys}$ and $\Delta\langle S^Q_{env}\rangle_{\{s\}} = Q/T$. Other choices of basis would give different values for the entropy changes. This strongly supports the choice of the $\{|s\rangle|\epsilon\rangle\}$ reference basis as the unique basis that gives standard results in the classical microcanonical limit.

4.5. Time-evolving Lorentzian states

Now we relate the preceding considerations to two illuminating situations that are both computationally transparent and analytically tractable. The model system and environment are the same as in Chapter III and Ref. [2]. There we observed in computations that there was excess entropy production. However, in the weak coupling/infinite density of states limit, the excess entropy went to zero, and classical microcanonical results were obtained: the free energy - entropy relation Eq. 4.2. Chapter III was about time evolution of a wave packet constructed from a superposition of many $|s\rangle|\epsilon\rangle$ zero order states. The initial wave packet had a single $\mathcal{S}$

state and many $\mathcal{E}$ states in the product. The idea was to mimic a reasonable initial state within a microcanonical energy shell, with the width of the shell corresponding to the range of environment zero order energies. The classical limit was obtained as the coupling k and density of states ρ were varied.

However, it is not so clear under what general conditions classical behavior will be recovered, and what governs the magnitude of excess entropy production. What role is played by the width of the microcanonical shell? Here we probe this by comparing the time evolution of two very different types of initial state. One is a superposition of many $\mathcal{SE}$ initial states, corresponding to a microcanonical shell of significant width. The second is a single zero order $\mathcal{SE}$ state. Here the width of the microcanonical shell is essentially zero. The suspicion is that nonclassical effects will be much more pronounced with this state. Then classical behavior would be something that is attained only by taking a superposition of many zero order $\mathcal{SE}$ states, corresponding to a finite microcanonical shell width. This surmise is essentially what we will observe in the following simulations, as described next.

4.5.1. Initial states

We investigate these questions with two kinds of simulations. One takes a random superposition of $|s\rangle|\epsilon\rangle$ zero-order states under an overall Lorentzian window. The second takes a single $|s\rangle|\epsilon\rangle$ zero-order state—an extreme case of a Lorentzian, with zero width. The results, shown in Figs. 4.1 and 4.2, will be discussed in the following sections.

The reason for considering Lorentzians is as follows. The energy eigenstates are Lorentzian superpositions of zero order states, as pointed out by Deutsch in his introduction [21] of the eigenstate thermalization hypothesis (ETH). Following

the analysis of Appendix B, a single $|s\rangle|\epsilon\rangle$ zero order state then consists of a Lorentzian superposition of eigenstates, and evolves into a Lorentzian of zero order states. Furthermore, an initial Lorentzian time-dependent superposition evolves into a (wider) Lorentzian superposition. Thus, with Lorentzian initial states, down to the limit of zero-width Lorentzian $|s\rangle|\epsilon\rangle$ state, we evolve to Lorentzian final states. This gives a unified class of states for systematic analysis. There are analytical results that can be brought to bear on the statistics of these Lorentzians, and also the entropy production. Furthermore, the Lorentzian width has a nice correspondence to the idea of a microcanonical shell width. Hence, Lorentzians are ideally suited for the kind of systematic investigation we want to undertake.

We consider initial states with the system in a single level $|s\rangle$ and the environment described by fluctuations $\tilde{g}_{s,\epsilon}$ about a Lorentzian distribution L_0

$$|\Psi_L^0\rangle \sim \sum_\epsilon \tilde{g}_{s,\epsilon}\sqrt{L_0}|s\rangle|\epsilon\rangle \tag{4.21}$$

The Lorentzian distribution at time $t = 0$ is

$$L_0(E_s + E_\epsilon) = \frac{1}{\pi}\frac{\gamma_0/\rho_0}{(E_s + E_\epsilon - E_0)^2 + \gamma_0^2} \tag{4.22}$$

where ρ_0 is the density of environment states that pair with the initial system level $|s\rangle$ and E_0 and γ_0 are parameters that respectively describe the central energy of the Lorentzian and the half-width at half-max. The $\tilde{g}_{s,\epsilon}$ are complex random Gaussian variates that give random deviations to the $|s\rangle|\epsilon\rangle$ basis state probabilities about the Lorentzian average. These are taken as as

$$\tilde{g}_{s,\epsilon} = \frac{g_{s,\epsilon} + ig'_{s,\epsilon}}{\sqrt{2}} \tag{4.23}$$

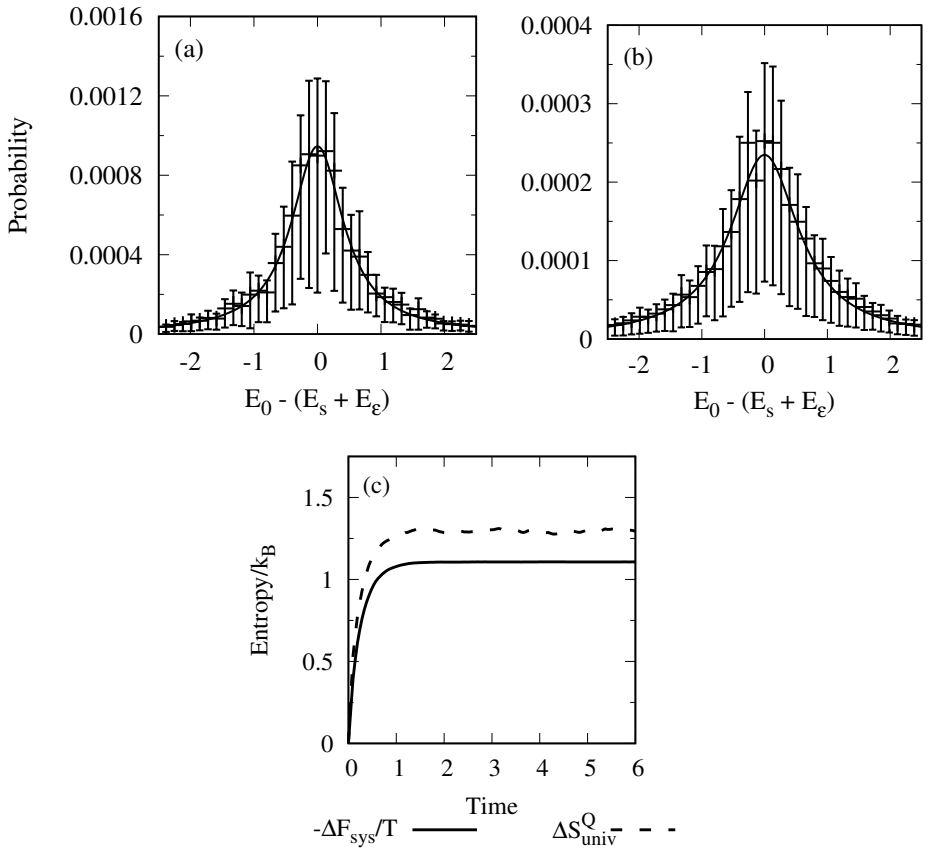

FIGURE 4.1. Average probabilities $|\langle s|\langle\epsilon|\Psi\rangle|^2$ for nearby $|s\rangle|\epsilon\rangle$ basis states for (a) an initial Lorentzian state from Eq. 4.21 with half-width at half-max $\gamma_0 = 0.5$ and (b) the corresponding time-evolved state of Eq. 4.26. The asymmetric error bars show the first and third quartiles of the distribution of probabilities that go into the averages shown by the data points. (c) Entropy production ΔS^Q_{univ} and free energy change $-\Delta F_{sys}/T$ during the time evolution.

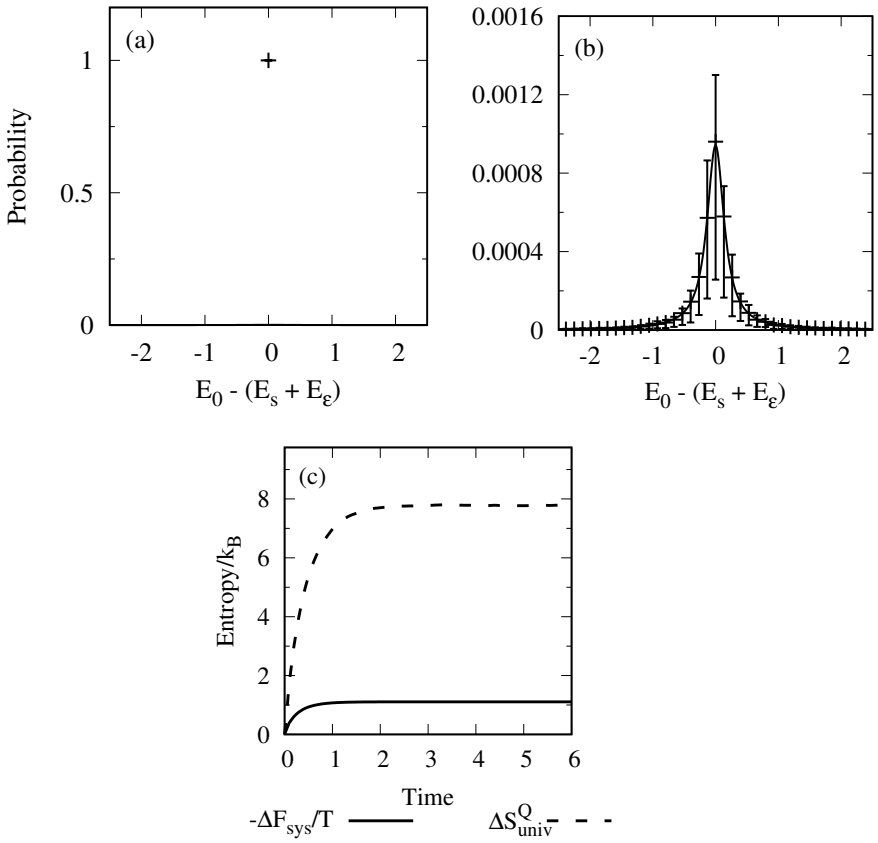

FIGURE 4.2. Average probabilities $|\langle s|\langle\epsilon|\Psi\rangle|^2$ for nearby $|s\rangle|\epsilon\rangle$ basis states for (a) an initial $|s\rangle|\epsilon\rangle$ state from Eq. 4.25 and (b) the corresponding time-evolved state of Eq. 4.26. The asymmetric error bars show the first and third quartiles of the distribution of probabilities that go into the averages shown by the data points. (c) Entropy production ΔS^Q_{univ} and free energy change $-\Delta F_{sys}/T$ during the time evolution.

where $g_{s,\epsilon}$ and $g'_{s,\epsilon}$ are random numbers from Gaussian distributions, e.g.

$$p(g_{s,\epsilon}) = \frac{1}{\sqrt{2\pi}} e^{-g_{s,\epsilon}^2/2} \tag{4.24}$$

With this definition the average variation is $\langle |\tilde{g}_{s,\epsilon}|^2 \rangle = 1$ so that the basis state probabilities follow the Lorentzian on average.

Panel (a) of Fig. 4.1 shows an example of an initial random Lorentzian state as in Eq. 4.21 with an initial width $\gamma_0 = 0.5$. The data points in the figure show averaged squared coefficients $|c_{s,\epsilon}|^2 = |\langle s|\epsilon|\Psi\rangle|^2$ and the asymmetric error bars show the first and third quartiles of the coefficient distributions for each average. The average squared coefficients follow the Lorentzian from Eq. 4.22. The quartiles shown for the error bars are in good agreement with the quartiles expected from the Gaussian random deviations $\tilde{g}_{s,\epsilon}$, as discussed in detail in Appendix B.

We are also concerned with the time-evolution of initial single $|s\rangle|\epsilon\rangle$ basis states

$$|\Psi^0_{s,\epsilon}\rangle = |s\rangle|\epsilon\rangle. \tag{4.25}$$

These can be viewed as the limit $\gamma_0 \to 0$ of the random Lorentzian initial states in Eq. 4.21, where the Lorentzian distribution approaches a δ function. Panel (a) of Fig. 4.2 shows an $|s\rangle|\epsilon\rangle$ initial state as in Eq. 4.25, with just a single nonzero coefficient $c_{s,\epsilon} = 1$. This is an example of a very non-classical starting state, where the "width" of the initial microcanonical energy shell is zero.

4.5.2. Time evolution and quantum spreading

Now consider the time evolution of the random Lorentzian states of Eq. 4.21 and of the single $|s\rangle|\epsilon\rangle$ states of Eq. 4.25. We found in Appendix B that both of these

evolve to equilibrium states that can be described statistically by random fluctuations about a Lorentzian average,

$$|\Psi_L^f(t)\rangle, |\Psi_{s,\epsilon}^f(t)\rangle \sim \sum_{s,\epsilon} \tilde{g}_{s,\epsilon} \sqrt{L_f} |s\rangle|\epsilon\rangle, \tag{4.26}$$

with a final state Lorentzian

$$L_f(E_s + E_\epsilon) = \frac{1}{\pi} \frac{\gamma_f/\rho_f}{(E_s + E_\epsilon - E_0)^2 + \gamma_f^2}, \tag{4.27}$$

where ρ_f is the total density of $|s\rangle|\epsilon\rangle$ states and γ_f is the half-width at half-max of the final Lorentzian, to be discussed further below.

The half-width at half-max γ_f was found in Appendix B to be increased by the "spreading factor" $2\pi k^2 \rho$ relative to the initial state width γ_0:

$$\gamma_f = \gamma_0 + 2\pi k^2 \rho_f. \tag{4.28}$$

Eqs. 4.26-4.28 apply to both the equilibrated, time-evolved Lorentzian initial states of Eq. 4.21 and the time-evolved $|s\rangle|\epsilon\rangle$ states of Eq. 4.25, where for the latter it is understood that the value $\gamma_0 = 0$ is used in the final width in Eq. 4.28, so that $\gamma_f = 2\pi k^2 \rho_f$.

Panel (b) of Figs. 4.1 and 4.2 show the time-evolved states. Both evolve to random fluctuations about the Lorentzians L_f from Eq. 4.27 with the appropriate widths γ_f from Eq. 4.28. The variations in the coefficients are very well characterized by the Gaussian random variations $\tilde{g}_{s,\epsilon}$ in Eq. 4.26, discussed in detail in Appendix B.

4.5.3. Entropy production for the time-evolving $|s\rangle|\epsilon\rangle$ and Lorentzian states

We now consider the entropy production for these examples of time-evolving states. Panel (c) of Fig. 4.1 shows the entropy production ΔS^Q_{univ} as the initial Lorentzian superposition in panel (a) evolves to the wider final Lorentzian distribution in panel (b). ΔS^Q_{univ} is compared with the classical entropy change $-\Delta F_{sys}/T = \Delta S^{micro}_{univ}$. There is some excess entropy production, as expected from Chapter III and Ref. [2], but overall it is fairly close to microcanonical. Panel (c) of Fig. 4.2 shows the entropy production for the initial single $|s\rangle|\epsilon\rangle$ state that evolves to a final random Lorentzian. Now there is a very large amount of excess entropy production. It seems that the finite microcanonical shell width of the state that is in an initial superposition plays an essential role in getting the approach to classical behavior, because it limits the *relative* spreading of the wave packet in time, as suggested in Eq. 4.19. In contrast, quantum spreading of the single $\mathcal{SE}$ state is relatively very large or undefined. To understand this connection systematically, we will take advantage of analytic expressions for superposition states with a Lorentzian profile, using results from Appendix C. We will see that considerable insight is gained following this path.

4.6. Master relationships for S^Q_{univ} and ΔS^x for time-evolving Lorentzian states

Now we want to attain a systematic and intuitive understanding of the entropies in the simulations and how they change during equilibration, in comparison with analytical results based on the initial and final state statistics from Section 4.5. The basic results are seen in Figs. 4.3-4.5 and show evident regularities. The initial states are either random Lorentzians or a single $|s\rangle|\epsilon\rangle$ basis state, as in Eqs. 4.21 and 4.25.

We will find that the entropies for these two types of initial states can be united in the approximate "master entropy" Eq. 4.32, which accounts for the pattern of Fig. 4.3. Both types of initial states evolve to final states that are also random Lorentzians as in Eq. 4.26. This will lead to an analytical approximation for the excess entropy production in Eq. 4.36 and Fig. 4.4. Finally we consider entropy production in the approach to the microcanonical limit of Ref. [2], where classical behavior is expected. Fig. 4.5 shows that superpositions approach classical entropy production $\Delta S^x = 0$ while the $|s\rangle|\epsilon\rangle$ initial states do not. The results account for the regularities in Figs. 4.3-4.5 and are in accord with our earlier heuristic arguments about S^Q and ΔS^x in Section 4.4, based on ideas about the microcanonical shell and quantum spreading of the environment state during equilibration.

4.6.1. Entropy of the States

An analytic relationship for the entropy of the random Lorentzian states, related below to Boltzmann's entropy formula $S = k_B \ln W$ and the idea of a microcanonical shell width, can be obtained following the straightforward but somewhat involved derivation of Appendix C. The derivation approximates the entropy sum Eq. 4.5 as an integral over the random Lorentzian coefficients as in Eqs. 4.21 and 4.26. The integral approximation should work well when the Lorentzian is wide enough to have a quasi-continuous distribution. The result is

$$S_L = \ln(4\pi\gamma\rho) - g_0 \tag{4.29}$$

where ρ is the density of states and γ is the half-width at half-max of the Lorentzian. These have the values ρ_0 and γ_0 for the initial Lorentzian states, as described below

Eq. 4.21, and ρ_f and γ_f for the final states, as described in the discussion around Eq. 4.28.

The first term on the right of Eq. 4.29 gives the entropy of a perfect Lorentzian (without the random variations $\tilde{g}_{s,\epsilon}$). This has the microcanonical-like form suggested previously in Eq. 4.17,

$$\ln(4\pi\gamma\rho) = \ln(\rho\delta E) = \ln W_{\text{eff}} \tag{4.30}$$

with $W_{\text{eff}} = \rho\delta E$ an effective number of states in an energy shell of width $\delta E = 4\pi\gamma$. The second term

$$g_0 = \langle |\tilde{g}_{s,\epsilon}|^2 \ln |\tilde{g}_{s,\epsilon}|^2 \rangle = 1 - \gamma_{EM} \tag{4.31}$$

gives the deviation from the Lorentzian entropy due to the random fluctuations in the basis state probabilities $\tilde{g}_{s,\epsilon}$, with $\gamma_{EM} = 0.577\ 215...$ the Euler-Mascheroni constant. We thus have obtained the desired relationship between S^Q, Boltzmann's entropy formula, and the number of states with a given shell width and density of states.

How well this works is seen in Fig. 4.3 which shows the entropies for a time-evolved $|s\rangle|\epsilon\rangle$ state, for initial random Lorentzian states with various initial widths $5 \times 10^{-6} \leq \gamma_0 \leq 0.25$, and for the time-evolved Lorentzian states with final widths $\gamma = \gamma_f$ from Eq. 4.28. The simulation results are well described by the approximate S_L of Eq. 4.29 along the diagonal line of the figure, when $\gamma\rho$ is not too small. For small $\gamma\rho$ on the left of the figure, the initial states approach the limit of the single $|s\rangle|\epsilon\rangle$ basis state. In this limit, the integral approximation that goes into the derivation of S_L breaks down. This gives $S_L < 0$ when $\gamma < e^{g_0}/4\pi\rho$, whereas $S^Q_{univ} \geq 0$ by definition. A better approximate formula is obtained by setting the entropy to zero

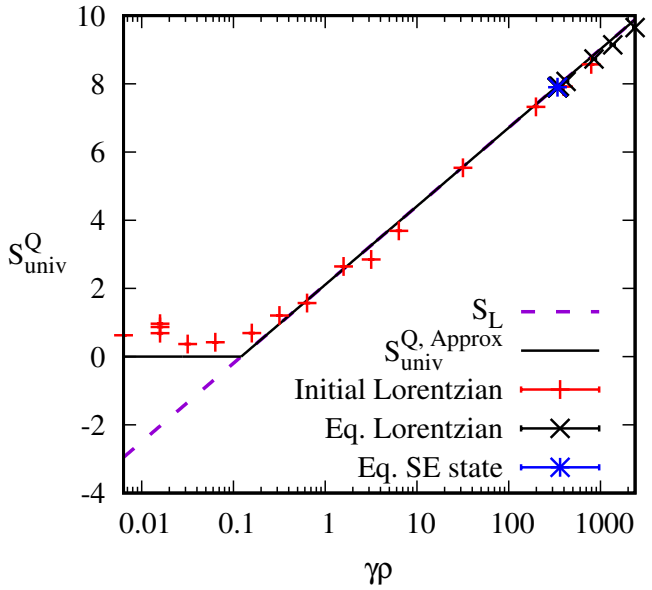

FIGURE 4.3. Entropies from the simulations follow the master equation Eq. 4.32.

when S_L becomes negative, essentially approximating the entropy of the very narrow states by the value for a single $|s\rangle|\epsilon\rangle$ state. This gives the complete generic "master" formula for the entropy of the time evolving random Lorentzian states, plotted as a solid line:

$$S^Q_{univ} \approx \begin{cases} \ln(4\pi\gamma\rho) - g_0 & : \quad \gamma \geq e^{g_0}/4\pi\rho \\ 0 & : \quad \text{otherwise} \end{cases} \tag{4.32}$$

This is the same as the previous relation S_L, except that it stops changing when it reaches the minimum value zero, giving the abrupt bend in the figure. The simulation results are in good agreement with this predicted behavior, with fluctuations around $S^Q_{univ} = 0$ at small $\gamma\rho$, and following the curve for S_L at larger $\gamma\rho$. In sum, the approximate master entropy relation Eq. 4.32 is giving a good account of the simulation results.

4.6.2. Entropy production

We next consider entropy changes and excess entropy production during the approach to equilibrium. The aim is to see how excess entropy relates to the intuitive idea of spreading of the quantum wave packet, and also the width of the microcanonical shell. First, we consider random initial Lorentzian states that are well described by the approximate entropy S_L of Eq. 4.29, when $\gamma_0 \geq e^{g_0}/4\pi\rho_0$ in Eq. 4.32. The entropy change for these states is

$$\Delta S_L = \ln \frac{\rho_f}{\rho_0} + \ln \frac{\gamma_f}{\gamma_0}, \tag{4.33}$$

with γ_f from Eq. 4.28. The first term $\ln \rho_f/\rho_0$ gives the classical entropy change from heat flow, following the microcanonical definition Eq. 4.15. The second term gives the quantum excess entropy production

$$\Delta S_L^x = \ln \frac{\gamma_f}{\gamma_0} = \ln \frac{\delta E_f}{\delta E_0} \tag{4.34}$$

due to quantum spreading of the environment state wave packet. This analytic relation is similar to the somewhat more complex empirical curve for fitting ΔS^x in Ref. [2] with a less structured type of $\mathcal{SE}$ state, which did not maintain a consistent Lorentzian profile as we have here. For our Lorentzians we obtain the simple formula of Eq. 4.34, in terms of only the initial and final widths γ_0 and γ_f. This corresponds simply to the increase in the effective width of the energy shell, as anticipated in Eq. 4.19.

The diagonal line on the left of Fig. 4.4 shows the approximate ΔS_L^x of Eq. 4.34 compared with $\Delta S^x = \Delta S^Q_{univ} + \Delta F_{sys}/T$ from the simulations. Moving from left to right in the figure, we are decreasing γ_0 to increase the ratio γ_f/γ_0. The approximate

relation is giving a good account of the results on the left of the figure, where γ_f/γ_0 is not too large.

Now consider the right side of Fig. 4.4. The ΔS^x are reaching close to a maximum value for a single $|s\rangle|\epsilon\rangle$ state, corresponding to the limit of small γ_0 with large γ_f/γ_0 in the figure. For small γ_0, we want to approximate the initial state as a single $|s\rangle|\epsilon\rangle$ state, like what we did for S^Q_{univ} in Eq. 4.32. For a single $|s\rangle|\epsilon\rangle$ initial state the initial entropy is zero. The final state has the Lorentzian entropy S_L. Then $\Delta S^Q_{univ} = S_L$. The maximum excess entropy production is then calculated by subtracting the microcanonical $\ln \rho_f/\rho_0$,

$$\Delta S^{x,max} = \ln(4\pi\gamma_f\rho_f) - g_0 - \ln\frac{\rho_f}{\rho_0} = \ln(8\pi^2k^2\rho_f\rho_0) - g_0, \tag{4.35}$$

where in the last line we have used the value $\gamma_f = 2\pi k^2\rho_f$ for a single $|s\rangle|\epsilon\rangle$ initial state, when $\gamma_0 = 0$ in Eq. 4.28. This gives the "master" equation for the excess entropy production

$$\Delta S^x \approx \begin{cases} \ln(\gamma_f/\gamma_0) & : \quad \gamma_0 \geq e^{g_0}/4\pi\rho_0 \\ \ln(8\pi^2k^2\rho_f\rho_0) - g_0 & : \quad \text{otherwise} \end{cases} \tag{4.36}$$

This master relation for ΔS^x is shown by the black solid line in Fig. 4.4. It follows ΔS^x_L from Eq. 4.34 up until this reaches the maximum value for a single $|s\rangle|\epsilon\rangle$ initial state, where the master relation bends and becomes flat in the right of the figure. This is in good agreement with our simulation results, which follow ΔS^x_L in the left of the figure then fluctuate around the maximum value in the right of the figure.

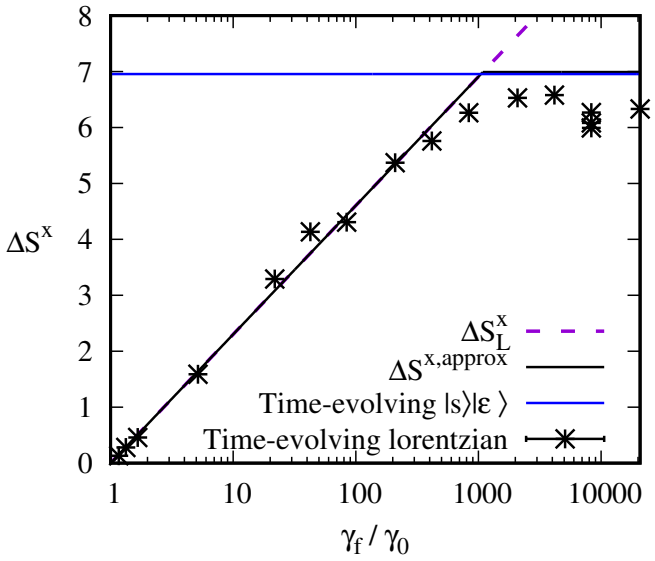

FIGURE 4.4. Excess entropy production for initial random Lorentzians (black stars) and for an initial $|s\rangle|\epsilon\rangle$ state (blue bar) follow the master equation Eq. 4.36.

4.6.3. Excess entropy production and the microcanonical limit

We have just seen that the source of the excess entropy production is the relative increase in the width of the environment state from quantum spreading during $\mathcal{SE}$ equilibration, with larger γ_f/γ_0 giving greater deviations from a fixed microcanonical energy shell, with larger ΔS^x. What is less clear so far is the role of the size of the environment and the $\mathcal{SE}$ coupling strength.

We have been dealing with a finite model environment with finite coupling, in contrast to the textbook situation with an infinite environment $\rho_f \to \infty$ and negligible coupling $k \to 0$. Ref. [2] showed with superposition states that microcanonical results $\Delta S^x = 0$ were obtained in this limit, based on the idea of an energy shell with fixed width and negligible coupling. Do we also see the approach to the classical $\Delta S^x = 0$ here, even for the highly non-classical $|s\rangle|\epsilon\rangle$ initial states?

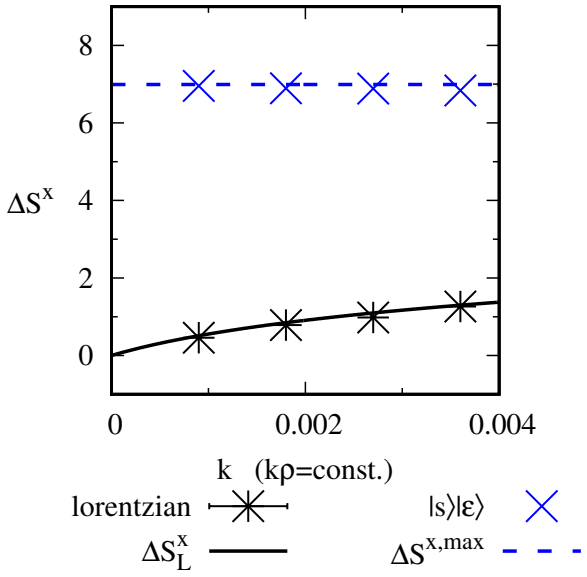

FIGURE 4.5. Excess entropy production for Lorentzian initial states with widths $\gamma_0 = 0.0625$ and $|s\rangle|\epsilon\rangle$ initial states, with different model environments heading towards the microcanonical limit $k \to 0, \rho \to \infty, k\rho = const.$ in the bottom left. The Lorentzians approach the classical result $\Delta S^x = 0$, while the $|s\rangle|\epsilon\rangle$ states have non-classical entropy production $\Delta S^x \gg 0$ in the microcanonical limit.

Fig. 4.5 shows ΔS^x in a series of calculations heading toward the "microcanonical limit" $k \to 0, \rho_f \to \infty$, with $k\rho_f = const.$ as needed to maintain thermalization within the simulations. First consider the Lorentzian states in the figure. These approach classical behavior $\Delta S^x = 0$ in Eq. 4.36 as quantum spreading in the environment becomes negligible, with $\gamma_f \to \gamma_0$ in Eq. 4.28. Now consider the $|s\rangle|\epsilon\rangle$ states in the figure. They have very nearly constant ΔS^x corresponding to the maximum from Eqs. 4.35 and 4.36. The maximum ΔS^x for an $|s\rangle|\epsilon\rangle$ initial state depends only on the products $k\rho_f$ and $k\rho_0$, which are both invariant in the limit, so there is no approach to classical behavior with a relatively fixed energy shell. Instead, quantum spreading is always a significant source of entropy production, and classical behavior is never observed for the $|s\rangle|\epsilon\rangle$ states.

4.7. Summary and concluding remarks

We have systematically explored the phenomenon of excess entropy production in time-dependent equilibration processes, in terms of the quantum thermodynamic entropy proposed in Refs. [1, 2] for a system-environment pure state. Our interest is the role of quantum spreading and the idea of the microcanonical shell width to understand the range of excess entropy, between the classical microcanonical limit and the limit of maximal excess entropy production with a single zero-order initial state.

Using the Shannon information entropy, we defined the quantum entropy S^Q_{univ} in terms of the ZO $\mathcal{SE}$ energy basis. The choice of the ZO basis is made on the grounds that thermodynamically one would be interested in observation of the system ZO state, and that straightforward definition of the energy in the microcanonical shell then involves the sum of ZO system and environment energies. We showed that there is an exact division of S^Q_{univ} into S^Q_{sys} and S^Q_{env}. With this, we found that our choice of basis for the definition of S^Q_{univ} uniquely gives standard thermodynamic results in the classical limit of weak coupling and large basis, including the standard classical relations $\Delta S_{univ} = -\Delta F_{sys}/T$ and $\Delta S_{env} = Q/T$ between the environment entropy and heat flow. The entropy is readily understood with Boltzmann's equation $S = k_B \ln W$ with W being given by shell width $\times$ density of states $\delta E \times \rho = 4\pi\gamma\rho$ according to Eq. 4.29, down to the limit $S = 0$ as seen in Fig. 4.3.

ΔS_{univ} can be understood according to Eq. 4.36 and as seen in Fig. 4.4 as being due to two components. One is classical "ergodization" as the system thermalizes and heat flows into the environment, with consequent increase in the density of states, giving the contribution $\ln \rho_f/\rho_0$. The second contribution is excess entropy production ΔS^x as seen in in Fig. 4.4, due to quantum spreading of the microcanonical shell,

represented by $\ln \gamma_f/\gamma_0$ in Eq. 4.36. The spreading is independent of the original width γ_0. Therefore ΔS^x is limited by the original width in $\ln \gamma_f/\gamma_0$. Initial states like a microcanonical wave packet, with small spreading compared to the original wave packet width, approach the classical limit. On the other hand, initial states that approach the extreme limit of a single $\mathcal{SE}$ zero order state have maximal, massive entropy production, very different from classical. Since the spreading is the same for Lorentzian states, the critical factor is the microcanonical shell width of the original Lorentzian. The excess happens in the environment, not as heat flow Q/T within the microcanonical shell, but rather as quantum spreading of the microcanonical shell.

In sum, we have the following picture. The quantum entropy S^Q_{univ} describes time-dependent thermodynamic evolution. The entropy can be formally divided into system and environment contributions. In the limit of small coupling and large bath, the classical limit with Eq. 4.2 is recovered. Away from this limit, there is excess entropy production $\Delta S^x > 0$. This excess entropy production takes place in the environment and is in addition to the classical contribution Q/T. The excess entropy is due to time-dependent quantum spreading. In general, it can be quite large, with a single $\mathcal{SE}$ zero-order state being the extreme case.

4.8. Connection to later work

This chapter has developed a much deeper understanding for the source and behavior of the excess entropy production ΔS^x associated with the quantum entropy S^Q_{univ} in time-dependent quantum pure state thermalization. The excess entropy production can be massive for non-classical types of states, with a direct relation to the spreading of the wavepacket that is particularly transparent for a class of Lorentzian states evolving in time. However, we haven't yet seen any new types

of quantum thermodynamic behavior associated with ΔS^x, as might be expected from this new source of entropy in the second law. Are there new effects in quantum thermodynamics related to maximizing the total entropy S^Q_{univ}, including excess entropy production ΔS^x, that wouldn't be expected from the classical entropy change alone? We explore this question in the next two chapters. The next chapter begins by exploring thermodynamics in finite size quantum systems, making use of a small quantum variable temperature "bath" in place of the standard type of fixed temperature bath explored so far. This will lead into a final examination of a very novel type of behavior in Chapter VI, where two of these finite baths are linked together by a system, with unequal couplings and rates of excess entropy production in the two baths. The entropy S^Q_{univ} with excess entropy production will have an important role to play, with implications for future developments in the foundations of quantum thermodynamics.

CHAPTER V

SIMULATING QUANTUM THERMODYNAMICS OF A FINITE SYSTEM AND BATH WITH VARIABLE TEMPERATURE

This chapter includes previously published material co-authored by Michael E. Kellman [4]. Michael Kellman and I both contributed to developing the model and theory, analyzing the results, and writing the manuscript. I performed the computations.

5.1. Introduction

This paper considers computational simulation of a process of energy flow as a quantum system becomes entangled with a very small temperature bath. In the corresponding "classical" thermodynamic system, we would have an idea of a *variable temperature* as energy flows into the finite bath. Here we ask, does a simulacrum of thermodynamic behavior emerge when we make the bath very small? Do reasonable ideas of a variable temperature hold, and is there something akin to thermal equilibrium with a Boltzmann distribution? We will find that with a very small "thermal" environment, as small as five oscillators, it is possible to get behavior that is very much like thermodynamic behavior. On the other hand, anomalies are observed related to the notion of temperature with the small bath. The work here builds on earlier simulations with a cruder, constant temperature bath [1, 2, 6, 35–37]. Questions of variable temperature in a very small quantum thermodynamic system and bath are of more than abstract interest. Our simulations may not be too much

simpler than what is called for in problems of practical import. Quantum nanodevices can be imagined whose performance may depend on considerations similar to those here. Similar in spirit to the approach taken here, quantum thermalization behavior of a pure quantum state has recently been observed experimentally in Bose-Einstein condensates containing as few as six-atoms [24]. Recently [26, 27, 38], work on molecular "quantum chaos" is being conceptualized as a venue for the exploration of contemporary ideas about the foundations of quantum thermodynamics, to which we turn next.

There have been a variety of simulations of quantum thermodynamic processes, including the very basic elementary process of heat flow into a bath [1, 2, 6, 35–37]. These have been successful in recovering standard thermodynamic behavior, with attainment of thermal equilibrium and a Boltzmann distribution for the system, with a properly behaving temperature. However, these investigations have used rather simple models of the temperature bath, sometimes with a grossly discrete model of energy levels [1, 6, 37], in others with an approximation to continuous levels in the bath [2, 35, 36], but always to our knowledge with a model of an effectively infinite bath with fixed temperature in mind. Usually also, a very simple coupling between system and environment is assumed, typically, a random matrix coupling without significant structure. Paralleling (and sometimes preceding) these simulations, there has been a great deal of work [1, 2, 7, 8, 10–21, 23, 26–34] examining theoretical foundations of quantum thermodynamics. Generally, this has focused on the large N limit of quantum entangled systems. In our simulations here the focus is rather on the extent to which thermodynamic-like behavior persists as the total system becomes very small. There have been simulations examining ergodicity and energy flow in small total systems [19, 20, 26, 27, 52, 53], but these have not involved the type of

variable temperature analysis that is our focus here. We construct a finite, variable temperature bath, also making use of a structured coupling which is far more selective than the random matrix coupling used in many earlier simulations. We will find that we can build a simulation model with features very much like a variable temperature and thermalization, but with significant anomalies due to the finite bath, with some challenges to overcome having to do with the nature of the coupling.

As noted briefly above, and in more detail in the concluding section, there are real molecular systems that could be considered as laboratories for "post-classical" thermodynamic effects. Consideration of small size is a recent "dimension" of quantum thermodynamics beyond that introduced long ago with the advent of quantum levels. A third innovation might come with novel effects from combining quantum time evolution with multiple small baths of the kind developed here for a single bath.

5.2. Model system-environment "universe"

In this section, we detail the system and environment in our model; we treat the system-environment interaction separately, in Sections 5.5 and 5.6.

We will deal with a total system or "universe" pure state for a coupled and entangled system and environment, or temperature bath. The total Hamiltonian includes system $\mathcal{S}$, environment $\mathcal{E}$, and interaction $\mathcal{SE}$ components

$$\hat{H} = \hat{H}_{\mathcal{S}} + \hat{H}_{\mathcal{E}} + \hat{H}_{\mathcal{SE}} \tag{5.1}$$

For the basis set we will use a truncation of the full $\mathcal{SE}$ tensor product basis to a subset that contains all of the $\mathcal{SE}$ basis states $|n\rangle \otimes |\epsilon\rangle$ in the energy range

$$0 \leq E_n + E_\epsilon \leq 13, \tag{5.2}$$

similar to the "thermal basis" described in Ref. [2]. The numerical convergence with this basis will be discussed in Section 5.6. Time evolution of the pure $\mathcal{SE}$ state $|\Psi\rangle$ is carried out by numerically diagonalizing $\hat{H}$ and then calculating a series of timesteps using the Schrödinger equation $|\Psi(t)\rangle = \exp(-i\hat{H}t)|\Psi(0)\rangle$ ($\hbar = 1$). In this section we will develop the system and environment basis sets and Hamiltonians $\hat{H}_\mathcal{S}$ and $\hat{H}_\mathcal{E}$; later sections develop $\hat{H}_\mathcal{SE}$.

The system Hamiltonian consists of a set of five evenly spaced levels

$$\langle n|\hat{H}_\mathcal{S}|n\rangle = \hbar\omega_\mathcal{S} n, \tag{5.3}$$

with frequency $\omega_\mathcal{S} = 0.5$ and quantum number $n = 0, 1, ..., 4$. These choices of $\omega_\mathcal{S}$ and n give a maximum system energy $E_\mathcal{S}^{\max} = 2$ that is reasonably small compared to the initial $\mathcal{SE}$ state total energies we will consider in this paper $\langle\hat{H}\rangle \gtrsim 4$, where $\hat{H}$ is the total Hamiltonian of Eq. 5.1. With larger $E_\mathcal{S}^{\max}$ we have found that it is more difficult to get good system thermalization, since very few environment levels are paired with the highest energy system levels at the total energy $\langle\hat{H}\rangle$ when $E_\mathcal{S}^{\max} \approx \langle\hat{H}\rangle$. This choice of $\omega_\mathcal{S}$ and $n = 0, 1, ..., 4$ ensures that there is always a fair amount of energy in the environment, so that it can act properly as a heat bath to the system in our simulations.

We want to have an environment or bath $\mathcal{E}$ with certain properties more general than in earlier work [1, 2, 6, 35–37], and more similar to real physical systems. We want the temperature to vary with energy, instead of being fixed. We would also like for the energy and temperature to be close to proportional, $T \sim E$, to the extent

possible in a finite model, and exactly so in the limit of a large bath. Furthermore, we may want the bath to have some significant structure, so that the couplings might also have some structure, unlike the abstract undefined environment levels with random couplings used earlier. To do all of these things, we will construct the bath as a collection of oscillators.

Consider first a set of degenerate oscillators with equal frequencies and level spacings $\hbar\omega = 1$. This "Einstein heat capacity" system has the well known degeneracy pattern and density of states

$$\rho_{\mathrm{Ein}}(\eta, n_{\mathrm{tot}}) = \frac{(\eta - 1 + n_{\mathrm{tot}})!}{(\eta - 1)! n_{\mathrm{tot}}!}, \tag{5.4}$$

where $\rho_{\mathrm{Ein}}(\eta, n_{\mathrm{tot}})$ is the number of ways to distribute n_{tot} total energy quanta into η oscillators. A more physically realistic model will generalize to oscillators of different frequencies, so as to obtain something resembling a continuous distribution of levels, while approximately maintaining the overall pattern of Eq. 5.4. To this end, we will extend the distribution ρ_{Ein} to variable frequencies and energies using a continuous function $\rho_{\mathcal{E}}$ that interpolates between the discrete points in Eq. 5.4. Then, we will devise a set of distinct harmonic oscillator frequencies $\{\omega_{\mathrm{osc}}\}$ that approximates the continuous distribution. The total environment Hamiltonian is expressed as the sum of oscillator Hamiltonians

$$\hat{H}_{\mathcal{E}} = \sum_{\mathrm{osc}=1}^{\eta} \hat{H}_{\mathrm{osc}}, \tag{5.5}$$

where the $\hat{H}_{\mathrm{osc}}$ have energy eigenvalues

$$\langle n_{\mathrm{osc}} | \hat{H}_{\mathrm{osc}} | n_{\mathrm{osc}} \rangle = \hbar\omega_{\mathrm{osc}} n_{\mathrm{osc}}, \tag{5.6}$$

where n_{osc} is the quantum number of a given oscillator. We will analyze the density of states $\rho_{\hat{H}_\mathcal{E}}$ of the Hamiltonian $\hat{H}_\mathcal{E}$, finding good agreement with the continuous density $\rho_\mathcal{E}$, and then analyze the temperature dependence of the model.

We begin by developing a continuous density function $\rho_\mathcal{E}$ in place of the highly degenerate density of Eq. 5.4. The most straightforward way to do this is to replace the factorials in (5.4) with Gamma functions

$$\rho_\mathcal{E}(E_\mathcal{E}) = \frac{\Gamma(\eta + E_\mathcal{E})}{\Gamma(\eta)\Gamma(E_\mathcal{E}+1)}, \tag{5.7}$$

where the discrete number of total quanta n_{tot} has been replaced by a continuous environment energy $E_\mathcal{E}$. The Γ function extends the density to non-integer values of the energy $E_\mathcal{E}$, and agrees with the original density ρ_{Ein} at integer $E_\mathcal{E} = n_{\text{tot}}$, since for example $\Gamma(E_\mathcal{E}+1) = E_\mathcal{E}! = n_{\text{tot}}!$ when $E_\mathcal{E} = n_{\text{tot}}$ is an integer. The top of Fig. 5.1 shows how the continuous density $\rho_\mathcal{E}$ extends the degenerate oscillator density ρ_{Ein} to non-integer $E_\mathcal{E}$.

The next step is to devise a set of oscillator frequencies for the Hamiltonian $\hat{H}_\mathcal{E}$ in Eq. 5.5 with a density $\rho_{\hat{H}_\mathcal{E}}$ that follows the interpolating function $\rho_\mathcal{E}$. An $\eta = 5$ oscillator bath will be used for the simulations. This value of η is large enough to give a density of states with an exponential-like dependence on energy, which will be imperative for Boltzmann thermalization of the system $\mathcal{S}$, but also small enough to make the computations tractable. The frequencies are generated as random numbers, to make the bath generic. We first tried generating random numbers $0.5 \leq \hbar\omega_{\text{osc}} \leq 1.5$ then rescaling the $\hbar\omega_{\text{osc}}$ so that their average was the same as the degenerate oscillator frequency $\hbar\omega = 1$ seen in the top of Fig. 5.1. However, when constructing the Hamiltonian $\hat{H}_\mathcal{E}$ in Eq. 5.5 using these frequencies, it was found that the resulting density of states $\rho_{\hat{H}_\mathcal{E}}$ was always greater than the desired $\rho_\mathcal{E}$ of Eq. 5.7.

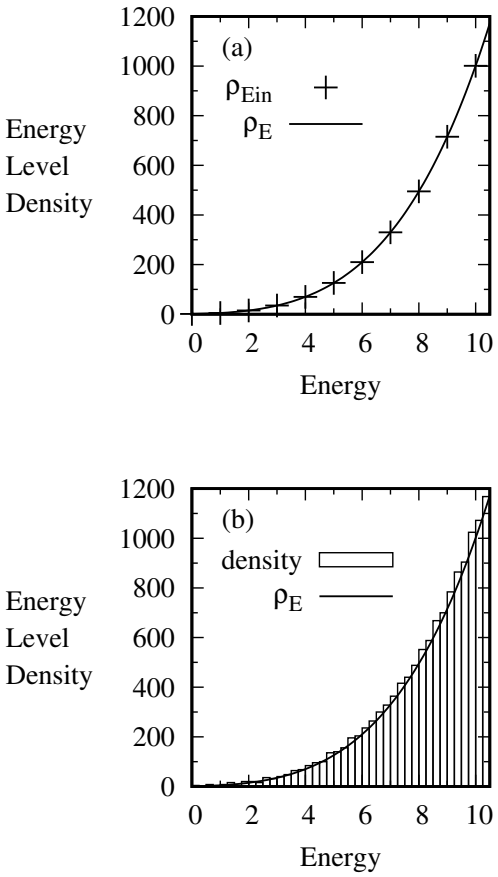

FIGURE 5.1. (a) The continuous density $\rho_{\mathcal{E}}$ from Eq. 5.7 interpolates between the degenerate oscillator densities $\rho_{\rm Ein}$ from Eq. 5.4. (b) Oscillator density of states histogram for the five oscillator bath with the frequencies in Table 5.1.

Instead, good agreement $\rho_{\hat{H}_{\mathcal{E}}} \approx \rho_{\mathcal{E}}$ is consistently found by rescaling the random $\hbar\omega_{\rm osc}$ values according to their geometric mean,

$$\sqrt[\eta]{\prod_{\rm osc=1}^{\eta} \hbar\omega_{\rm osc}} = \hbar\omega = 1, \tag{5.8}$$

as discussed in detail shortly. Eq. 5.8 sets the unit of energy in this paper and also sets the relationship between the collection of variable frequencies $\{\hbar\omega_{\rm osc}\}$ and the degenerate oscillator frequency $\hbar\omega$ assumed in connection with Eq. 5.4. The relation

Eq. 5.8 has previously been noted by Landau and Lifshitz [54] where it was also found to give the necessary link between variable and fixed frequency oscillators in a different context.

The $\hat{H}_{\mathcal{E}}$ that we use with Eq. 5.5 uses the frequencies given in Table 5.1 that come from randomly chosen values that have been rescaled according to Eq. 5.8. The results are robust for other choices of random and rescaled $\{\hbar\omega_{\rm osc}\}$. The density of states $\rho_{\hat{H}_{\mathcal{E}}}$ for this set of frequencies is shown in the histogram boxes in the bottom of Fig. 5.1, and is in excellent agreement with $\rho_{\mathcal{E}}$ of Eq. 5.7. Recall that $\rho_{\mathcal{E}}$ also agrees with the fixed frequency $\rho_{\rm Ein}$ as seen in the top of Fig. 5.1. This demonstrates that Eq. 5.8 gives the desired correspondence between the densities of states for the variable and identical frequency oscillators:

$$\rho_{\hat{H}_{\mathcal{E}}} \approx \rho_{\mathcal{E}} = \rho_{\rm Ein} \tag{5.9}$$

at integer energies $E_{\mathcal{E}} = n_{\rm tot}$ and

$$\rho_{\hat{H}_{\mathcal{E}}} \approx \rho_{\mathcal{E}} \tag{5.10}$$

at non-integer energies (where the single-frequency $\rho_{\rm Ein}$ is undefined in Eq. 5.4). The correspondence between the somewhat random $\rho_{\hat{H}_{\mathcal{E}}}$ and the well-controlled, analytical $\rho_{\mathcal{E}}$ will allow us to determine analytical temperature relationships for our oscillator bath using the relatively simple function $\rho_{\mathcal{E}}$. This is developed in the next section.

$\hbar\omega_1$	$\hbar\omega_2$	$\hbar\omega_3$	$\hbar\omega_4$	$\hbar\omega_5$
0.620 246	0.735 401	1.146 315	1.316 886	1.453 415

TABLE 5.1. Oscillator frequencies in the five harmonic oscillator environment shown to six decimal places.

5.3. Temperature

This rather involved section addresses key questions about the "thermal" character introduced by the small finite bath in our model. Does the standard infinite bath relation $E \sim T$ hold at high energy? What is the low temperature behavior of the finite bath? While sensible notions of temperature will emerge, we will also see that there are anomalies in both of these aspects, related to the finite size of the bath.

We usually think of temperature in terms of a microcanonical ensemble with a very large, effectively infinite bath, so that the temperature is constant. The temperature comes from the standard relation

$$\frac{1}{T} = \frac{\partial S}{\partial E} \tag{5.11}$$

applied to the total system+environment $\mathcal{SE}$ as the density of states is varied with energy. In the situation envisaged in Fig. 5.2, we start by thinking instead of a temperature $T_{\mathcal{E}}$ for the bath environment initially in isolation from the system. There are a multiplicity of initial separate system-bath combinations, each with the same total energy E; an example is the red $\mathcal{SE}$ state pair in the left of Fig. 5.2. Each $\mathcal{SE}$ combination has its own initial system energy $E_{\mathcal{S}}$, bath energy $E_{\mathcal{E}}$, and bath temperature $T_{\mathcal{E}}$. The bath temperature $T_{\mathcal{E}}$ is based on a fixed $E_{\mathcal{E}}$ microcanonical energy that is defined only before the interaction with the system has begun—the system in our simulations starts in a single zero-order state—so there is no meaningful independent system temperature. Then, heat flows between system and bath, leading to a finite change in a temperature that we want to be defined for the final equilibrium state, and perhaps in between as well. The final temperature $T_{\mathcal{SE}}$ after the heat flow comes from the microcanonical ensemble for the total system $\mathcal{SE}$, which consists of

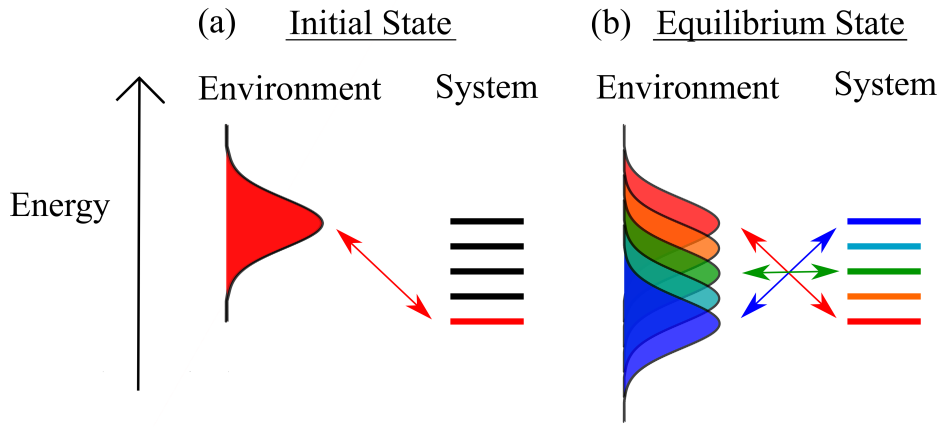

FIGURE 5.2. (a) Schematic example of an $\mathcal{SE}$ initial state with the system in the lowest energy level and the environment in a high-energy Gaussian initial state as described in Section 5.4. The temperature is $T_{\mathcal{E}}(E_{\mathcal{E}})$ from Eq. 5.13. (b) Schematic of the same state after $\mathcal{SE}$ equilibration, where now there is an $\mathcal{SE}$ state pair for each system level, all at the same total $\mathcal{S} + \mathcal{E}$ energy (examples of $\mathcal{SE}$ state pairs are shown by the arrows). The temperature is $T_{\mathcal{SE}}$ from Eq. 5.23, which is the average of the $1/T_{\mathcal{E}}$ across all of the $\mathcal{SE}$ state pairs.

the union of all the system-bath sub-ensembles, all with total $\mathcal{SE}$ energy E, as in the right of Fig. 5.2. An interesting relation Eq. 5.23 will be found to hold between the inverse temperature $1/T_{\mathcal{SE}}$ of the complete ensemble of the $\mathcal{SE}$ total system, and the average of the inverse temperatures $1/T_{\mathcal{E}}$ of the baths of the sub-ensembles. In fact, it will be possible to define a time-varying "master temperature" $T_{\mathcal{SE}}(t)$ in Eq. 5.24 for the time-dependent intermediate state $|\Psi(t)\rangle$ in the equilibration process. Thus, we will obtain a satisfying unified description of all the possible processes of the type in Fig. 5.2.

5.3.1. Temperature for initial isolated environment

First, we develop the temperature $T_{\mathcal{E}}$ for a finite environment that is thermally isolated from the system. (This will turn out to be the initial state temperature in

the time-dependent temperature $T_{\mathcal{SE}}(t)$ to be developed in Section 5.3.3.) We will compare this finite bath to an infinite "true" temperature bath of infinitely many oscillators. The system is in a single zero-order initial state n_0, corresponding to our initial state in Fig. 5.2. The total energy is E, the system has energy $E_{\mathcal{S}} = E_{n_0}$, and the environment has energy $E_{\mathcal{E}} = E - E_{\mathcal{S}}$. The temperature is defined using the standard thermodynamic relation of Eq. 5.11. This is evaluated using the Boltzmann entropy $S = k_B \ln W(n_0, E)$, with $W(n_0, E)$ the number of $\mathcal{SE}$ states $|n_0, \epsilon\rangle$ in a microcanonical energy shell $[E - \delta E/2, E + \delta E/2]$, again with the system in the level n_0. Since n_0 is fixed, $W(E) = \rho_{\mathcal{E}}(E_{\mathcal{E}})\delta E$ is just the number of environment states, where $\rho_{\mathcal{E}}$ in Eq. 5.7 is the smoothed continuous density function describing the density of discrete states in our Hamiltonian $\rho_{\hat{H}_{\mathcal{E}}}$, following Eqs. 5.9 and 5.10. The initial temperature is then related only to the environment, and we will label it $T_{\mathcal{E}}$, and rewrite it in terms of the density $\rho_{\mathcal{E}}$ as

$$\frac{1}{T_{\mathcal{E}}} = \frac{d\rho_{\mathcal{E}}/dE_{\mathcal{E}}}{\rho_{\mathcal{E}}}. \tag{5.12}$$

Using Eq. 5.7 for $\rho_{\mathcal{E}}$ then gives

$$\frac{1}{T_{\mathcal{E}}} = \psi(E_{\mathcal{E}} + \eta) - \psi(E_{\mathcal{E}} + 1) = \sum_{m=1}^{\eta-1} \frac{1}{E_{\mathcal{E}} + m}, \tag{5.13}$$

where $\psi(x) = (d\Gamma(x)/dx)/\Gamma(x)$ is the digamma function. The last equality comes analytically from $\eta - 1$ applications of the recurrence relation [55] $\psi(x) = \psi(x-1) + 1/(x-1)$ to the term $\psi(E_{\mathcal{E}} + \eta)$.

It is not clear just from looking at Eq. 5.13 how our temperature $T_{\mathcal{E}}$ for the finite bath will behave in comparison to standard temperature-energy relations involving an infinite fixed-temperature bath. In the next two subsections we will make this

comparison, using the paradigmatic standard of an average oscillator in an infinite oscillator bath. Section 5.3.1.1 will discuss the convergence of $T_{\mathcal{E}}$ from Eq. 5.13 to the standard temperature-energy relation as the size of the bath is increased, with convergence to the high energy relation $T \sim E$. Section 5.3.1.2 will discuss deviations related to the finite size of the bath, including deviations from $T = 0$ at low energy, and deviations in the heat capacity even at high energy.

5.3.1.1. Comparison of finite and infinite bath: energy-temperature relation

The heat bath described above is a finite collection of oscillators. We will compare this to a true temperature bath consisting of an infinite collection of oscillators. For this, we use the energy-temperature relation from Einstein and Planck for a harmonic oscillator in an infinite temperature bath:

$$\langle n_{\text{osc}} \rangle = \frac{1}{e^{1/T} - 1} \tag{5.14}$$

($\hbar\omega = 1$ and $k_B = 1$), where $\langle n_{\text{osc}} \rangle$ is the expected number of energy quanta in the oscillator. (This relation was obtained by Einstein in his heat capacity model [56] by treating a solid as a collection of identical oscillators in an exterior temperature bath using the canonical ensemble. The result is the same regardless of the ensemble setup, microcanonical or canonical.) We will find that our $T_{\mathcal{E}}$ for the finite bath behaves much like a standard temperature, but also has significant differences from the Einstein relation Eq. 5.14, leading also to deviations in the heat capacity from the Einstein model. However, we also find that $T_{\mathcal{E}}$ agrees properly with Eq. 5.14 in the limit of a large number of oscillators. The development is based on the correspondence

$\rho_{\mathcal{E}} \approx \rho_{\hat{H}_{\mathcal{E}}}$ in Eqs. 5.9 and 5.10, recalling the remarks there about the analytical function $\rho_{\mathcal{E}}$.

These relationships are represented in Fig. 5.3 and later for the heat capacity in Fig. 5.4. It will be instructive to consider the total energy of the "Einstein oscillator" including both energy quanta and the zero-point energy, $\langle E_{\rm osc}^{(+{\rm zp})} \rangle = \langle n_{\rm osc} \rangle + 1/2$. The orange (light gray) curve in Fig. 5.3 shows the relationship between $\langle E_{\rm osc}^{(+{\rm zp})} \rangle$ and temperature based on Eq. 5.14. The curve begins at the zero-point energy at $T = 0$, then quickly approaches the well-known quantum equipartition relation

$$\lim_{\langle n_{\rm osc} \rangle \to \infty} T = \langle n_{\rm osc} \rangle + \frac{1}{2} = \langle E_{\rm osc}^{(+{\rm zp})} \rangle, \tag{5.15}$$

shown by the purple (medium gray) line in the background of the figure.

For comparison, Fig. 5.3 also shows the relationship between $\langle E_{\rm osc} \rangle + 1/2$ and $T_{\mathcal{E}}$ for finite oscillator baths with various η, again, based on the correspondence $\rho_{\mathcal{E}} \approx \rho_{\hat{H}_{\mathcal{E}}}$ in Eqs. 5.9 and 5.10. The average energy per oscillator from energy quanta $\langle E_{\rm osc} \rangle \equiv E_{\mathcal{E}}/\eta$ is the analog for our bath of $\langle n_{\rm osc} \rangle$ for the Einstein oscillator in Eqs. 5.14 and 5.15. The quantity 1/2 then shifts this up by the Einstein oscillator zero-point energy to allow for a direct comparison in the figure between our $T_{\mathcal{E}}$ and the temperature in the Einstein model. In general, the exact zero-point energy in our model will not be 1/2 in our units (unlike the Einstein model), but will instead depend on the frequencies of the oscillators. Here, the 1/2 is an arbitrary added quantity for the finite baths, inserted for comparison to the Einstein bath.

For the $\eta = 5$ bath we use for our simulations, shown by the black solid curve, the temperature behavior is significantly different than the orange (light gray) infinite bath curve. As we increase the number of oscillators η we find that the curves get closer to the standard orange curve for an infinite bath. For example, the dashed-

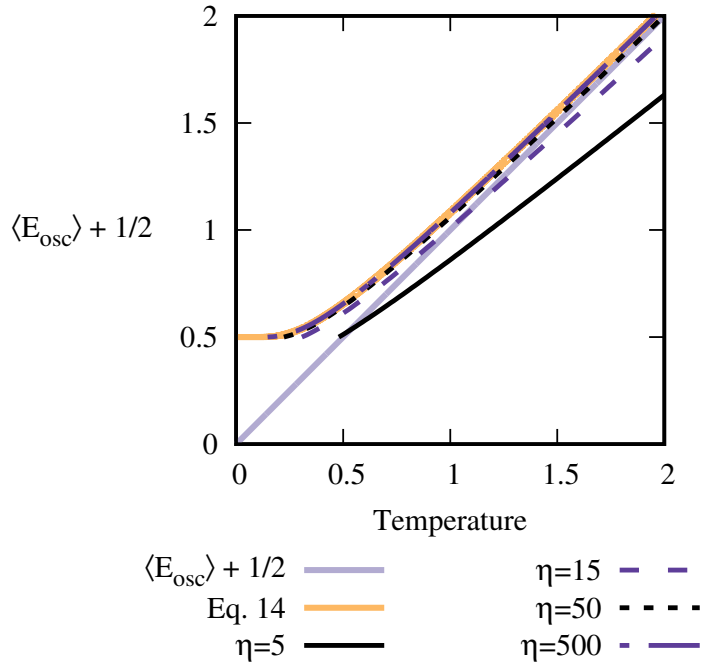

FIGURE 5.3. Temperatures $T_{\mathcal{E}}$ converge to the Einstein solid temperature relation as the number of bath oscillators $\eta \to \infty$. Deviations outside this limit are due to the finite size of the bath.

dotted dark purple (dark gray) line for $\eta = 500$ oscillators rests on top of the orange line for the infinite bath T. The convergence towards Eq. 5.14 with increasing η confirms that our temperature gives the standard relation for an infinite bath in the thermodynamic limit $\eta \to \infty$, as expected with a reasonable temperature definition. With this in mind, we next discuss in more detail the much more interesting question of anomalies in temperature behavior associated with small number of oscillators η in the finite bath.

5.3.1.2. Anomalous temperature behavior associated with a very small bath

The very small size of the $\eta = 5$ bath leads to anomalous temperature behavior at both high and low energies, as seen in Fig. 5.3. First, consider the behavior of $T_{\mathcal{E}}$ at low energies. Recall that we treat this as a continuous variable that will be related to the continuous variable $E_{\mathcal{E}}$ in Eq. 5.13. The temperatures for all of the finite η oscillator baths in Fig. 5.3 are nonzero at the minimum value of energy 1/2 in the figure (when $E_{\mathcal{E}} = 0$ in Eq. 5.13, the rationale for the 1/2 being that given in the last subsection). The non-zero minimum temperatures seem to be an unavoidable consequence of combining a finite bath with the standard temperature definition Eq. 5.12. The temperature is only zero when $d\rho_{\mathcal{E}}/dE_{\mathcal{E}} = \infty$ in Eq. 5.12—an evidently impossible condition for a finite bath with a limited number of states. However, as seen in Fig. 5.3, the curves for increasing η converge to the standard infinite bath relation in which $T = 0$ at the minimum energy 1/2.

At high energy, $T_{\mathcal{E}}$ approaches the asymptotic relation

$$\lim_{E_{\mathcal{E}} \to \infty} T_{\mathcal{E}} = \frac{E_{\mathcal{E}} + \eta/2}{\eta - 1} = \left(\langle E_{\text{osc}} \rangle + \frac{1}{2} \right) \frac{\eta}{\eta - 1}, \tag{5.16}$$

where again $\langle E_{\text{osc}} \rangle = E_{\mathcal{E}}/\eta$ refers to the average energy per non-identical oscillator of the finite bath, although it also applies to an infinite "Einstein bath" of identical oscillators. Eq. 5.16 comes from the analytical limit of the right-hand side of Eq. 5.13, which we evaluated using *Mathematica*. Eq. 5.16 differs from the high-energy Einstein relation Eq. 5.15 by the factor of $\eta/(\eta - 1)$. This difference is negligible in the thermodynamic limit $\eta \to \infty$ but very significant for small η, as seen by the differing slopes for the solid black and orange (light gray) lines in Fig. 5.3 at high energy.

The differing slopes correspond to a difference in heat capacities

$$C = \frac{d\langle E_{\rm osc}\rangle}{dT} \tag{5.17}$$

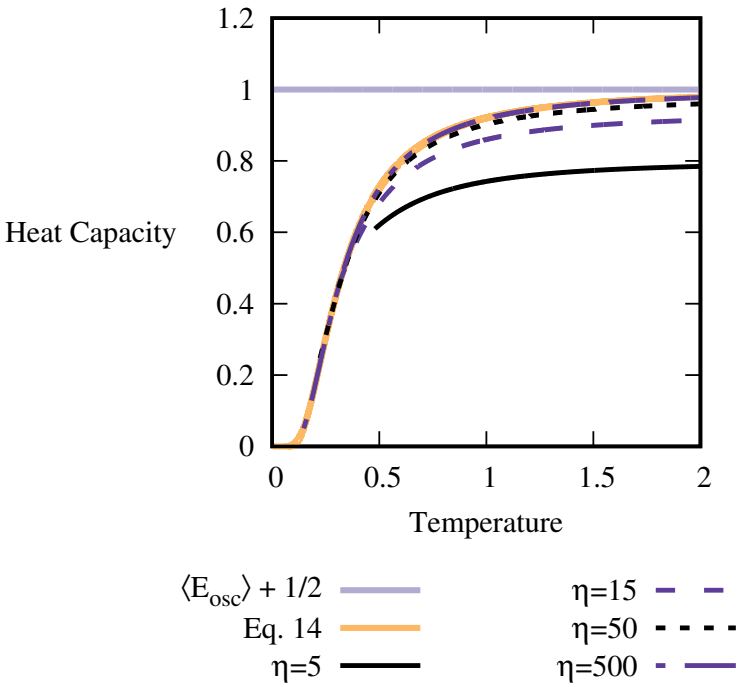

FIGURE 5.4. Heat capacities for the energy-temperature curves in Fig 5.3.

between the different temperature-energy relations. The heat capacities for all of the temperature-energy curves in Fig. 5.3 are plotted in Fig. 5.4. The heat capacity curves are similar to the standard Einstein behavior at low temperature, but they are systematically lower at high temperature, where they approach asymptotic values $C \to (\eta{-}1)/\eta < 1$, less than both the Einstein relation and the standard equipartition result.

We will find in Section 5.7 that the anomalous temperature behavior seen in Fig. 5.3 is critical in obtaining the correct thermalized Boltzmann distribution for the

system: the anomalous scaling behavior $\sim \eta/(\eta-1)$ in the figure must be taken into account to correctly describe the equilibrium $\mathcal{S}$ Boltzmann distribution and the $\mathcal{SE}$ thermodynamic behavior.

5.3.2. System-environment microcanonical temperature

We now consider the equilibrium $\mathcal{SE}$ state and the temperature $T_{\mathcal{SE}}$ for the complex entangled state $|\Psi(t)\rangle$ shown schematically in the right of Fig. 5.2; this will be the equilibrium value of the time-dependent temperature $T_{\mathcal{SE}}(t)$ to be developed in Section 5.3.3.

$T_{\mathcal{SE}}$ is defined following the same reasoning leading to Eq. 5.12, giving

$$\frac{1}{T_{\mathcal{SE}}(E)} = \frac{d\rho_{\mathcal{SE}}/dE}{\rho_{\mathcal{SE}}}. \tag{5.18}$$

To evaluate the temperature we will examine $\rho_{\mathcal{SE}}$ as the density of zero-order states, just as we did for the isolated bath temperature $\rho_{\mathcal{E}}$. While there is some arbitrariness in doing this now with $\rho_{\mathcal{SE}}$, it is operationally simple, and seems at least as reasonable a choice as other possibilities. It is consonant with what we have done with $\rho_{\mathcal{E}}$, and will lead to the simple result Eq. 5.23.

The total density of $\mathcal{SE}$ zero-order states at energy E has contributions from all of the $\mathcal{SE}$ state pairs that are in the microcanonical energy shell $E - \delta E/2 \leq E_{\mathcal{S}} + E_{\mathcal{E}} \leq E + \delta E/2$, that is, each of the $\mathcal{SE}$ state pairs shown schematically in Fig. 5.2. The total density of $\mathcal{SE}$ states is the sum of bath densities that pair with each system level n at the total energy $E = E_{\mathcal{E}} + E_n$,

$$\rho_{\mathcal{SE}}(E) = \sum_n \rho_{\mathcal{E}}(E - E_n). \tag{5.19}$$

The $\mathcal{SE}$ temperature can then be written as

$$\frac{1}{T_{\mathcal{SE}}(E)} = \sum_n \frac{d\rho_{\mathcal{E}}(E-E_n)/dE}{\sum_m \rho_{\mathcal{E}}(E-E_m)}. \tag{5.20}$$

The derivatives can be rewritten in terms of $\rho_{\mathcal{E}}$ and $T_{\mathcal{E}}$ using Eq. 5.12, giving

$$\frac{1}{T_{\mathcal{SE}}(E)} = \sum_n \frac{\rho_{\mathcal{E}}(E-E_n)}{\sum_m \rho_{\mathcal{E}}(E-E_m)} \frac{1}{T_{\mathcal{E}}(E-E_n)}. \tag{5.21}$$

The fraction involving the densities gives the number of microcanonical states with the system in the level E_n relative to the total number of microcanonical states. This is simply the microcanonical probability of the system level E_n,

$$\frac{\rho_{\mathcal{E}}(E-E_n)}{\sum_m \rho_{\mathcal{E}}(E-E_m)} = p_{\text{micro}}(E_n). \tag{5.22}$$

Putting this into Eq. 5.21 gives the simple result

$$\frac{1}{T_{\mathcal{SE}}(E)} = \sum_n \frac{p_{\text{micro}}(E_n)}{T_{\mathcal{E}}(E-E_n)} = \left\langle \frac{1}{T_{\mathcal{E}}(E-E_n)} \right\rangle_{\text{micro}}. \tag{5.23}$$

Equation 5.23 says that the reciprocal temperature $1/T_{\mathcal{SE}}$ for the full $\mathcal{SE}$ microcanonical ensemble is simply the average of the reciprocal environment temperatures $1/T_{\mathcal{E}}$ for each of the $\mathcal{SE}$ state-pairs within the microcanonical ensemble.

It is interesting that the derivation of $T_{\mathcal{SE}}$ in Eqs. 5.18-5.23 used only the standard temperature definition in Eqs. 5.12 and 5.18 and the choice of the zero-order basis for the densities of states $\rho_{\mathcal{E}}$ and $\rho_{\mathcal{SE}}$, used to formulate the sum in Eq. 5.19. In this respect the relation Eq. 5.23 is completely general, so it could also be used for other $\mathcal{SE}$ thermodynamic models which could potentially be much different from the simple oscillator model we use here.

5.3.3. Continuously varying time-dependent temperature

The temperature relations in the previous sections were derived using the standard expression Eq. 5.11 for the microcanonical ensemble, applied to the initial and final equilibrium states of the $\mathcal{SE}$ universe. It is useful to consider a time-dependent generalization of the microcanonical temperature that can be defined *during* thermalization. This uses time-dependent system probabilities from the system reduced density operator $\hat{\rho}_{\mathcal{S}}(t)$ in place of the microcanonical probabilities in Eq. 5.23, giving

$$\frac{1}{T_{\mathcal{SE}}(E,t)} = \sum_n \frac{\rho_{\mathcal{S}}^{n,n}(t)}{T_{\mathcal{E}}(E-E_n)} = \left\langle \frac{1}{T_{\mathcal{E}}(E-E_n)} \right\rangle_{\hat{\rho}_{\mathcal{S}}(t)} \tag{5.24}$$

where $\rho_{\mathcal{S}}^{n,n}$ is the probability of the system energy level E_n. Note that this time-dependent temperature agrees with the initial temperature $T_{\mathcal{E}}$ in Eq. 5.13 and with the final temperature $T_{\mathcal{SE}}$ in Eq. 5.23. $T_{\mathcal{SE}}(t)$ is the "master temperature" that describes the entire equilibration and thermalization process. Using Eq. 5.24 we will be able to follow the time-dependent changes in temperature as $\mathcal{S}$ and $\mathcal{E}$ begin in the initial state, exchange energy during thermalization, and eventually reach thermal equilibrium. This $T_{\mathcal{SE}}(t)$ is what we will be looking at as the "temperature" throughout the simulation.

5.4. Initial states for the simulations

The calculations start at $t = 0$ with separable $\mathcal{SE}$ initial states

$$|\Psi_{n_0}\rangle = |n_0\rangle|\epsilon_0\rangle, \tag{5.25}$$

where the initial system level is $|n_0\rangle$ and the initial environment state $|\epsilon_0\rangle$ has Gaussian distributed basis state probabilities

$$|\epsilon_0\rangle \sim \sum_{\epsilon} \exp\left(-\frac{(E_\epsilon - E_{\epsilon_0})^2}{4\sigma_{\mathcal{E}}^2}\right)|\epsilon\rangle, \tag{5.26}$$

with $\sigma_{\mathcal{E}} = 0.5$ (the results are similar for other $0.1 \leq \sigma_{\mathcal{E}} \leq 1$ that we have tested). In Eq. 5.26 the environment state is centered at an energy

$$E_{\epsilon_0} = E_0 - E_{n_0} \tag{5.27}$$

which varies with n_0, so that we are able to generate states that have the same nominal $\mathcal{SE}$ central energy $E_0 = E_{\epsilon_0} + E_{n_0}$ but different system levels n_0. This will be useful for examining temperature equilibration, where the final state in principle will depend on the total energy but not on n_0. An example of the total probability per unit energy for an $n_0 = 4$ initial state $|\Psi_{n_0}\rangle$ at energy $E_0 = 5$ is shown in the top of Fig. 5.5. Each histogram bar in the figure shows the sum of $\mathcal{SE}$ basis states probabilities within the surrounding zero-order energy unit; the actual state is naturally much more complex in the zero-order basis. Note the logarithmic scale in the figure; the state is pretty sharply peaked around its nominal central energy. A slight asymmetry can be observed about the central energy $E_0 = 5$. This is because there are more basis states per unit energy above E_0 than below due to the increasing environment density of states. The asymmetry makes the average energy of the state slightly larger than the nominal energy E_0 in a way that depends on the environment density, which in turn depends on the environment energy E_{ϵ_0} and the system level n_0. This gives a slightly different initial state energy for each n_0, but the energies are close to the same.

We next consider the time evolution of this state, first with a random matrix coupling which we will find leads to pathological behavior, then with a more refined coupling that will be found to give physically satisfactory results.

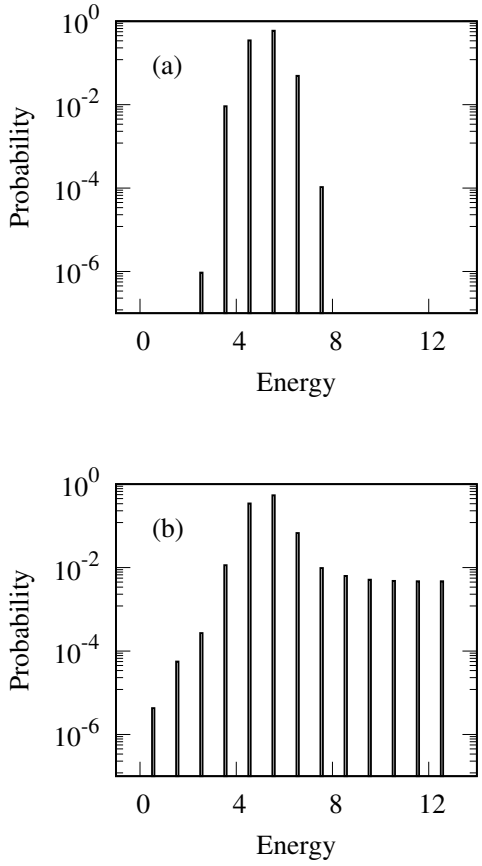

FIGURE 5.5. Histogram of total quantum state probabilities per unit energy for an initial Gaussian state (a) and corresponding time-evolved equilibrium state (b) with a random matrix coupling with $k = 0.0027$. The total probability per unit energy does not converge to zero at high energy for the equilibrium state, indicating a problem with the coupling.

5.5. Random matrix coupling and runaway thermalization dynamics

In this section we begin developing the quantum dynamics with the coupling Hamiltonian $\hat{H}_{\mathcal{SE}}$ of Eq. 5.1. We begin with a standard type of coupling, the

random matrix coupling, used to model systems with classically chaotic dynamics [20], and often invoked in accounting for the existence of thermalization in quantum thermodynamics [20, 36, 37]. We used this in earlier simulations [1, 2, 6] with good results. However, we find here that with the introduction of a variable temperature, the random coupling introduces pathological behavior of runaway spreading of the wave packet. Furthermore, the random coupling is a serious limitation in itself—many important real systems are not well modeled by random couplings, for example in models of coupled molecular vibrational modes [52, 53, 57, 58]. Thus, to understand thermalization for more realistic systems, we will want to explore more discriminating coupling forms.

The construction of $\hat{H}_{\mathcal{SE}}$ in Eq. 5.1 as a random matrix coupling begins with a matrix $\hat{R}$ filled with off-diagonal elements

$$\langle n|\langle\epsilon|\hat{R}|\epsilon'\rangle|n'\rangle = R_{n\epsilon,n'\epsilon'}. \tag{5.28}$$

The $R_{n\epsilon,n'\epsilon'}$ are random complex numbers $R_{n\epsilon,n'\epsilon'} = X_{n\epsilon,n'\epsilon'} + iY_{n\epsilon,n'\epsilon'}$ as in Ref. [37]. This is more generic than our previous work in Refs. [1, 2, 6], where we used real $R_{n\epsilon,n'\epsilon'}$ to minimize numerical effort. We generate the real and imaginary parts $X_{n\epsilon,n'\epsilon'}$ and $Y_{n\epsilon,n'\epsilon'}$ each as random numbers from a Gaussian distribution with standard deviation $\sigma = 1$ with probabilities

$$p(X_{n\epsilon,n'\epsilon'}) \sim e^{-X^2_{n\epsilon,n'\epsilon'}/2\sigma^2}, \tag{5.29}$$

and similarly for the imaginary parts $Y_{n\epsilon,n'\epsilon'}$. We set the diagonal elements to zero to preserve the oscillator energies in the zero-order basis, as was done previously in Ref. [2]. The interaction Hamiltonian is then constructed by multiplying $\hat{R}$ by a

parameter k that sets the overall coupling strength, $\hat{H}_{\mathcal{SE}} = k\hat{R}$. This multiplication scales the random numbers so that their standard deviation becomes $\sigma = k$, consistent with the description in our earlier work [1, 2, 6] (e.g. in Eq. 10 of Ref. [6]). We chose k to be the size of the average level spacing of the system-environment universe at our initial state energy $E_0 = 5$, since we have found that smaller k do not give proper thermalization.

Fig. 5.5 shows time evolution with this coupling. With this coupling the initial Gaussian state associated with the top panel evolves in time to the state of the bottom panel. The time evolution evidently leads to runaway spreading of the wavepacket with probability in high energy states that does not appear to be converging to zero. This is not how a physically reasonable state should behave.

It is important to understand why this coupling causes runaway behavior here, because it was not observed, at least so prominently, in our earlier simulations with a fixed temperature bath. The coupling causes some spreading of the wavepacket to basis states of all energies, with the amount of probability per basis state decreasing rapidly as the states get farther off resonance from the initial state energy $E_0 = 5$. This might seem to entail decreasing probabilities at the top edge of the basis. However, the number of $\mathcal{E}$ basis states per unit energy increases very rapidly with increasing energy in the variable temperature bath, as shown in Fig. 5.1, so that many more basis states contribute to the total probability in each successive energy unit. Taken together, the total probability per unit energy doesn't converge to zero as it should, as clearly seen in Fig. 5.5. This runaway coupling is a problem that needs to be addressed next.

5.6. Selective coupling "tames" thermalization dynamics

We will see that by defining a suitably much more selective coupling, physical results are obtained with both thermalization and contained spreading of the time-dependent quantum $\mathcal{SE}$ state. The basic idea is to "tame" the coupling to limit the range of transitions, especially to high energy states.

As before with the random matrix coupling, we begin with a coupling constant k and a random matrix $\hat{R}$ as in Eq. 5.28. To construct $\hat{H}_{\mathcal{SE}}$, we take each individual matrix element of $k\hat{R}$ and multiply it by an exponential "taming" factor that depends on the quantum number differences between the coupled states:

$$\langle n|\langle\epsilon|\hat{H}_{\mathcal{SE}}|\epsilon'\rangle|n'\rangle = kR_{n\epsilon,n'\epsilon'} \exp\left(-\gamma_{\mathcal{S}}|\Delta n| - \gamma_{\mathcal{E}} \sum_{\text{osc}=1}^{\eta} |\Delta n_{\text{osc}}|\right) \tag{5.30}$$

where $|\Delta n| = |n - n'|$ is the quantum number difference between the coupled system states and $\sum_{\text{osc}} |\Delta n_{\text{osc}}|$ is the total quantum number difference for the individual oscillators in the coupled environment states. The parameters $\gamma_{\mathcal{S}}$ and $\gamma_{\mathcal{E}}$ suppress the coupling between $\mathcal{SE}$ states depending on how much they vary in quantum number, for example the coupling that moves one quantum between the system and bath is stronger than the coupling that moves two quanta. This limits the strength of transitions to high energy states, since they typically differ significantly in their quantum number distributions, thereby addressing the runaway problem.

A coupling scheme similar to Eq. 5.30 has been put forward by Gruebele [52, 53] in the context of intramolecular vibrational energy transfer, where he has argued that the exponential quantum-number dependence of the coupling is an approximate generic feature in molecular vibrational systems. Deutsch [20] has also said that a similar exponentially-tamed random matrix coupling can be obtained through a

second-order perturbation theory analysis and that the exponential taming is needed to prevent runaway behavior in large quantum thermodynamic systems.

The tamed coupling has three parameters $k, \gamma_{\mathcal{S}}$, and $\gamma_{\mathcal{E}}$ that we choose somewhat arbitrarily for our model, with an aim towards obtaining physical thermalization behavior. The k sets the "baseline" coupling strength; if k is too small then thermalization will be impossible. The $\gamma_{\mathcal{E}}$ restricts the $\mathcal{E}$ transitions to address the runaway problem; it must be large enough to restrict the spreading with large energy differences, as needed for convergence, but also small enough to allow transfer between nearby $\mathcal{E}$ levels, as needed for thermalization. The $\gamma_{\mathcal{S}}$ controls how easily the system can transition between its levels; it must be small enough that all of the system levels can be accessed during the dynamics.

In our simulations we choose a coupling constant $k = 0.15$. This is much larger than the k we used with the random matrix coupling, to balance the exponential taming factors. We choose a relatively small system taming factor $\gamma_{\mathcal{S}} = 0.125$ and a large environment factor $\gamma_{\mathcal{E}} = 1$. This parameter choice gives good system thermalization behavior while limiting the environment transitions strongly enough to get good convergence within our basis. The effectiveness of this coupling and parameter choice is demonstrated by the time-evolved state in Fig. 5.6. The state corresponding to this figure began as an initial Gaussian state as seen in the top of Fig. 5.5, then it was evolved in time to equilibrium under the full Hamiltonian Eq. 5.1 containing the tamed coupling interaction $\hat{H}_{\mathcal{SE}}$ from Eq. 5.30. As seen in the histogram boxes in Fig. 5.6, the total probability per unit energy is converging to zero at the top edge of the basis. This shows that the tamed coupling has fixed the runaway problem of the random matrix coupling that was seen in the bottom of

Fig. 5.5. Using the tamed coupling we found good convergence with a maximum $\mathcal{SE}$ energy $E^{max} = 13$ for the simulations in this paper.

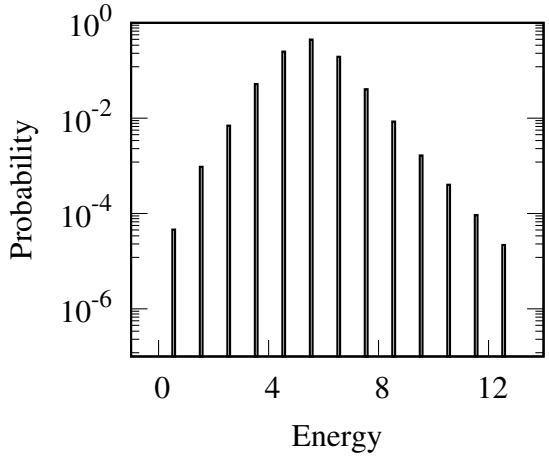

FIGURE 5.6. Time-evolved state with the "tamed" coupling Eq. 5.30 has probabilities that converge to zero at high energy. The initial state was the same as panel (a) of Fig. 5.5.

The tamed coupling is a physically reasonable choice needed to solve a real problem of runaway behavior with the random matrix coupling in the oscillator bath model. Tamed couplings similar to ours in Eq. 5.30 have a long history of successful use in modeling molecular vibrational dynamics [52, 53] similar to our oscillator model here. A type of tamed coupling can also be understood in Franck-Condon factors in vibronic transitions, where couplings decrease for greater vibrational quantum number differences between coupled vibrational modes. In sum the tame coupling of Eq. 5.30 is a physically realistic choice that overcomes a significant problem with the simpler random matrix coupling and gives physical results in our oscillator bath model.

5.7. Results: equilibration and thermalization in the simulations

Now we examine key aspects of the system dynamics during the approach to equilibrium: behavior of the time-dependent temperature; and the question of equilibrated Boltzmann distribution with thermalization. Is there thermodynamic-like behavior? But do we also see anomalous small-size temperature effects suggested by Fig. 5.3?

5.7.1. Variable temperature and small-size effects

First we consider the computed time evolution of a set of initial states, constructed as described in Section 5.4 with different initial system levels n_0 but the same nominal energies $E_0 = 6$. The total energies for the various n_0 are somewhat larger, as discussed in Section 5.4, with $6.116 \leq \langle \hat{H} \rangle \leq 6.156$, where $\hat{H}$ is the total Hamiltonian Eq. 5.1. Taking $E = \langle \hat{H} \rangle$ in Eq. 5.23 we get for these states a narrow range of equilibrium microcanonical temperatures $1.912 \leq T_{\mathcal{SE}} \leq 1.922$. Roughly speaking, we can think of all the states as sharing the common energy $E \approx 6.14$, hopefully corresponding in the simulations to a common final equilibrium temperature $T_{\mathcal{SE}} \approx 1.92$, where $1/T_{\mathcal{SE}}$ is the weighted average over all the initial state $1/T_{\mathcal{E}}$ at the common energy E, as in Eq. 5.23. We therefore test in the simulations whether the time-dependent temperature $T_{\mathcal{SE}}(t)$ of Eq. 5.24 equilibrates to the common temperature $T_{\mathcal{SE}} \approx 1.92$.

Fig. 5.7 shows the time-dependent behavior of the temperatures $T_{\mathcal{SE}}(t)$ for each of the initial states n_0. For each n_0, the temperature begins in its respective value for an isolated system and environment, $T_{\mathcal{SE}}(t = 0) = T_{\mathcal{E}}$ (from Eqs. 5.24 and 5.13). Time evolution takes the temperatures to equilibrium, where they do in fact fluctuate

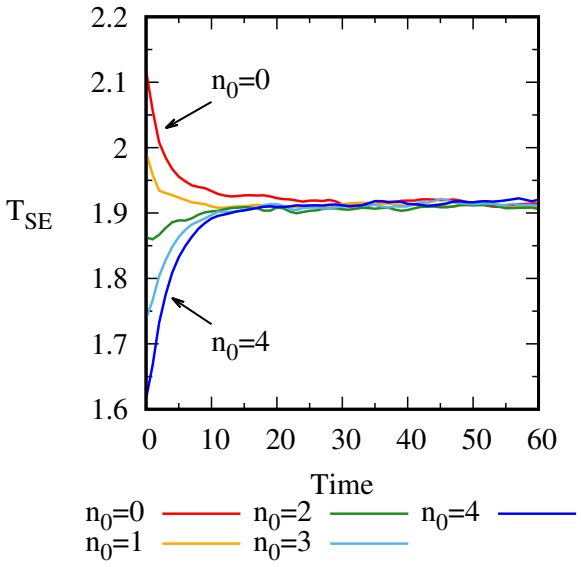

FIGURE 5.7. Time-dependent temperatures $T_{\mathcal{SE}}(t)$ (Eq. 5.24) for a series of calculations with approximately the same $\mathcal{SE}$ energy $E \approx 6.14$ but different starting $\mathcal{S}$ levels n_0. Each temperature evolves to approximately the same final temperature $T_{\mathcal{SE}} \approx 1.92$ from Eq. 5.23.

around the common approximate value $T_{\mathcal{SE}} \approx 1.92$. Thus, we are getting the common microcanonical $T_{\mathcal{SE}}$ value corresponding to energy $E \approx 6.14$, as hoped for. This result validates the path of development in Section 5.3 regarding a variable temperature. Observed small temperature fluctuations at equilibrium are due to the time-dependent fluctuations in the system density operator $\hat{\rho}_{\mathcal{S}}(t)$, whose behavior will be discussed shortly in Section 5.7.2.

It is a noteworthy prediction based on the considerations of Section 5.3 that the finite bath equilibrium temperatures in Fig. 5.7 should be considerably higher than would be expected using the infinite bath T from Eq. 5.14 based on the average number of quanta per degenerate oscillator $\langle n_{\text{osc}} \rangle = \langle E_{\text{osc}} \rangle$. To test this, we calculated $\langle E_{\text{osc}} \rangle = \langle E_{\mathcal{E}} \rangle / \eta$ as the time-averaged equilibrium value for times $30 < t \leq 60$ averaged over all of the simulations shown in Fig. 5.7, giving $\langle E_{\text{osc}} \rangle = 1.117 \pm 0.004$.

The infinite bath limit temperature Eq. 5.14 from this $\langle E_{\rm osc}\rangle$ is $T = 1.564 \pm 0.004$, much smaller than our temperature $T_{\mathcal{SE}} = 1.92$. This is because the finite bath temperatures $T_{\mathcal{E}}$ in Eq. 5.13 (which go into the calculation of the $T_{\mathcal{SE}}$ via Eq. 5.23) increase more rapidly with energy than the infinite bath T, as was seen in Fig. 5.3. Thus, the anomalous temperature scaling of the small environment is demonstrably evident from this analysis of Fig. 5.7. We will have more to say about the anomalous temperature in the next subsection.

5.7.2. Approach to thermal equilibrium and anomalous size effects

Next, we consider the behavior of the system in the approach to thermal equilibrium. Fig. 5.8 shows an example of the time-dependent system probabilities $\rho_{\mathcal{S}}^{n,n}$ from the reduced density operator for an initial $\mathcal{S}$ level $n_0 = 0$ (the dynamics are similar for the other n_0). As the state begins to evolve in time, much of the initial state probability is quickly lost to the other levels, followed by a much slower decay to the equilibrium Boltzmann distribution marked by the dotted lines. The behavior can be fit by an empirical power law

$$\rho_{\mathcal{S}}^{n_0,n_0}(t) = \frac{1}{\sqrt{1+(t/\tau)^{\delta}}}\left(1 - \frac{e^{-E_{n_0}/T_{\mathcal{SE}}}}{Z}\right) + \frac{e^{-E_{n_0}/T_{\mathcal{SE}}}}{Z} \tag{5.31}$$

where τ and δ are fit parameters and $\exp(-E_{n_0}/T_{\mathcal{SE}})/Z$ is the equilibrium Boltzmann probability at the temperature $T_{\mathcal{SE}}$, as will be discussed further shortly. Power law decays have been discussed by Gruebele [53, 59] as a generic feature in molecular vibrational systems that can be described by couplings similar to our Eq. 5.30. The decay describes the nearly exponential drop of the initial state n_0 probability at short times and the longer decay to equilibrium. The other levels n reach equilibrium at different timescales depending on how far they are from the initial level $n_0 = 0$, for

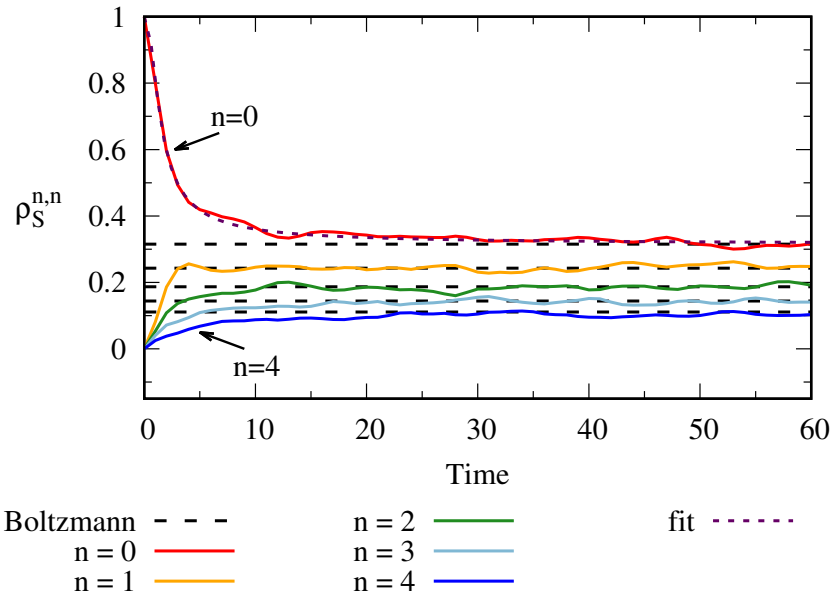

FIGURE 5.8. System level probabilities evolve in time to the Boltzmann distribution at temperature $T_{\mathcal{SE}}(E = \langle \hat{H} \rangle)$ from Eq. 5.23. The decay of the initial state $n_0 = 0$ is described by Eq. 5.31 with $\tau = 1.02 \pm 0.03$ and $\delta = 2.38 \pm 0.06$.

example, $n = 1$ reaches its equilibrium probability relatively quickly whereas it takes much longer for the $n = 4$ level. This stands in contrast to the dynamics under the simple random matrix coupling, where each system level evolves at approximately the same rate [6], without any sense of "proximity" between nearby energy levels that facilitates their energy transfer. Beyond simply being essential to converge the calculations, as discussed in Section 5.6, it seems to us that the tamed coupling is also giving a much more realistic dynamics.

At long times, the system level probabilities fluctuate about a Boltzmann-appearing distribution $\rho_{\mathcal{S}}^{n,n} \sim \exp(-E_n/T_{\mathcal{SE}})$ at the temperature $T_{\mathcal{SE}}$, shown as a black dotted line for each E_n. The agreement with the Boltzmann distribution at $T_{\mathcal{SE}}$ is examined in Fig. 5.9 across a range of initial state energies $E = \langle \hat{H} \rangle$ and corresponding temperatures listed in Table 5.2. The time-averaged system

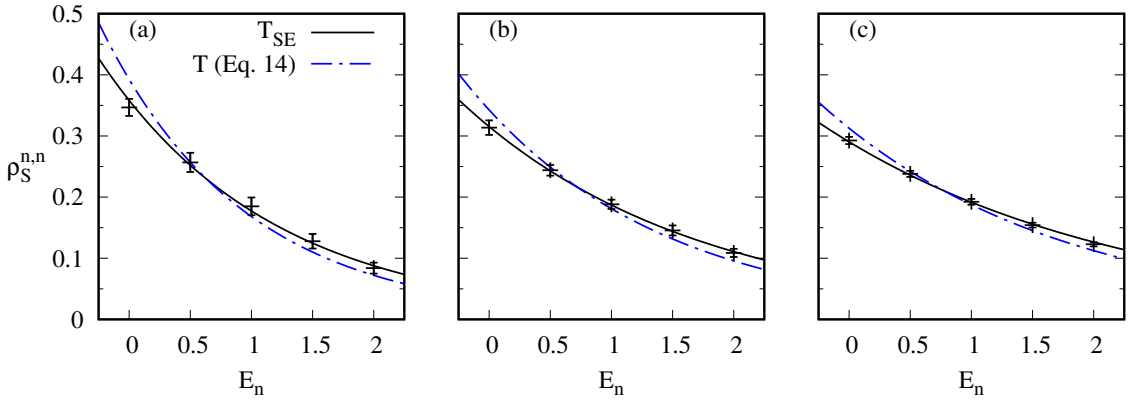

FIGURE 5.9. Time-averaged equilibrium system probabilities for three initial states (a), (b), and (c) with the energies and temperatures in Table 5.2. The Boltzmann distributions $\rho_{\mathcal{S}}^{n,n} \sim \exp(-E_n/T_{\mathcal{SE}})$ at the analytical temperatures $T_{\mathcal{SE}}$ give very good descriptions of the system level probabilities $\rho_{\mathcal{S}}^{n,n}$, while the Boltzmann distributions at the infinite bath T do not.

probabilities from the simulations are in very good agreement with the analytical Boltzmann distributions at temperatures $T_{\mathcal{SE}}$ from Eq. 5.23. For comparison, in Fig. 5.9 we also show the Boltzmann distributions for the infinite bath temperatures T calculated for the states, based on the average energy per bath oscillator observed in the simulations, see Table 5.2 and the discussion in the last paragraph of Section 5.7.1. The resulting temperatures are systematically lower than the $T_{\mathcal{SE}}$ values, and the corresponding Boltzmann distributions do a poor job of describing the system probabilities. Thus, the observed thermalization to $T_{\mathcal{SE}}$ strongly reinforces that this is the correct thermodynamic temperature to describe the total system $\mathcal{SE}$.

At this point it is appropriate to remark on the question of "eigenstate thermalization" in our simulations. The eigenstate thermalization hypothesis (ETH), that eigenstates of a suitable system-environment Hamiltonian reflect thermal properties [20, 21, 23], is widely regarded as an explanation for thermalization phenomena. ETH is often justified through an appeal to chaotic dynamics of the

kind that classically corresponds to a random matrix Hamiltonian. Chaotic dynamics become less certain the more that there is a "taming" of the coupling, as used in this paper to get convergence of the dynamics, and ETH thereby becomes less certain as well. Nonetheless, all of our initial states thermalize to their expected temperatures, and this is consistent with ETH. In future work, we plan to explore the breakdown of ETH as reduced coupling strength makes questionable chaotic dynamics, ETH behavior, and thermalization itself.

Another point worth remark is alternatives to the random matrix-based couplings used in this paper. Simple couplings based on linear combinations of raising and lowering operators are used in many quantum thermodynamic investigations [23]. Accordingly, we have run calculations where we adopt a linear $k\hat{x}_i\hat{x}_j$ coupling. We find that this gives controlled spreading with semi-quantitative thermalization. However, in comparison the thermalization is significantly better with the random matrix tamed coupling calculations reported above. The likely reason the random matrix works better for our setup is that our five-oscillator bath has approximate frequency resonances. This is typical of many physical systems, e.g. a molecule embedded in a bath, which will almost inevitably have such "anharmonic resonances." A random coupling will better capture the effects of these resonances. On the other hand, there are systems, e.g. of coupled bosons, where the $\hat{x}_i\hat{x}_j$ type coupling is more appropriate. Based on our calculations, we believe that variable temperature baths can be devised appropriate to a variety of physical situations in "tailor-made" fashion.

5.8. Summary and prospects

This paper has considered a quantum description of energy flow from a system into a very small variable temperature bath. We defined a system, consisting of a

State	E	$T_{\mathcal{SE}}$	$\langle E_{\rm osc}\rangle$	T (Eq. 5.14)
(a)	4.148	1.422	0.750 ± 0.005	1.180 ± 0.006
(b)	6.118	1.913	1.121 ± 0.003	1.568 ± 0.003
(c)	8.099	2.406	1.499 ± 0.002	1.957 ± 0.002

TABLE 5.2. Energy and temperature data for Fig. 5.9. The energies $E = \langle \hat{H} \rangle$ are from the full Hamiltonian in Eq. 5.1 and the $T_{SE}(E)$ were calculated from Eq. 5.23. The average bath-oscillator energies $\langle E_{\rm osc}\rangle = E_{\mathcal{E}}/\eta$ were averaged over the same time window $30 < t \leq 60$ as the system probabilities in Fig. 5.9 and the infinite bath T were calculated from Eq. 5.14 with $\langle n_{\rm osc}\rangle = \langle E_{\rm osc}\rangle$.

finite number of levels, and an environment, consisting of levels of a finite collection of harmonic oscillators (which constitutes the bath). A set of identical oscillators was first considered, paralleling the Einstein heat capacity model. To get something more like a continuous state distribution, we then took a collection of non-identical oscillators. This gives a distribution of levels that closely tracks that of the bath of identical oscillators, but also has the desired feature of breaking the degeneracy, giving a quasi-continuous level distribution. The level pattern of this bath has a density of states that gives temperature-like behavior, using the standard statistical thermodynamic microcanonical relation between temperature, energy, and density of states. This defines the "temperature" $T_{\mathcal{E}}$ for the finite bath. This temperature differs significantly from that of the infinite oscillator bath, as seen in simulations with a bath with only $\eta = 5$ oscillators. We compared the energy-temperature relations for a single oscillator within the infinite bath (the well-known result of Einstein from his famous heat capacity paper) to the corresponding relation for a finite bath. There are systematic differences, which are pronounced for $\eta = 5$, and asymptotically approach the infinite bath at large η. The small bath has higher temperature for a given amount of energy per oscillator. Very unlike the infinite bath, it also terminates at a temperature $T_{\mathcal{E}} > 0$, as seen in Fig. 5.3.

Having devised the finite bath with temperature $T_{\mathcal{E}}$, we considered the process of heat flow from the system into this bath. Simulations were performed of the process of heat flow to the finite bath in quantum time evolution. First we used a random-matrix coupling of the kind that has been employed in many contexts, including successful quantum thermodynamic simulations [1, 2, 6, 37]. This however led to "runaway spreading" of the quantum $\mathcal{SE}$ wave function. This is closely connected with the variable temperature of the bath—a feature not present in earlier thermodynamic simulations. The problem is that the density of states increases rapidly with increasing temperature, and the non-discriminate random coupling overpowers the quantum time evolution. To solve this, we switched to a more selective coupling similar to the kind that has long been used [52, 53] in molecular simulations. This selective coupling "tames" the spreading of the wave function, so that runaway behavior is avoided. The tamed coupling appears to be a realistic new feature needed to solve a real problem in the simulations.

Next came computational examination of the temperature $T_{\mathcal{SE}}$ defined for the microcanonical ensemble of the $\mathcal{SE}$ total system "universe," including the time-dependent temperature $T_{\mathcal{SE}}(t)$ that varies continuously between the initial bath temperature $T_{\mathcal{E}}$ and the final $\mathcal{SE}$ temperature $T_{\mathcal{SE}}$. In simulations with the $\eta = 5$ oscillator bath, starting with different initial system states but the same total system-environment energy, we tracked the temperature from its various initial values (because the bath has different energies depending on the system state) to its final value at equilibrium. All the simulations went to essentially the same final temperature $T_{\mathcal{SE}}$, as desired. The simulations with the bath of $\eta = 5$ oscillators with selective coupling show equilibration to a Boltzmann-type distribution at the temperature $T_{\mathcal{SE}}$ implied by the initial energy of the total system. As noted above,

this temperature is markedly different from that of an infinite bath with the equivalent energy per bath oscillator. In short, there are marked effects of the small finite bath on thermal behavior with variable temperature in the quantum simulations.

It is interesting to consider real situations in which to explore these finite size quantum thermodynamic effects. Experiments on very small Bose-Einstein condensates, containing as few as six atoms [24], may point the way to size-dependent variable temperature behavior similar to the oscillator model we have studied here. Several investigators have proposed small molecules as laboratories for fundamental exploration of quantum thermodynamics and statistical mechanics. Leitner [26, 27] has reviewed a method of using the eigenstate thermalization hypothesis to understand ergodicity and localization of energy within time-dependent molecular systems. Pérez and Arce [38] performed simulations of dynamics on a potential energy surface of the molecule OCS, which has a long history as an exemplar of problems of classically chaotic molecular dynamics. They treat one of the vibrational modes of OCS as a "system," and the other two modes as an "environment," akin to what we do here, but with a two-mode bath that is much smaller even than what has been considered here. They find a kind of thermalization of the system when it is excited with sufficient energy to have chaotic classical dynamics. However, they did not engage in the kind of analytic treatment of temperature of the present paper. If we go to a four-atom molecule, for example the important species C_2H_2 (acetylene) or H_3O^+ (hydronium ion), we could take as system one of the modes, e.g. a C-H stretch, leaving 5 vibrational modes as the bath, just as we do here. This ignores rotational degrees of freedom; one could do experiments with angular momentum $J = 0$; or alternately, allow J excitations, which would become increasingly important at higher J, where rotation-vibration coupling

would become important, giving the rotational degrees of freedom as a second bath or environment $\mathcal{E}'$. It is worth noting that molecular systems interacting with small baths are of interest in other contexts as well, e.g. in calculations of entanglement dynamics and spectroscopic signals [60, 61].

As an alternative to the molecular dynamics simulations of Ref. [38], one could also use "effective Hamiltonians" of the kind that have had vast use in molecular spectroscopy [57, 58]. It is notable that these Hamiltonians usually employ one or more "polyad numbers" that constitute approximate constants of motion, valid on a limited time scale. This makes these attractive systems in which to explore the effects of approximate constants as barriers to thermalization, a topic of considerable interest [20] in contemporary theory of quantum thermodynamics. The effective molecular polyad Hamiltonian can then be enhanced with polyad-breaking perturbations [62–64] that correspond to real molecular dynamical effects. These hierarchical dynamical systems could be ideal laboratories for investigation of thermodynamic processes on multiple time scales.

As a final comment, taking a wider perspective on the work here, it may be worthwhile to consider that there are (at least) three dimensions of "post-classical" effects in quantum thermodynamics. The first of course is quantization of energy levels, introduced in the very beginnings of quantum physics by Planck in his black-body theory and by Einstein in his famous heat capacity paper. A second is finite size, as exemplified in this paper by the very small size (five oscillators) of the variable temperature bath. A third involves quantum time evolution. This might come with more complicated setups of finite size and time evolution than explored here. One might consider a system linking two baths of different sizes; or a system linking two finite baths where the coupling of the system to each bath is different. These

would require far larger simulations than performed here. We can readily imagine experimental realizations of these situations, e.g. with supramolecular arrangements of two or more molecules weakly linked by a third.

5.9. Connection to later work

This chapter has developed a model for a quantum "temperature bath" of a small number of oscillators. The temperature $T_{\mathcal{SE}}$ depends on the size of the bath in a novel type of way that deviates from the temperature-energy relation for an infinite bath, but with $T_{\mathcal{SE}}$ the environment behaves as a proper temperature bath, with thermalization of an interacting system to the Boltzmann distribution at temperature $T_{\mathcal{SE}}$. With this properly functioning variable temperature quantum bath, we will now move onto a much more interesting situation where two of the baths considered here interact and exchange heat along the path to temperature equilibrium. In classical thermodynamics, this leads to equal temperatures in the baths, associated with maximizing the entropy of the universe in the second law. In quantum thermodynamics, the entropy S^Q_{univ} includes the non-classical component of excess entropy production in addition to the classical component, as developed in Chapters III-IV. Can this lead to new types of temperature equilibration behavior in quantum pure state thermodynamics, associated with maximizing the total S^Q_{univ} including non-classical excess entropy production? The next chapter will address this question, with much to say about the fundamental role of S^Q_{univ} and the possibility for novel types of quantum thermodynamic effects associated with excess entropy production.

CHAPTER VI

ASYMMETRIC TEMPERATURE EQUILIBRATION WITH HEAT FLOW FROM COLD TO HOT IN A QUANTUM THERMODYNAMIC SYSTEM

This chapter includes previously unpublished material co-authored by Michael E. Kellman [5]. Michael Kellman and I both contributed to developing the model and theory, analyzing the results, and writing the manuscript. I performed the computations.

6.1. Introduction

In this paper we explore a computational model of a multicomponent quantum thermodynamic network in which surprising phenomena are manifest, due to finite-size time-dependent quantum effects. We observe, in a straightforward manner of speaking, that by introducing a deliberate asymmetry, heat can be made to flow from cold to hot in a pure state system consisting of two separate variable temperature baths, coupled through a "linker system." We explore the description of these phenomena in terms of a recently introduced [1, 2] quantum entropy S^Q for a pure state, and show that this gives results in accord with the standard classical second law formulation $\Delta S_{univ} \geq 0$. In contrast, a description in terms of a von Neumann entropy treatment, similar to that described by Landau and Lifshitz [65] in their approach to thermodynamics for large quantum systems, fails to account for the equilibration to the unequal temperatures. There have been other approaches to formulating the second law in quantum thermodynamics, beginning with mixed states [28] or pure states expressed in a "quantum phase space" basis [30], but to our knowledge these have not been associated with new types of quantum thermodynamic

effects as we have here with S^Q in the second law. This work is part of a broad program reexamining the foundations of statistical mechanics in the context of quantum pure states evolving in time [1–4, 6–38], with the results here demonstrating novel aspects of the quantum thermodynamic behavior.

An essential element of our setup is the variable temperature baths. In a recent paper [4], we introduced a computational model for such a bath and showed that it thermalizes with a system, while exhibiting quantum thermodynamic effects related to the finite size of the bath. The variable temperature bath generalized earlier work [1, 2, 6, 35–37] on quantum thermodynamic simulations that used a constant temperature bath.

6.2. Complex model system with two baths

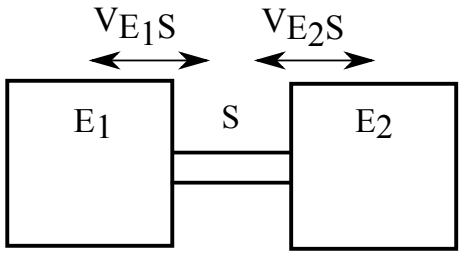

FIGURE 6.1. Two bath-environments $\mathcal{E}_1$ and $\mathcal{E}_2$ are linked together by a two level system $\mathcal{S}$. The baths exchange heat through the system, with system-environment couplings $\hat{V}_{\mathcal{E}_1 S}$ and $\hat{V}_{\mathcal{E}_2 S}$.

Fig. 6.1 shows the setup of present interest: two variable temperature finite baths or environments $\mathcal{E}_1$ and $\mathcal{E}_2$ that are uncoupled from each other, except for a system S that acts as a linker. Each bath is coupled to the linker, but the baths are coupled to each other only indirectly, through the linker. Suppose the baths start out at different temperatures. In ordinary classical thermodynamics, the baths and linker system would equilibrate to a common temperature. This would be true even

if the couplings to each bath were not the same. However, we hypothesize that if we introduce such an asymmetry into a small quantum thermodynamic system, there might be asymmetry of temperature in the final equilibrated state. This is indeed what we will find. In this and the following sections, we describe the setup sketched in Fig. 6.1, present the results of the computational simulations, and give an account in terms of the quantum entropy S^Q.

We consider a linker system $\mathcal{S}$ with zero-order Hamiltonian $\hat{H}_\mathcal{S}$ that connects together two finite temperature baths or environments $\mathcal{E}_1$ and $\mathcal{E}_2$ with Hamiltonians $\hat{H}_{\mathcal{E}_1}$ and $\hat{H}_{\mathcal{E}_2}$. The baths do not interact directly, but rather interact with the system via coupling operators $\hat{V}_{\mathcal{E}_1\mathcal{S}}$ and $\hat{V}_{\mathcal{E}_2\mathcal{S}}$. The total Hamiltonian is

$$\hat{H} = \hat{H}_\mathcal{S} + \hat{H}_{\mathcal{E}_1} + \hat{H}_{\mathcal{E}_2} + \hat{V}_{\mathcal{E}_1\mathcal{S}} + \hat{V}_{\mathcal{E}_2\mathcal{S}}. \tag{6.1}$$

The system consists of two levels with energy spacing $\hbar\omega_\mathcal{S} = 1$ and eigenstates $\{|n\rangle\} = \{|0\rangle, |1\rangle\}$:

$$\langle n|\hat{H}_\mathcal{S}|n\rangle = n. \tag{6.2}$$

The environment (bath) Hamiltonians $\hat{H}_{\mathcal{E}_1}$ and $\hat{H}_{\mathcal{E}_2}$ are for identical collections of η harmonic oscillators, each with frequencies $\{\omega_{\rm osc}\}$. The zero-order eigenstates for bath $\mathcal{E}_1$ are $|\epsilon_1\rangle = |n_1^{(\epsilon_1)}, n_2^{(\epsilon_1)}, ..., n_\eta^{(\epsilon_1)}\rangle$ with Hamiltonian matrix elements

$$\langle \epsilon_1|\hat{H}_{\mathcal{E}_1}|\epsilon_1\rangle = \sum_{\rm osc=1}^{\eta} \hbar\omega_{\rm osc} n_{\rm osc}^{(\epsilon_1)}, \tag{6.3}$$

with similar expressions for bath $\mathcal{E}_2$ with $|\epsilon_2\rangle$ and $\hat{H}_{\mathcal{E}_2}$. The frequencies of the bath oscillators are taken as random numbers that are scaled to set their geometric mean $(\prod_{osc=1}^{\eta} \hbar\omega_{\rm osc})^{1/\eta} = 1$, in accord with Ref. [4] where this finite environment model was

developed as a small variable temperature bath in simulations of a system interacting with a single environment. The frequencies we use are listed in Table 6.1.

η	$\hbar\omega_1$	$\hbar\omega_2$	$\hbar\omega_3$	$\hbar\omega_4$	$\hbar\omega_5$
4	0.696 987	0.987 490	1.088 054	1.335 340	
5	0.620 246	0.735 401	1.146 315	1.315 886	1.453 415

TABLE 6.1. Oscillator frequencies for the $\eta = 4$ and $\eta = 5$ oscillator environments, shown to six decimal places.

The interactions $\hat{V}_{\mathcal{E}_1\mathcal{S}}$ and $\hat{V}_{\mathcal{E}_2\mathcal{S}}$ in Eq. 6.1 are selective random matrix couplings used in Ref. [4], similar to those that have long been used in modeling energy transfer between molecular vibrational modes [52, 53]. For example, $\hat{V}_{\mathcal{E}_1\mathcal{S}}$ begins with a random matrix $\hat{R}_{\mathcal{E}_1}$ with elements $\langle n|\langle\epsilon_1|\hat{R}_{\mathcal{E}_1}|\epsilon_1'\rangle|n'\rangle = R_{n\epsilon_1,\epsilon_1'n'}$ generated as random numbers from Gaussian distributions with standard deviation $\sigma = 1$. Each of these matrix elements is then scaled by a coupling constant k_1 and by "taming factors" $\exp(-\gamma_{\mathcal{S}}|\Delta n|)$ and $\exp(-\gamma_{\mathcal{E}}\sum_{\rm osc}|\Delta n_{\rm osc}^{(\epsilon_1)}|)$ that will be explained shortly. The final form of the coupling matrix elements is:

$$\langle n|\langle\epsilon_1|\hat{V}_{\mathcal{E}_1\mathcal{S}}|\epsilon_1'\rangle|n'\rangle = k_1 R_{n\epsilon_1,\epsilon_1'n'} e^{-\gamma_{\mathcal{S}}|\Delta n|} e^{-\gamma_{\mathcal{E}}\sum_{\rm osc}|\Delta n_{\rm osc}^{(\epsilon_1)}|}, \tag{6.4}$$

with a similar expression for $\hat{V}_{\mathcal{E}_2\mathcal{S}}$. We set the diagonal elements to zero to preserve the oscillator energies in the zero-order basis, as was done previously in Ref. [4], and use real numbers only in the coupling to minimize the numerical overhead.

The parameters $\gamma_{\mathcal{S}} = 0.1$ and $\gamma_{\mathcal{E}} = 0.5$ determine how the coupling scales with quantum number differences $|\Delta n|$ and $\sum_{\rm osc}|\Delta n_{\rm osc}^{(\epsilon_1)}|$ of the coupled system and environment states. The larger value for $\gamma_{\mathcal{E}}$ is needed to obtain physical results where the environment doesn't spread out too much in energy [4]. The smaller value of $\gamma_{\mathcal{S}}$ gives good system thermalization in the dynamical calculations. The parameters

$\gamma_{\mathcal{S}}$ and $\gamma_{\mathcal{E}}$ have been reduced relative to the values we used for a single system and bath in Ref. [4], as we found this to be more successful in obtaining good energy flow between the baths. The coupling constants k_1 and k_2 will vary as described in the results to follow.

For the basis set we use a "thermal basis" [2, 4] that is a truncated version of the full tensor product basis $\mathcal{H} = \mathcal{H}_{\mathcal{E}_1} \otimes \mathcal{H}_{\mathcal{S}} \otimes \mathcal{H}_{\mathcal{E}_2}$. The thermal basis contains all basis states in the energy range

$$0 \leq E_{\mathcal{S}} + E_{\mathcal{E}_1} + E_{\mathcal{E}_2} \leq E^{\max}. \tag{6.5}$$

A similar truncated basis was found to give good thermodynamic behavior in Ref. [4] with a single variable temperature bath of the type we use here. We find good convergence with $\eta = 4$ oscillators using $E^{\max} = 16$ and $E^{\max} = 17$ in Sections 6.5.1 and 6.5.2 respectively, where the coupling constants k_1 and k_2 take different values. For $\eta = 5$ oscillators per bath, we also use $E^{\max} = 17$. With 5 oscillators the calculations are not quite converged. We are unable to go to higher $E^{\max}$ due to the computational demands of increasing the basis, but the results are qualitatively completely consistent for different $E^{\max}$.

6.3. Temperature and the baths

In this paper we will be talking about asymmetries in temperature of two baths, with "heat flow from cold to hot." This necessitates a careful consideration of temperature. Implicitly, we must be talking about "temperatures" of the individual baths. But general formulations of statistical mechanics, and certainly our prior work defining temperature baths [1, 2, 4, 6], rely on a microcanonical ensemble implementation of the thermodynamic temperature $T = (\partial S/\partial E)^{-1}$ for the total

system. In our case here, this would be the two baths + system $\mathcal{E}_1, \mathcal{E}_2$, and $\mathcal{S}$. We implement this same type of microcanonical temperature definition here for the total system, and use it to define (or perhaps contrive) sensible temperatures for the individual baths. This is a somewhat lengthy process, placed in Appendix D; a brief sketch follows.

To define the single bath temperatures we use the standard thermodynamic relationship between temperature, entropy, and energy applied to the baths, for example

$$\frac{1}{T_{\mathcal{E}_1}} = \frac{\partial S_{\mathcal{E}_1}}{\partial E_{\mathcal{E}_1}}, \tag{6.6}$$

where $S_{\mathcal{E}_1}$ and $E_{\mathcal{E}_1}$ are the bath entropy and average energy, with a similar expression for second bath temperature $T_{\mathcal{E}_2}$. We evaluate $T_{\mathcal{E}_1}$ in Eq. 6.6 analytically as a function of the bath energy in Appendix D. The approach uses standard microcanonical relations to calculate $S_{\mathcal{E}_1}$ and $E_{\mathcal{E}_1}$ for a given total $\mathcal{E}_1\mathcal{S}\mathcal{E}_2$ energy. The temperature $T_{\mathcal{E}_1}$ is then calculated by numerically taking the derivative in Eq. 6.6. This results in a temperature-energy relation $T_{\mathcal{E}_1} = T_{\mathcal{E}_1}(E_{\mathcal{E}_1})$ for the finite baths, with a similar relation for $T_{\mathcal{E}_2}$. The temperatures increase monotonically with the bath energy, with curves similar to the standard type of temperature-energy relationship for an oscillator in an infinite bath. The temperatures from Eq. 6.6 are what we will use throughout our results to compare temperatures in the baths.

6.4. Initial states and time-propagation

The initial pure $\mathcal{E}_1\mathcal{S}\mathcal{E}_2$ state is a product state:

$$|\Psi^0\rangle = |\psi^0_{\mathcal{S}}\rangle|\psi^0_{\mathcal{E}_1}\rangle|\psi^0_{\mathcal{E}_2}\rangle \tag{6.7}$$

The system begins in a single level $|\psi^0_{\mathcal{S}}\rangle = |n\rangle$. We take the environment states $|\psi^0_{\mathcal{E}_1}\rangle$ and $|\psi^0_{\mathcal{E}_2}\rangle$ as Gaussian superpositions following Ref. [4], for example:

$$|\psi^0_{\mathcal{E}_1}\rangle \sim \sum_{\epsilon_1} \exp(i\delta_{\epsilon_1}) \exp(-(E^0_{\mathcal{E}_1} - E_{\epsilon_1})^2/4\sigma^2)|\epsilon_1\rangle, \tag{6.8}$$

where the δ_{ϵ_1} are random phases, $E^0_{\mathcal{E}_1}$ is the central energy of the Gaussian, E_{ϵ_1} is the energy of the zero-order basis state $|\epsilon_1\rangle$, and $\sigma = 0.5$ is the width of the Gaussian. A similar expression holds for $|\psi^0_{\mathcal{E}_2}\rangle$. We will take different values for $E^0_{\mathcal{E}_1}$ and $E^0_{\mathcal{E}_2}$ in different simulations, as we vary initial energies and temperatures in the baths. A different type of initial bath state with random variations about a Gaussian gave very similar results to those we report here, so our results do not appear to depend significantly on our specific choice of $|\psi^0_{\mathcal{E}_1}\rangle$ and $|\psi^0_{\mathcal{E}_2}\rangle$ in Eq. 6.8.

The time-dependent behavior of the total state $|\Psi(t)\rangle$ is calculated using a converged Chebyshev polynomial expansion of the time-dependent state. The expansion is known to give a highly accurate and efficient approximation to the true dynamics. Detailed accounts of the implementation of the method can be found in Refs. [66, 67].

6.5. Equilibration of the system and baths

In this section we discuss results of the time propagation with equal and unequal couplings to the two baths. In a classical system we would expect the change in couplings to change the rate of approach to equilibrium for the baths, but not their final temperatures, which we would expect classically to be equal for the two baths. Does the same temperature independence hold here with the quantum baths with variable couplings?

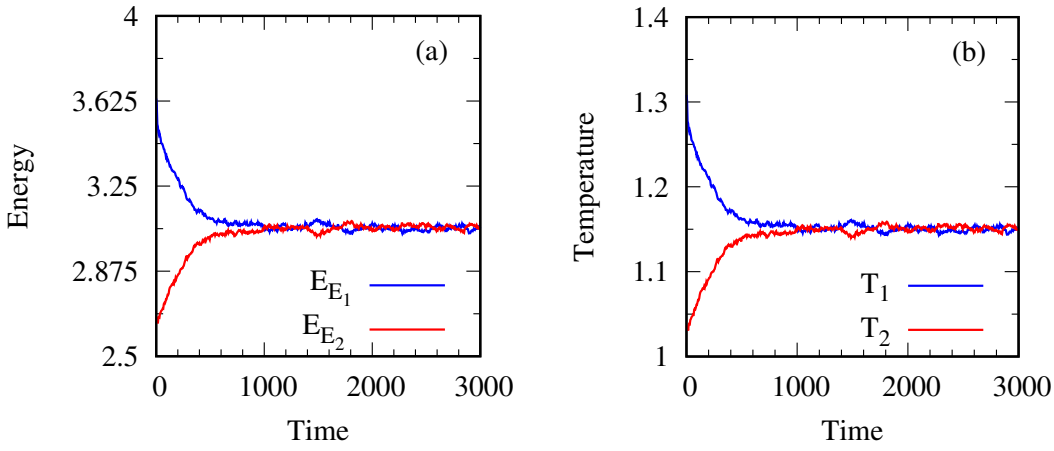

FIGURE 6.2. Equilibration dynamics with two baths with equal couplings $k_1 = k_2 = 0.085$. Panel (a) shows the average zero-order energies of the baths, (b) shows the corresponding temperatures from Eq. 6.6.

6.5.1. Energy equilibration with equal bath couplings

First we will examine the time-dependent behavior with equal coupling constants $k_1 = k_2 = 0.085$ in Eq. 6.4. We begin with different initial energies $E^0_{\mathcal{E}_1}$ and $E^0_{\mathcal{E}_2}$ in Eqs. 6.7 and 6.8. The time-dependent behavior of the bath energies is shown in panel (a) of Fig. 6.2. The two baths approach an equilibrium state where their energies fluctuate about approximately equal values $E_{\mathcal{E}_1} \approx E_{\mathcal{E}_2}$. In panel (b), we show the time-dependent temperature behavior, based on the single bath temperature $T_{\mathcal{E}}(E_{\mathcal{E}})$, as outlined in Section 6.3 and developed in Appendix D. The temperatures behave similarly to the energies, ending in an equilibrium state where the two baths fluctuate about the same temperature. This is standard thermodynamic behavior, as fully expected.

6.5.2. Energy equilibration with unequal bath couplings

Now we consider our central result, the temperature asymmetric equilibration when the couplings to the two baths are unequal, with $k_1 = 0.085$ and $k_2 = 3k_1$ in Eq. 6.4. In Fig. 6.3 we show three cases where the initial state bath energies are the same or different from one another, (a) $E^0_{\mathcal{E}_1} > E^0_{\mathcal{E}_2}$, (b) $E^0_{\mathcal{E}_1} = E^0_{\mathcal{E}_2}$, and (c) $E^0_{\mathcal{E}_1} > E^0_{\mathcal{E}_2}$. All states go to the same qualitative type of final state where the energy in the strongly coupled bath is greater than the energy in the weakly coupled bath $E_{\mathcal{E}_2} > E_{\mathcal{E}_1}$. Similar statements describe the individual temperatures of the baths. This is decidedly different from standard thermodynamic behavior! In panel (a) it is no exaggeration to speak of heat flowing from cold to hot. In all three cases, an asymmetric temperature equilibrium holds.

6.6. Entropy

We have seen unusual behavior in this quantum system: an equilibrium in which two temperature baths reach different temperatures, with cases that can be described as having heat flow from cold to hot until an asymmetric equilibrium is reached. In thermodynamics, we are used to explaining equilibration outcomes with reference to the second law. In terms of entropy, this is the statement that S_{univ} reaches a maximum, given any constraints. Is anything like this available to us here? It might seem not, because quantum statistical mechanics has the von Neumann entropy, and for a pure state, the von Neumann entropy is zero, hence seems to have no relevance. However, we have recently introduced a new quantum thermodynamic entropy S^Q which is nonzero for a pure state [1, 2]. We also sometimes call this entropy S^Q_{univ} to designate that it is an entropy for the total system-environment "universe" pure state. We have observed in simulations that in ordinary quantum thermodynamic situations,

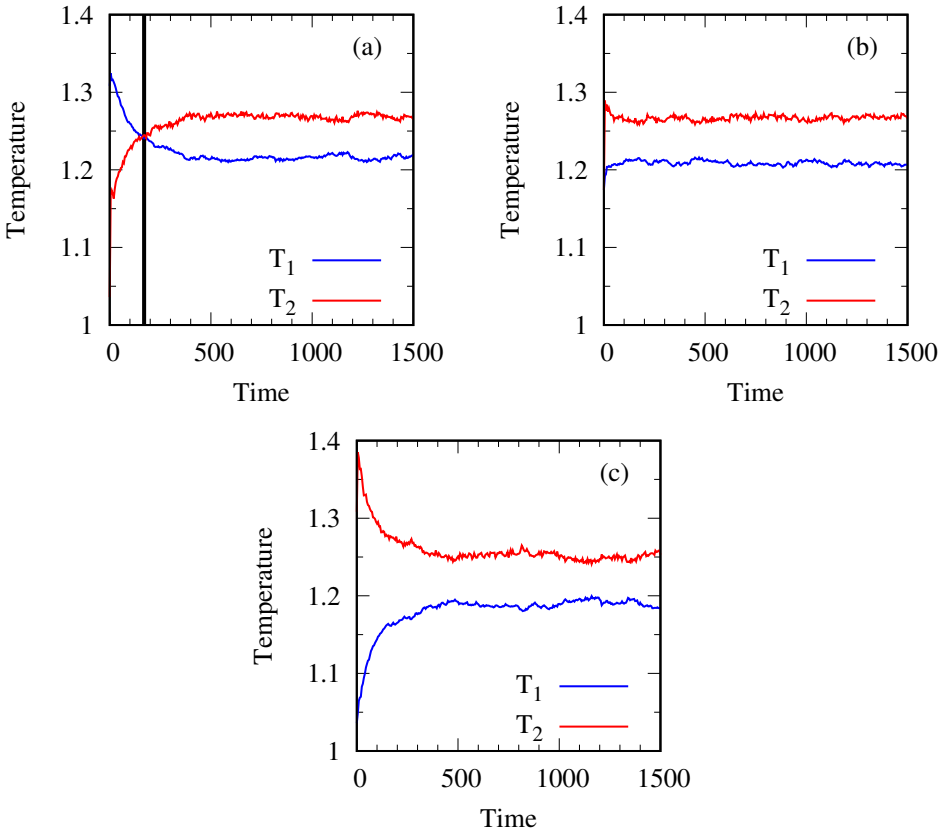

FIGURE 6.3. Baths with unequal couplings $k_1 = 0.085$ and $k_2 = 3k_1$ evolve to equilibrium states with unequal temperatures in the baths. The panels show simulations with different initial bath energies (a) $E^0_{\mathcal{E}_1} > E^0_{\mathcal{E}_2}$, (b) $E^0_{\mathcal{E}_1} = E^0_{\mathcal{E}_2}$, and (c) $E^0_{\mathcal{E}_1} < E^0_{\mathcal{E}_2}$.

e.g. heat flow into a single bath, this entropy maximizes at thermal equilibrium, in accord with the second law. The question arises whether S^Q has salience for the unusual situation of asymmetric temperature equilibration considered here. We will also try to apply a von Neumann-type entropy analysis using subsystems of the total system, devised with a procedure along lines discussed by Landau and Lifshitz [65]. We will see that S^Q succeeds in giving a second law entropy account of the unusual equilibration. In contrast, the procedure using the von Neumann entropy fails. We now describe the two approaches, then compare their description of the equilibration process.

6.6.1. Pure state quantum entropy S^Q

The quantum thermodynamic entropy S^Q was developed in Ref. [1] for an isolated system-environment "universe" in a pure state $|\Psi\rangle$. It is based on an expansion of the state in terms of the system-environment zero-order basis $|\Psi\rangle = \sum_{s,\epsilon_1,\epsilon_2} c_{s,\epsilon_1,\epsilon_2}|s\rangle|\epsilon_1\rangle|\epsilon_2\rangle$. The entropy is then taken along the lines of a Shannon definition using the zero-order probabilities $p_{s,\epsilon_1,\epsilon_2} = |c_{s,\epsilon_1,\epsilon_2}|^2$ as

$$S^Q_{univ} = -\sum_{s,\epsilon_1,\epsilon_2} p_{s,\epsilon_1,\epsilon_2} \ln p_{s,\epsilon_1,\epsilon_2} \tag{6.9}$$

The time evolution of S^Q for our simulations, shown in Figs. 6.4 and 6.5, will be discussed along with calculations in the von Neumann-type approach, to which we turn next.

6.6.2. Von Neumann entropy approach

Now we consider an approach based on a von Neumann entropy construct. Of course, the von Neumann entropy is zero for the total system pure state. Instead,

we follow a procedure similar to that of Landau and Lifshitz [65]. We partition the total system $\mathcal{S} + \mathcal{E}_1 + \mathcal{E}_2$ to define a von Neumann entropy for each of $\mathcal{S}$, $\mathcal{E}_1$, and $\mathcal{E}_2$. Specifically, we define the sub-entropies by finding the von Neumann entanglement entropy of each sub-system with respect to the other two sub-systems. Thus $S_{\mathcal{S}}$ is defined with respect to $\mathcal{E}_1$ and $\mathcal{E}_2$, and so forth for the other combinations. Then, we find the total entropy as the sum of the the three sub-entropies

$$S^{vN}_{\text{total}} = S^{vN}_{\mathcal{S}} + S^{vN}_{\mathcal{E}_1} + S^{vN}_{\mathcal{E}_2}. \tag{6.10}$$

This procedure seems very reasonable for large total systems, and is likely to give essentially the same, classical results no matter how we do the divisions. But in our small quantum system, with the non-classical phenomena in Figs. 6.4 and 6.5, the behavior of S^{vN}_{total} seems *a priori* not at all predictable.

6.6.3. Comparison of entropy calculations

Fig. 6.4 shows the two calculations of the entropy of the universe for the simulation with four oscillators in the panel (a) of Fig. 6.3, with the black line indicating the time of the temperature crossing. The entropy is calculated as the pure state entropy S^Q (top) and as the total von Neumann entropy S^{vN}_{total} (bottom).

Fig. 6.4 shows that S^Q rises during the heat transfer process, and is rising still at $T_1 = T_2$. It keeps rising (to within computational fluctuation) until it reaches a maximum at the equilibrium state where $T_1 > T_2$. This shows that S^Q is in fact giving a very nice account of our results, consistent with a second law explanation $\Delta S^Q \geq 0$, with $\Delta S^Q = 0$ at the nonclassical equilibrium with unequal temperatures. In contrast, the von Neumann entropy S^{vN}_{total} maximizes close to the time of the temperature equalization, then *decreases* as the equilibration proceeds to different

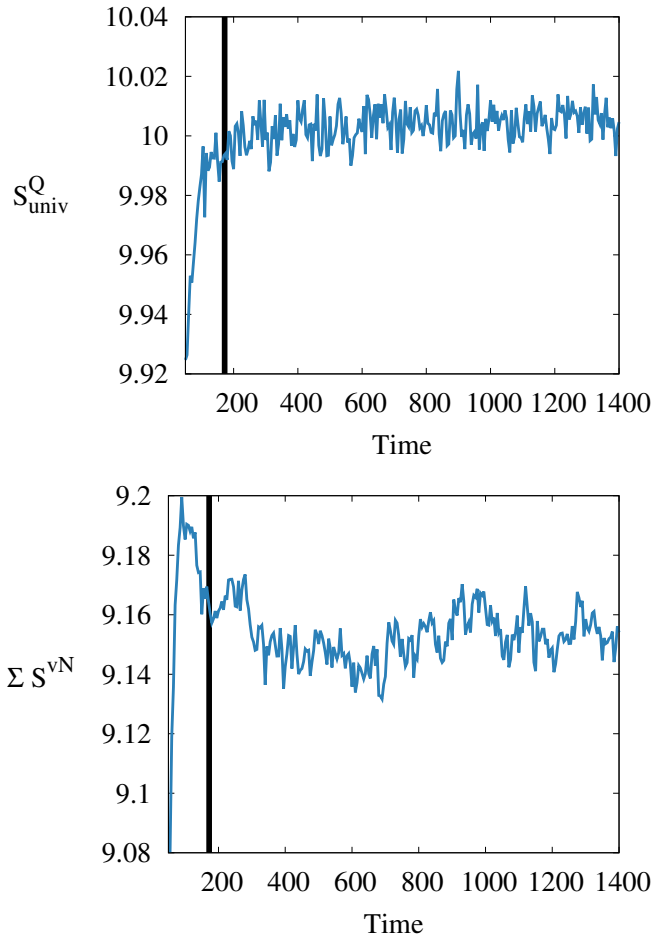

FIGURE 6.4. Universe entropy production S^Q_{univ} in Eq. 6.9 and S^{vN}_{total} in Eq. 6.10 for the calculation in the top of Fig. 6.3 with $\eta = 4$ oscillators per bath. The black line shows the time of the temperature crossing.

temperatures. Thus the von Neumann entropy is maximized near the classical state of equilibrium, with equal temperatures, and does not account for the asymmetric quantum equilibrium in terms of the second law.

Fig. 6.5 shows results where we have increased the number of oscillators per bath to $\eta = 5$. These calculations are not quite converged, as mentioned previously at the end of Section 6.2, but the behavior in Fig. 6.5 is robust to changes in the basis size. Here, we see an even more striking increase in S^Q_{univ} after the temperatures

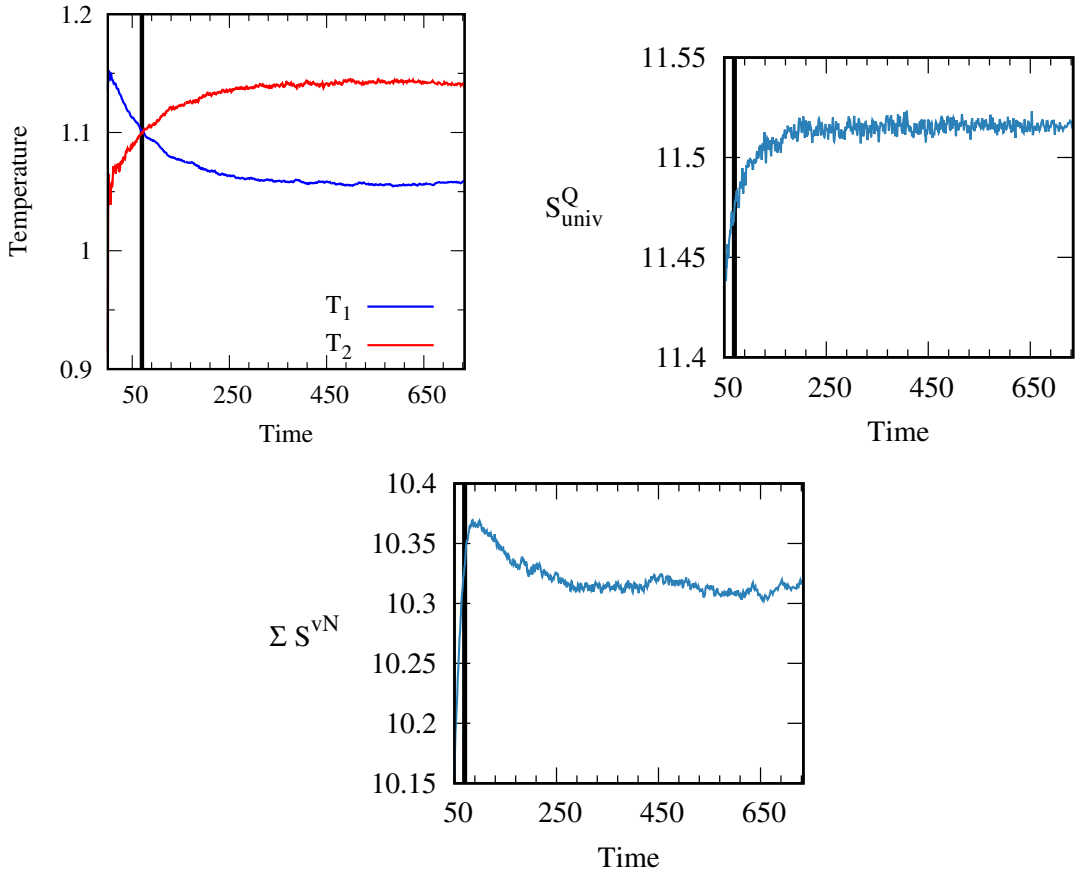

FIGURE 6.5. Temperature equilibration similar to Figs. 6.3 and 6.4 but with $\eta = 5$ oscillators per bath. The increase in S^Q_{univ} and decrease in $\sum S^{vN}$ after the temperature separation is even more striking.

cross, along the way to the asymmetric equilibrium. On the other hand, the von Neumann entropy is again maximized near the time of the temperature crossing, with a significant decrease as the state approaches the asymmetric equilibrium. This result strongly supports that S^Q_{univ} is giving a correct account of the equilibration behavior while S^{vN}_{total} is not.

6.7. Why the effect takes place

We have seen a sizable temperature difference attained in the baths at equilibrium when they have asymmetric couplings, with coupling constants $k_2 > k_1$ in Eq. 6.4. In essence, heat can flow from cold to hot, as seen in Fig. 6.3. Here we discuss the physical origin of this effect, its relation to the asymmetric coupling, and to "excess quantum entropy production" in attaining a maximum of S^Q_{univ} at the asymmetric temperature equilibrium.

We argue that the basic source of these effects in the asymmetric system is that couplings induce quantum spreading of the wavepacket within the baths during the quantum time evolution. Interactions among non-resonant energy levels cause the baths to spread to higher and lower zero-order energy basis states $|\epsilon_1\rangle$ and $|\epsilon_2\rangle$. The quantum spreading accesses many more high energy basis states than low energy states, since the density of bath states at higher energy is much larger than the density at lower energy. This asymmetric spreading to mostly high energy basis states has the effect of increasing the energy of each of the baths, with a compensating decrease in the coupling energies, so that the total energy $\langle \hat{H} \rangle$ of Eq. 6.1 is constant.

Fig. 6.6 shows details of the average coupling energies, bath energies, and the system energy near the beginning of a simulation, analogous to panel (b) of Fig. 6.3, where the baths begin at the same energy. There is a rapid decrease in each of the coupling energies, associated with an increase in the bath energies and the system energy. This is due to spreading of the wavepacket that predominantly accesses higher energy bath basis states, as discussed above. However, the more strongly coupled bath has a much greater change in its associated coupling energy $\langle V_{\mathcal{E}_2 \mathcal{S}} \rangle$ and bath energy $E_{\mathcal{E}_2} = \langle \hat{H}_{\mathcal{E}_2} \rangle$.

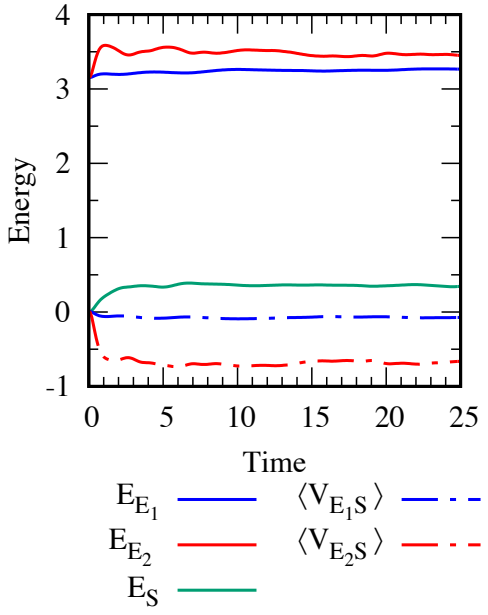

FIGURE 6.6. Energy terms in the total Hamiltonian $\hat{H}$ of Eq. 6.1.

After the initial increase in both bath energies, there is a slower partial transfer of energy from bath to bath via the system, but the energies never equalize. The asymmetric spreading to high energy states remains localized primarily in the strongly coupled bath. The energy difference from the asymmetric spreading gives a small but significant final temperature difference between the baths. Similar initial increases in the bath energies and decreases in coupling energy are seen for all the different initial states in Fig. 6.3. The spreading of the wavepacket to higher energies, along with the incomplete transfer of this energy between the baths, is the basic source of the asymmetric temperature equilibrium.

Having discussed the physical source of the temperature separation, we now consider its connection with in the quantum entropy and the second law. The entropy S^Q_{univ} of Eq. 6.9 depends on the probabilities $p_{\epsilon_1,s,\epsilon_2}$ of the zero-order basis states $|\epsilon_1\rangle|s\rangle|\epsilon_2\rangle$. The changes in the $p_{\epsilon_1,s,\epsilon_2}$ and S^Q_{univ} can be thought of qualitatively as a sum of a classical and a quantum "excess entropy" component,

with $\Delta S^Q_{univ} = \Delta S^{classical} + \Delta S^x$. The classical $\Delta S^{classical}$ is related to heat flow between the system and baths; alone this would lead to equal temperatures in the baths. However, ΔS^Q_{univ} also depends on the quantum excess entropy production ΔS^x related to the quantum spreading of the wavepacket to non-resonant energy levels [2]. The asymmetric spreading of the wavepacket with asymmetric couplings leads to temperature separation in the baths as described above. Thus there is a direct connection between $\Delta S^Q_{univ}, \Delta S^x$, and the temperature separated equilibrium state. This evidently gives a ΔS^Q_{univ} that follows the second law $\Delta S > 0$ during the temperature equilibration, as seen in Figs. 6.4 and 6.5.

In contrast, the total von Neumann entropy of Eq. 6.10 is more indirect than S^Q_{univ}, in that it depends on the eigenvalues of the reduced density operators for the $\mathcal{E}_1, \mathcal{S}$, and $\mathcal{E}_2$ subsystems. These eigenvalues evidently do not encode information about the temperature equilibration in such a way that the total von Neumann entropy is maximized at equilibrium, as would be expected if the second law holds. Thus, the von Neumann entropy fails to give a second law account of the asymmetric temperature equilibration behavior observed in Figs. 6.4 and 6.5. In contrast, the new quantum entropy S^Q_{univ} is successful in explaining the temperature separation in terms of the second law.

It seems likely to us that the unequal spreading within the baths is encoded into the eigenstates, so that eigenstates usually have temperature separations between the baths. If so, the temperature separation is likely inevitable at equilibrium, where the coherences between the eigenstates are effectively random and the average behavior of the eigenstates dominates. This same line of reasoning about the average eigenstate behavior is often cited in the eigenstate thermalization hypothesis account of quantum thermodynamics [19, 20], but to our knowledge this hasn't yet been

extended to novel quantum thermal effects as we have here. Our hypothesis about temperature separation in the eigenstates appears to us to be entirely consistent with the temperature separation behavior of Fig. 6.3, where a variety of initial states all reach approximately the same final temperature-separated equilibrium. It may also be interesting to consider the role of coherences and entanglement between the subsystems $\mathcal{E}_1, \mathcal{S}$, and $\mathcal{E}_2$ in producing the anomalous heat flow behavior. Coherence between subsystems has been related to a novel type of quantum thermodynamic effect in increasing heat engine power [68] and it is possible that subsystem coherence also plays an important role here.

6.8. Summary

In this paper we considered a quantum total system "universe" where surprising behavior is observed with heat flow from cold to hot along the path to an asymmetric temperature equilibrium. The total system contained two environment "baths" $\mathcal{E}_1$ and $\mathcal{E}_2$ of four or five oscillators each [4] linked together by a system $\mathcal{S}$, with $\mathcal{E}_1\mathcal{S}\mathcal{E}_2$ collectively in a quantum pure state. The baths exchanged heat indirectly through the system, with system-bath couplings that we varied in strength to examine the resulting temperature equilibration behavior.

To analyze temperature equilibration we needed a description for the temperatures of the individual baths, as opposed to the more standard type of temperature for the total system from the microcanonical ensemble. To develop temperatures for the single baths, we began with the microcanonical ensemble for the total system and from this derived the bath entropies and energies to define a temperature using the standard thermodynamic definition $T = (\partial S/\partial E)^{-1}$. From

this we obtained sensible temperature-energy relationships $T_{\mathcal{E}_1}(E_{\mathcal{E}_1})$ and $T_{\mathcal{E}_2}(E_{\mathcal{E}_2})$ for the individual baths to assess their thermodynamic behavior.

We examined two types of situations of heat flow between the baths. First, we set equal coupling strengths to the two baths. We found that they evolved to an equilibrium with equal temperatures, completely consistent with classical expectations. Second, we tripled the coupling strength to one of the baths. We found that different initial states for the baths all evolved to similar final equilibrium states with asymmetric temperature distributions in the baths, with heat flow from cold to hot in one of the examples. This is not standard thermodynamic behavior! The asymmetric temperature equilibrium was attributed to asymmetric spreading of the wavefunction in the two baths, with the strongly coupled bath accessing higher energy states than the weakly coupled bath, giving it a higher energy and temperature.

The asymmetric temperature equilibrium we observed would not be observed classically since it does not maximize the classical entropy S_{univ} in accord with the second law $\Delta S_{univ} > 0$. The observance of this equilibrium here then seems to necessitate a different quantum account of the second law. We examined two different approaches to defining a quantum S_{univ} and examined their behavior in terms of the second law. The first formulation was based on a recently developed entropy S^Q_{univ} for the pure state, while a more conventional second approach was based on a sum of component von Neumann entropies for the system and baths.

We found that S^Q_{univ} was maximized in the temperature separated equilibrium, with $\Delta S^Q_{univ} > 0$ as heat flowed from cold to hot. This gives a thermodynamic account of the novel asymmetric temperature equilibration where S^Q_{univ} is maximized at equilibrium following the second law. We argued that the success of S^Q_{univ} in describing the temperature separation was related to "excess entropy production"

from spreading of the wavepacket [2] in the asymmetric equilibrium. The second approach with the sum of component von Neumann entropies failed to maximize at the observed equilibrium, instead maximizing around a point of equal temperatures in the baths as expected classically. Thus the more conventional approach based on von Neumann entropies failed, whereas S^Q_{univ} was entirely successful in giving a second law account of the observed behavior.

It is possible there could be a variety of new quantum thermodynamic effects that harness "excess entropy production" to maximize S^Q_{univ} in classically forbidden types of states, beyond the temperature equilibration phenomena studied here. This could be of great significance for future explorations in the foundations of quantum thermodynamics.

CHAPTER VII

CONCLUSIONS

This chapter contains previously unpublished material co-authored by Michael E. Kellman. Michael Kellman and I both contributed to developing the points from previous chapters that are summarized here, and to the ideas for the future research. I wrote this chapter.

This dissertation has addressed three fundamental problems in **formulating thermodynamics for a quantum pure state** $|\Psi_{\mathcal{SE}}\rangle$ of a system $\mathcal{S}$ and environment $\mathcal{E}$ in a thermodynamic process as outlined in Chapter I: demonstrating the recently developed [1] entropy S^Q_{univ} gives a second law account of quantum thermalization with a **correct classical limit** and exploring its **behavior outside this limit**; discovering new types of **specifically quantum thermodynamic behavior** related to finite size and strong coupling; and giving a quantum **second law account of the new quantum behavior**.

Chapter II reviewed the background information related to addressing the goals: the basic approach to quantum pure state thermodynamics, its relation to classical thermodynamics and statistical mechanics, and the recently developed entropy S^Q_{univ}. Chapters III-VI contributed to the three problems above, as summarized in the next section. After summarizing the main results, the final sections of this chapter discuss ideas for future research related to this work, concluding with some final remarks.

7.1. Summary of results

The first goal in this dissertation was to show that the recently proposed [1] quantum thermodynamic entropy S^Q_{univ} gives a proper account of the second law of

thermodynamics in a classical limit of quantum pure state thermodynamics and to explore its behavior outside this limit. Chapter III and Ref. [2] assessed the behavior of S^Q_{univ} in comparison with the classical relation between the entropy change of the universe and the free energy change of system in Eq. 3.2, to analyze the hoped-for approach to classical behavior with ΔS^Q_{univ}. To assess S^Q_{univ}, a model for a thermal process in a quantum system-environment $\mathcal{SE}$ "universe" was developed, with a system $\mathcal{S}$ of a few energy levels exchanging heat with a finite model for a fixed temperature environment $\mathcal{E}$ designed to have the essential characteristics of a true infinite temperature bath. The model made considerable improvements on the environment, initial state, and basis set used in the previous work of Ref. [1], to give a much more realistic account of the behavior of ΔS^Q_{univ}.

The behavior of S^Q_{univ} was analyzed in simulations of $\mathcal{SE}$ thermalization and entanglement. These generally showed a phenomenon of **"excess quantum entropy production" $\boldsymbol{\Delta S^x}$** beyond the classical entropy change expressed in terms of the free energy change of the system ΔF_{sys} and the temperature T in Eq. 3.2. The approach to classical behavior was formulated as the environment density of states increased $\rho \to \infty$ and the system-environment coupling became small $k \to 0$, in accord with the classical thermodynamic microcanonical ensemble where the bath is assumed infinite and the coupling negligible. The approach to this "macroscopic" "classical" limit was examined numerically in series of calculations with varying coupling k and density ρ. The ΔS^x monotonically approached zero throughout the numerical approach to the limit, however, the calculations remained somewhat removed from $\Delta S^x = 0$. To better probe the classical limit, an empirical ΔS^x curve was developed. The best fit curves empirical curves for ΔS^x were extrapolated to the classical macroscopic limit of an infinite bath $\rho \to \infty$ and weak coupling $k \to 0$, where it was observed

that $\Delta S^x \to 0$ to within the error of the fit. Based on this fit curve analysis, it was concluded that $\boldsymbol{\Delta S^Q_{univ}}$ **approaches the correct classical entropy change with** $\boldsymbol{\Delta S^x = 0}$ **in the classical limit** of a macroscopic environment $\rho \to \infty$ and weak coupling $k \to 0$.

Chapter IV and Ref. [3] explored **excess entropy production** $\boldsymbol{\Delta S^x}$ in relation to **strong coupling** as noted in Chapter III and Refs. [1, 2]. We considered an analytically tractable class of initial Lorentzian states, with a variable width in the calculations, down to the limit of zero width with a single system-environment basis state $|s\rangle|\epsilon\rangle$ as the initial state. The initial Lorentzians evolved in time with spreading of the wavepacket into wider Lorentzians, with a simple analytical relation between the initial and final widths of the Lorentzians. We derived the Lorentzian entropy as a microcanonical Boltzmann-like expression $S^Q_{univ} \sim \ln W_{\text{eff}}$ of Eqs. 4.29, 4.30 and 4.32 for an effective number of states W_{eff} under the Lorentzian. The total entropy production ΔS^Q_{univ} was separated into a classical component and an excess entropy production component that is due entirely to spreading of the wavepacket in the environment, given in terms of the increase in the width of the Lorentzian in Eqs. 4.34 and 4.36. In essence, the Lorentzian width plays the role of the microcanonical shell width in semi-classical theory, and the *relative* increase in this width gives the deviation from classical behavior. The excess entropy production can be very large, taking a maximal value for a single $|s\rangle|\epsilon\rangle$ state where the relative spreading is maximized, with $\Delta S^x \gg 0$ even in the "classical" type of limit with coupling $k \to 0$ and density of states $\rho \to \infty$. Thus with S^Q_{univ} there is a new quantum source of entropy production $\boldsymbol{\Delta S^x}$ **associated with strong coupling and spreading of the wavepacket in quantum thermodynamics**. This new source of entropy has significant consequences in quantum thermodynamics as explored in Chapter VI.

In sum, Chapters III and IV fulfill the first goal, showing that S^Q_{univ} gives an account of the second law in quantum pure state thermodynamics, with correct behavior in a type of classical limit. Outside of this limit, there is a new source of quantum excess entropy production ΔS^x, where quantum spreading of the wavepacket contributes additional entropy.

The second goal in this dissertation was to explore **new types of specifically quantum thermodynamic behavior**. We studied finite size and strong coupling, both of which are important aspects of small quantum systems that are not included in basic classical statistical mechanics, where the baths are assumed infinite and coupling negligible.

Chapter V and Ref. [4] considered **finite size in quantum temperature bath equilibration**, with a system $\mathcal{S}$ interacting with a bath $\mathcal{E}$ composed of as few as five oscillators. The analytical $\mathcal{E}$ temperature had significant deviations from the standard temperature-energy relationship for an oscillator in an infinite bath, with the finite bath temperature converging to the standard temperature in the limit as the number of bath oscillators $\eta \to \infty$. With small η the temperature was larger at a given energy than the infinite bath temperature. The behavior of the system, finite bath, and temperature was studied in simulations of $\mathcal{SE}$ heat flow and equilibration with a very small $\eta = 5$ oscillator bath. The system $\mathcal{S}$ evolved to a state of thermal equilibrium with the bath, with an equilibrium $\mathcal{S}$ Boltzmann thermal distribution at the finite bath temperature, which was much different from the Boltzmann distribution at the temperature expected for an infinite bath. Thus the finite environment $\mathcal{E}$ behaved properly as a temperature bath with a **new quantum thermodynamic effect** of the **anomalous temperature behavior with the finite bath**.

Chapter VI considered a situation **combining finite size and strong coupling, with two small baths** linked together by a system, with variable couplings to the two baths. Simulations of dynamics with equal couplings to the two baths showed the approach to equilibrium with equal temperatures in the baths, as expected in classical thermodynamics. However, in simulations with a strong coupling to one bath and a weak coupling to the other, the baths evolved to an **asymmetric temperature equilibrium** state with a higher temperature in the strongly coupled bath, with **heat flow from cold to hot** along the path to equilibrium. The asymmetric temperature was closely related to asymmetric spreading of the wavepacket in the two baths, where the strongly coupled bath accessed higher energy states giving it a higher temperature. Thus finite size and strong coupling combined to give a new type of quantum temperature equilibration behavior, with significant implications for the general foundations of quantum thermodynamics.

The final goal was to give a **second-law account of new thermodynamic behavior** with the entropy S^Q_{univ}. The entropy was calculated during the asymmetric temperature equilibration with two baths of Chapter VI, where it was found that $\boldsymbol{S^Q_{univ}}$ **reached a maximum at the temperature separated equilibrium** state in the simulations, with $\boldsymbol{\Delta S^Q_{univ} > 0}$ **as heat flowed from cold to hot** after a point of temperature equalization. The asymmetric temperature equilibrium was related to **excess entropy production** from asymmetric spreading of the wavepacket in the baths. Thus S^Q_{univ} gave a second law account of this new quantum thermodynamic effect, reaching a maximum at the asymmetric temperature equilibrium, very unlike the classical entropy S_{univ}.

The results for S^Q_{univ} were further compared with a more conventional approach to defining a quantum total universe entropy in Eq. 6.10, taken as a sum of component von Neumann entropies for the system and the two baths. The summed von Neumann entropy reached a maximum near a point of equal temperatures in the simulations, then decreased as heat flowed from cold to hot along the way to the final equilibrium. Thus the summed component von Neumann type of **more conventional approach to defining a quantum universe entropy failed** to give an account of the simulation results in terms of the second law: $\boldsymbol{S^Q_{univ}}$ **was needed to give a second law account of the novel quantum thermodynamic behavior**.

7.2. Future directions in quantum thermodynamics

These studies suggest several interesting ideas for future research in the foundations of quantum pure state thermodynamics. Experiments that study the theoretical effects of this dissertation may be well within reach, giving verification and further insights into the roles of finite size, strong coupling, and excess entropy production in quantum pure state thermodynamics. There may also be new quantum thermodynamic effects related to S^Q_{univ} and excess entropy production, in equilibration of systems with many thermodynamic variables or in non-thermalizing systems far from equilibrium. In this section I'll briefly describe these hopeful possibilities brought to light by this work on the fundamental role of S^Q_{univ} in the second law in quantum pure state thermodynamics.

7.2.1. Experimental studies of novel quantum thermodynamic effects

A variety of experiments may be in reach to study the new types of quantum pure state thermodynamic effects presented in this dissertation. Experiments are already

being performed on isolated pure state Bose-Einstein (BE) condensates to study their thermodynamic behavior. Ref. [24] found Boltzmann thermalization of a single atom in a BE condensates of six total atoms, with the other five atoms constituting the bath. This is very reminiscent of Chapter V where a system approached Boltzmann equilibrium in interaction with a five oscillator bath, with an anomalous temperature related to the finite size of the bath. This same type of anomalous temperature may already be present in the results of Ref. [24], who did not engage in the same type of basic temperature analysis as we did in Chapter V and Ref. [4]. It may also be possible in similar future experiments to introduce variable couplings between two subsystem "baths" to study the asymmetric temperature equilibration phenomenon of Chapter VI and Ref. [5].

Another experimental opportunity is in studies of dilute gas phase molecules that are effectively isolated from their surroundings on a limited timescale. There has been recent interest in using such molecules as fundamental probes of quantum pure state thermodynamics [26, 27, 38], since a wide variety of Hamiltonians are accessible with different molecules and pure states are relatively easy to prepare. Ref. [38] studied the dynamics of the OCS molecule on a potential energy surface, with a kind thermalization for one vibrational mode interacting with two other vibrational modes constituting the bath. Similar theoretical or experimental studies on small molecules could study the anomalous temperature-energy scaling associated with finite baths from Chapter V and Ref. [4]. For example, four-atom molecules with six vibrational modes can be analyzed in terms of a single vibrational mode $\mathcal{S}$ interacting with a bath $\mathcal{E}$ of the five other vibrations, similar to the model of Chapter V. Rotational degrees of freedom could also play a role, giving additional bath modes or serving as a secondary exterior bath.

The asymmetric temperature equilibration of Chapter VI could be studied in experiments on molecules with two "bath" groups of atoms linked together by a smaller "linker system" atom or group of atoms. These could show a variety of different asymmetric temperature equilibria in different molecules, where the Hamiltonian can be tuned by substituting different atoms in the baths or linker system. It would also be interesting to study how robust the temperature separation is to entanglement with further exterior systems, such as additional degrees of freedom in the molecules or other exterior degrees of freedom. If the temperature separation is robust to exterior entanglement, then it could have potential applications in solid state devices, where it might be harnessed to give new heat transport functionalities in interaction with other device components. Experimental studies such as these in molecules, Bose-Einstein condensates, or other pure state systems would give important support to the theoretical discoveries in this dissertation, with significance for the foundations of quantum pure state thermodynamics and potential technological applications.

7.2.2. Possibility for other new types of quantum thermodynamic effects

It's interesting to consider other types of novel thermodynamic effects that might be associated with the entropy S^Q_{univ} and excess entropy production ΔS^x, beyond the simple heat flow phenomena studied here. In this work, we saw that a maximum of S^Q_{univ} was attained at a novel type of asymmetric temperature equilibrium state, in an isolated "universe" with two conjugate thermodynamic variables of heat and temperature. However, in general thermodynamic processes there are additional thermodynamic variables of pressure, volume, chemical potentials, and mole numbers. In classical thermodynamics, all of these variables are balanced at equilibrium to

maximize S_{univ} in accord with the second law. In quantum thermodynamics, the equilibrium states that maximize S^Q_{univ} including ΔS^x could potentially have new types of asymmetries in these other thermodynamic variables, giving new families of equilibrium states related to excess entropy production beyond the asymmetric temperature equilibrium studied here. If this is the case, then S^Q_{univ} with ΔS^x would seem to introduce a great deal of flexibility into quantum pure state thermodynamics beyond what's allowed classically.

Another possibility for new effects lies in the study of systems away from equilibrium or non-thermalizing systems that never reach standard Boltzmann equilibrium. Some preliminary studies indicate that S^Q_{univ} may have much to say about the equilibration behavior of these systems. I've run calculations with a similar setup to Chapters III-IV, but with a significantly reduced coupling constant k that does not allow the system to reach standard Boltzmann thermal equilibrium. In these simulations there is *deficit entropy production* throughout the time evolution, with $\Delta S^Q_{univ} < -\Delta F_{sys}/T$, much different than the excess entropy production phenomena in thermalization that was studied throughout this dissertation. It's possible that deficit entropy production is a general feature of non-thermalizing systems in quantum pure state thermodynamics. If so, a non-thermalizing system could be identified early in its time evolution by comparing the entropy production with the free energy change, with a deficit of entropy production indicating that the system will never reach thermal equilibrium. This would seem to indicate great utility for the quantum entropy S^Q_{univ} in connecting non-thermal, quantum, and classical thermodynamic behaviors.

7.3. Final remarks

This dissertation has shown that it is possible to give a unified account of spontaneous quantum thermodynamic behavior in the second law with S^Q_{univ}, ranging from classical relations and phenomena to a surprising new specifically quantum thermodynamic effect of asymmetric temperature equilibration. The quantum statement of the second law with S^Q_{univ} thus seems well founded and fruitful, with potential applications in new types of effects that may still be awaiting discovery.

APPENDIX A

ANALYSIS OF THE SYSTEM-ENVIRONMENT DECOMPOSITION OF THE CLASSICAL MICROCANONICAL ENTROPY

This appendix includes unpublished material co-authored by Michael E. Kellman [3]. Michael Kellman and I both contributed to developing the theory and writing in this appendix.

In this appendix we show how a system-environment decomposition of the classical microcanonical Boltzmann entropy $S = k_B \ln W$ gives the standard result for the environment $\Delta\langle S_{env}^{micro}\rangle_{\{sys\}} = Q/T$ in Eq. 4.16.

The classical microcanonical ensemble is based on the idea of $W = \rho\delta E$ states in the microcanonical energy shell of width δE with density of states ρ. The entropy is given by Boltzmann's relation

$$S_{univ}^{micro} = -\sum_{s,\epsilon} p_{s,\epsilon}^{micro} \ln p_{s,\epsilon}^{micro} = \ln W, \tag{A.1}$$

where

$$p_{s,\epsilon}^{micro} = \frac{1}{W}. \tag{A.2}$$

The entropy can be decomposed into system and environment parts following Eq. 4.11

$$S_{univ}^{micro} = S_{sys}^{micro} + \langle S_{env}^{micro}\rangle_{\{sys\}}. \tag{A.3}$$

First consider the system component

$$S_{sys}^{micro} = -\sum p_s^{micro} \ln p_s^{micro}. \tag{A.4}$$

analogous to S_i in Eq. 4.11. The system probabilities are computed from Eq. 4.9 as

$$p_s^{micro} = \sum_{\epsilon=1}^{W_s} p_{s,\epsilon}^{micro} = \frac{W_s}{W} \tag{A.5}$$

where W_s is the number of bath states ϵ that pair with s in the microcanonical ensemble. Using Eq. A.5 to rewrite $\ln p_s^{micro}$ in Eq. A.4 gives

$$S_{sys}^{micro} = -\sum_s p_s^{micro}(\ln W_s - \ln W) = \ln W - \sum_s p_s^{micro} \ln W_s \tag{A.6}$$

Now consider the environment term

$$\langle S_{env}^{micro} \rangle_{\{sys\}} = \sum_s p_s^{micro} \left(-\sum_\epsilon p_{\epsilon|s}^{micro} \ln p_{\epsilon|s}^{micro} \right) \tag{A.7}$$

analogous to $\langle S_\lambda \rangle_{\{i\}}$ in Eq. 4.11. The conditional environment probabilities are calculated from Eq. 4.10 along with Eqs. A.2 and A.5,

$$p_{\epsilon|s}^{micro} = \frac{p_{s,\epsilon}^{micro}}{p_s^{micro}} = \frac{1}{W_s} \tag{A.8}$$

Using Eq. A.8 we can simplify the rightmost sum in Eq. A.7

$$-\sum_\epsilon p_{\epsilon|s}^{micro} \ln p_{\epsilon|s}^{micro} = \ln W_s, \tag{A.9}$$

then putting this into Eq. A.7 gives

$$\langle S_{env}^{micro} \rangle_{\{sys\}} = \sum_s p_s^{micro} \ln W_s. \tag{A.10}$$

The system and environment entropies Eqs. A.6 and A.10 clearly sum to the total microcanonical entropy $S_{univ}^{micro} = \ln W$ in Eq. A.1, as needed.

We now consider a thermalization process where we begin with a constrained microcanonical ensemble of W_0 states for the initial state. For example, this could correspond to a situation where the system begins in thermal isolation from the environment. The constraint is then removed, allowing heat to flow between the system and environment, resulting in a final state microcanonical ensemble with $W_f > W_0$. The total entropy change is

$$\Delta S_{univ}^{micro} = \ln \frac{W_f}{W_0} = \ln \frac{\rho_f}{\rho_0} \tag{A.11}$$

The last equality comes from the microcanonical relation $W = \rho \delta E$ with ρ the density of states in the microcanonical energy shell of width δE. The system entropy change from Eq. A.6 is

$$\Delta S_{sys}^{micro} = \ln \frac{W_f}{W_0} - \sum_{s_f} p_{s_f}^{micro} \ln W_{s_f} + \sum_{s_0} p_{s_0}^{micro} \ln W_{s_0} \tag{A.12}$$

The system entropy change can be greatly simplified through a series of manipulations we will perform on the final two sums of Eq. A.12. This will lead to the final simple result for the system entropy in Eq. A.20, and will also be useful in deriving the environment entropy change in Eq. A.22. First, the sums can be combined by inserting the identities $\sum_{s_0} p_{s_0}^{micro} = \sum_{s_f} p_{s_f}^{micro} = 1$,

$$- \sum_{s_f} p_{s_f}^{micro} \ln W_{s_f} + \sum_{s_0} p_{s_0}^{micro} \ln W_{s_0} = - \sum_{s_0, s_f} p_{s_0}^{micro} p_{s_f}^{micro} \ln \frac{W_{s_f}}{W_{s_0}}. \tag{A.13}$$

This is simplified by noting that for a heat bath environment $W \sim e^{E_{env}/T}$, where $E_{env} = E_{total} - E_s$ is the energy of the environment. Then the ratio W_{s_f}/W_{s_0} in the right of Eq. A.13 can be expressed as

$$W_{s_f}/W_{s_0} = e^{-(E_{s_f} - E_{s_0})/T} \tag{A.14}$$

where $E_{s_f} - E_{s_0} = \Delta E_{sys}$ is the energy difference between the final and initial system states s_f and s_0. Putting this into Eq. A.13 gives

$$-\sum_{s_0,s_f} p_{s_0}^{micro} p_{s_f}^{micro} \ln \frac{W_{s_f}}{W_{s_0}} = \sum_{s_0,s_f} p_{s_0}^{micro} p_{s_f}^{micro} \frac{E_{s_f} - E_{s_0}}{T} \tag{A.15}$$

Now we separate again into two terms

$$\sum_{s_0,s_f} p_{s_0}^{micro} p_{s_f}^{micro} \frac{E_{s_f} - E_{s_0}}{T}$$

$$= \frac{1}{T} \left(\sum_{s_0} p_{s_0}^{micro} \sum_{s_f} p_{s_f}^{micro} E_{s_f} - \sum_{s_f} p_{s_f}^{micro} \sum_{s_0} p_{s_0}^{micro} E_{s_0} \right) \tag{A.16}$$

Using the identities $\sum_s p_{s_0}^{micro} = \sum_s p_{s_f}^{micro} = 1$ this becomes

$$\frac{1}{T} \left(\sum_{s_f} p_{s_f}^{micro} E_{s_f} - \sum_{s_0} p_{s_0}^{micro} E_{s_0} \right) = \frac{\langle E_{sys,f} \rangle - \langle E_{sys,0} \rangle}{T} = \frac{\Delta \langle E_{sys} \rangle}{T} \tag{A.17}$$

Finally, we note that the system energy change is due solely to heat flow from the environment $\Delta \langle E_{sys} \rangle = -Q = -\Delta \langle E_{env} \rangle$, so we can express the result in Eq. A.17 equivalently as

$$\frac{\Delta\langle E_{sys}\rangle}{T} = \frac{-Q}{T}. \tag{A.18}$$

In total, Eqs. A.13-A.18 show that

$$-\sum_{s_f} p_{s_f}^{micro} \ln W_{s_f} + \sum_{s_i} p_{s_0}^{micro} \ln W_{s_0} = \frac{-Q}{T} \tag{A.19}$$

Putting this into Eq. A.12 the system entropy change takes the simple final form

$$\Delta S_{sys}^{micro} = \ln \frac{W_f}{W_i} - \frac{Q}{T}. \tag{A.20}$$

Now consider the entropy change of the environment. From the basic relation of Eq. A.10 this is

$$\langle \Delta S_{env}^{micro} \rangle_{\{sys\}} = \sum_{s_f} p_{s_f}^{micro} \ln W_{s_f} - \sum_{s_0} p_{s_0}^{micro} \ln W_{s_0}. \tag{A.21}$$

Using Eq. A.19 this is simply

$$\langle \Delta S_{env}^{micro} \rangle_{\{sys\}} = \frac{Q}{T}, \tag{A.22}$$

which is the standard thermodynamic result. Note this is an exact equality for a standard heat bath with the level density behavior of Eq. A.14. Thus we have proved $\Delta\langle S_{env}^{micro}\rangle_{\{sys\}} = Q/T$ in Eq. 4.16.

APPENDIX B

LORENTZIAN STATE DISTRIBUTIONS

This appendix includes previously unpublished material co-authored by Michael E. Kellman [3]. Michael Kellman and I both contributed to developing the theory. I wrote this appendix.

In this appendix we show how we obtain the time-evolving Lorentzian states discussed in Section 4.5. The time-evolution of an initial state $|\Psi(0)\rangle$ follows the Schrödinger equation, expressed in terms of the eigenstates $|\xi\rangle$ as

$$|\Psi(t)\rangle = e^{-i\hat{H}t}|\Psi(0)\rangle = \sum_{\xi} c_{\xi} e^{-iE_{\xi}t}|\xi\rangle. \tag{B.1}$$

Our approach will be to first analyze the structure of the eigenstates $|\xi\rangle$, then use the eigenstate structure to analyze the time-dependent behavior of the $|s\rangle|\epsilon\rangle$ and Lorentzian initial states.

Some of our important results for the average equilibrium behavior of time-dependent states, Eqs. B.3 and B.16 below, were obtained in nearly the same form by Deutsch in his well-known paper of 1991 [21, 22] where he developed the ideas behind the eigenstate thermalization hypothesis approach to quantum thermodynamics [20]. Our model varies somewhat from Deutsch's, so that our eigenstates require an additional parameter in Eq. B.3 that was not included in Deutsch's work. The widths of the eigenstates in from our calculations also vary from Deutsch's result by a factor of two, in agreement with a recent re-evaluation of Deutsch's work by Nation and Porras in Ref. [25].

In addition to analyzing the average equilibrium behavior of time-dependent states, we also extend beyond the work of Deutsch [21, 22] and Nation and Porras

[25] to analyze the fluctuations of a time-evolving state about its average and to develop the idea of a time-evolving initial Lorentzian state. Our advances provide the critical relations in Eq. 4.26, appearing again in this appendix as Eqs. B.8 and B.22.

B.1. Eigenstates

We build up to an analysis of time-dependent states beginning with the structure of the eigenstates $|\xi\rangle$. The eigenstates come from the system-environment Hamiltonian in Chapters III-IV and Refs. [2, 3], which includes a random interaction between a simple three-level system and an environment with a density of states that increases exponentially with energy. In the system-environment zero-order energy basis $\{|s\rangle|\epsilon\rangle\}$ the eigenstates are expressed as

$$|\xi\rangle = \sum_{s,\epsilon} c_{s,\epsilon}^{(\xi)} |s\rangle|\epsilon\rangle, \tag{B.2}$$

where the coefficients $c_{s,\epsilon}^{(\xi)}$ are real numbers since the Hamiltonian is real.

Deutsch [21, 22] and Nation and Porras [25] derived the eigenstate coefficients $c_{s,\epsilon}^{(\xi)}$ in a very similar model with a random interaction between evenly spaced system-environment levels. We find that our eigenstates can be very well fit by their result with the addition of a fit parameter ΔE_0, which is likely related to the exponential level density in our environment as opposed to the evenly spaced levels they considered. With this additional fit parameter, our eigenstates coefficients can be described statistically as

$$c_{s,\epsilon}^{(\xi)} \approx g_{s,\epsilon}^{(\xi)} \sqrt{L_\xi(E_s + E_\epsilon)}, \tag{B.3}$$

where $L_\xi(E_s + E_\epsilon)$ is a Lorentzian distribution and the $g^{(\xi)}_{s,\epsilon}$ give random variations about the Lorentzian average. The Lorentzian is

$$L_\xi(E_s + E_\epsilon) = \frac{1}{\pi} \frac{\gamma_\xi/\rho(E_\xi)}{(E_\xi - E_s - E_\epsilon - \Delta E_0)^2 + \gamma_\xi^2}, \tag{B.4}$$

with half-width at half-max

$$\gamma_\xi = \pi k^2 \rho(E_\xi), \tag{B.5}$$

where E_ξ is the eigenstate energy, $\rho(E_\xi)$ is the total density of system-environment zero-order states, and ΔE_0 is a fit parameter that sets the center of the Lorentzian. The small parameter ΔE_0 varies slightly between eigenstates, but we will approximate it as constant here to simplify the analysis, finding that this is entirely adequate for describing our results.

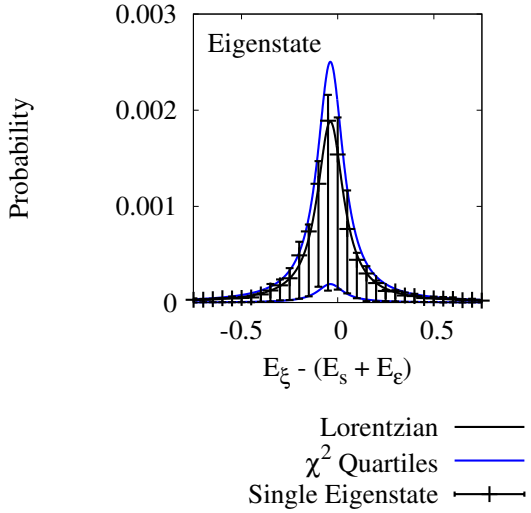

FIGURE B.1. Average squared coefficients $\langle |c^{(\xi)}_{s,\epsilon}|^2 \rangle$ for a single eigenstate follow the Lorentzian distribution of Eq. B.4. Error bars show the first and third quartiles of the distribution of $|c^{(\xi)}_{s,\epsilon}|^2$ in each data point. The quartiles of the coefficient distributions are in good agreement with the quartiles of the single degree of freedom χ^2 distribution with the Lorentzian mean, shown in blue.

Fig. B.1 shows an example of a single eigenstate calculated by exact diagonalization of our Hamiltonian. In the figure, we averaged squared-coefficients $|c_{s,\epsilon}^{(\xi)}|^2$ with nearby energies $E_s + E_\epsilon$ to get the averages $\langle |c_{s,\epsilon}^{(\xi)}|^2 \rangle$ shown as data points in the figure. The averages $\langle |c_{s,\epsilon}^{(\xi)}|^2 \rangle$ represent the average probability of measuring an $|s\rangle|\epsilon\rangle$ state of energy $E_s + E_\epsilon$ when in the eigenstate $|\xi\rangle$ of energy E_ξ. The averages are very well described by the Lorentzian $\langle |c_{s,\epsilon}^{(\xi)}|^2 \rangle \approx L_\xi(E_s + E_\epsilon)$, with L_ξ from Eq. B.4.

The asymmetric error bars in the figure show the first and third quartiles of the distribution of squared coefficients $|c_{s,\epsilon}^{(\xi)}|^2$ for each data-point average $\langle |c_{s,\epsilon}^{(\xi)}|^2 \rangle$. The quartiles are in good agreement with the quartiles of a single degree of freedom χ^2 distribution with mean $L_\xi(E_s + E_\epsilon)$. The χ^2 distribution describes a sum of squared random Gaussian variates. This suggests that the $g_{s,\epsilon}^{(\xi)}$ in Eq. B.3 behave as random standard Gaussian variates, so that the squared coefficients $|c_{s,\epsilon}^{(\xi)}|^2$ follow the χ^2 distribution with mean L_ξ. To check this, in Fig. B.2 we plot the distribution of the $g_{s,\epsilon}^{(\xi)} = c_{s,\epsilon}^{(\xi)} / \sqrt{L_\xi(E_s + E_\epsilon)}$, where they are indeed seen to follow a standard Gaussian distribution

$$p(g_{s,\epsilon}^{(\xi)}) = p\left(\frac{c_{s,\epsilon}^{(\xi)}}{\sqrt{L_\xi(E_s + E_\epsilon)}} \right) \sim e^{-{g_{s,\epsilon}^{(\xi)}}^2/2}. \tag{B.6}$$

The Gaussian variations for $g_{s,\epsilon}^{(\xi)}$ in Eq. B.6 explain the χ^2 distributed quartiles in Fig. B.1, and are consistent the work of Deutsch [21, 22] and Nation and Porras [25]. We have thus arrived at the description of the eigenstates in Eq. B.3, with the Lorentzian L_ξ of Eq. B.4 and the random variations $g_{s,\epsilon}^{(\xi)}$ of Eq. B.6.

The Gaussian fluctuations in the basis state probabilities of Eq. B.3 are related to the random structure of the interaction, as discussed by Deutsch [21, 22]. They also have a connection to the random states considered in the "typicality" approaches to quantum statistical mechanics [11–18]. These approaches seek to rationalize

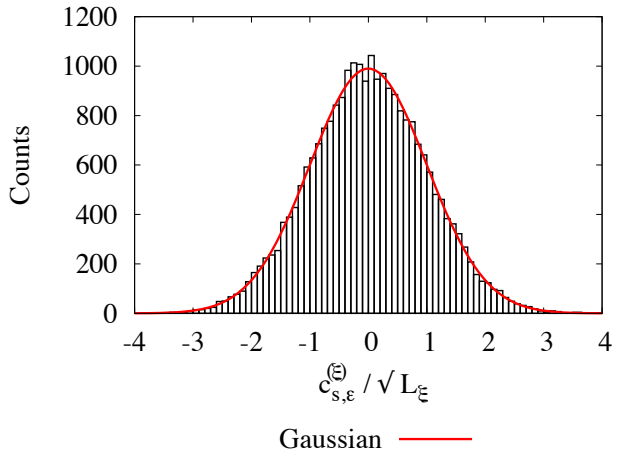

FIGURE B.2. Histogram counts of coefficient variations for an eigenstate. The variations $g^{(\xi)}_{s,\epsilon} = c^{(\xi)}_{s,\epsilon}/\sqrt{L_\xi}$ in the single eigenstate coefficients of Eq. B.3 follow the standard Gaussian distribution of Eq. B.6.

thermalization behavior by analyzing the statistics of random states. An unbiased sampling of random states is accomplished by taking coefficients as random Gaussian variates [14], similar to our Eq. B.6. Here, the eigenstates can be thought of as random or "typical" states within their Lorentzian windows, as seen in Fig. B.2.

B.2. Time evolution of an $|s\rangle|\epsilon\rangle$ initial state

Our goal in this section is to understand the behavior of a very simple time-dependent state from Eq. 4.25 that begins in single zero-order basis state

$$|\Psi_{s,\epsilon}(t)\rangle = e^{-i\hat{H}t}|s\rangle|\epsilon\rangle = \sum_{s',\epsilon'} c_{s',\epsilon'}(t)|s'\rangle|\epsilon'\rangle. \tag{B.7}$$

Our analysis will give the Lorentzian behavior for the time-evolved state $|\Psi_{s,\epsilon}(t)\rangle$ seen in Fig. 4.2 and Eqs. 4.26-4.28. We now briefly describe these results, repeated here in Eqs. B.8-B.10, before going into the mathematical details of how we obtain the results in the remainder of the section.

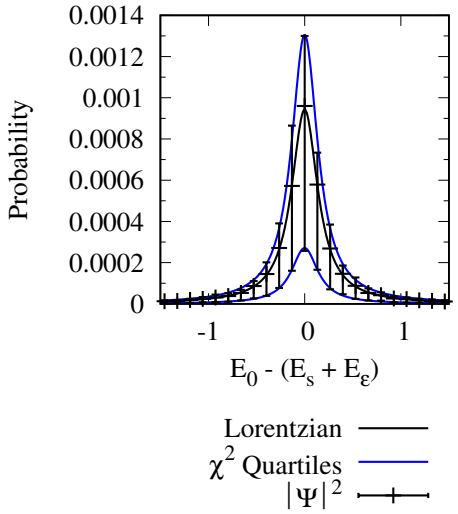

FIGURE B.3. Average squared coefficients $\langle |c_{s',\epsilon'}(t)|^2 \rangle$ for a time-evolved $|s\rangle|\epsilon\rangle$ state of Eq. B.7 follow a Lorentzian distribution with twice the width of the eigenstates (the state is the same as in Fig. 4.2). Error bars show the first and third quartiles of the distribution of the individual $|c_{s',\epsilon'}(t)|^2$ in each data point. The quartiles of the coefficient distributions are in good agreement with the quartiles of the two degree of freedom χ^2 distribution scaled by half the Lorentzian weight, shown in blue.

Fig. B.3 shows an example of average squared coefficients $\langle |c_{s',\epsilon'}(t)|^2 \rangle$ for a time-evolved $|s\rangle|\epsilon\rangle$ state of the type in Eq. B.7, at a time t at equilibrium (the results are similar for other choices of t). The state is the same as in Fig. 4.2. The average squared coefficients $\langle |c_{s,\epsilon}|^2 \rangle$ for the state follow a Lorentzian distribution with twice the width of the eigenstate seen previously in Fig. B.1; note the energy range in Fig. B.3 is doubled relative to Fig. B.1. The equilibrated state of Eq. B.7 can be expressed in the Lorentzian form from Eqs. 4.26-4.28,

$$|\Psi_{s,\epsilon}(t)\rangle \approx \sum_{s',\epsilon'} \tilde{g}_{s',\epsilon'} \sqrt{L_f^{(s,\epsilon)}} |s'\rangle|\epsilon'\rangle, \tag{B.8}$$

where the $\tilde{g}_{s',\epsilon'}$ are random complex fluctuations and $L_f^{(s,\epsilon)}$ is a Lorentzian centered at the initial $|s\rangle|\epsilon\rangle$ energy $E_0 = E_s + E_\epsilon$,

$$L_f^{(s,\epsilon)}(E_{s'} + E_{\epsilon'}) = \frac{1}{\pi} \frac{\gamma_f/\rho_f}{(E_{s'} + E_{\epsilon'} - E_0)^2 + \gamma_f^2}, \tag{B.9}$$

with half-width at half-max

$$\gamma_f = 2\pi k^2 \rho_f, \tag{B.10}$$

where $\rho_f = \rho(E_0)$ is the total density of system-environment states at E_0. The Lorentzian is similar to the eigenstate Lorentzian in Eqs. B.4 and B.5, except that the eigenstate energy has been replaced with the initial state energy $E_0 = E_s + E_\epsilon$, the width is doubled to $2\pi k^2 \rho_f$, and there is no median energy parameter ΔE_0.

The error bars in Fig. B.3 show the quartiles of the distributions of squared coefficients for each data point, they are in very good agreement with the quartiles of a two degree of freedom χ^2 distribution scaled by 1/2 the Lorentzian. This will be related to the structure of the random deviation terms $\tilde{g}_{s',\epsilon'}$ in Eq. B.8, which we will find to follow statistics where their real and imaginary parts can be treated as random Gaussian variates, as in Eq. 4.23. We now discuss how we obtain these results mathematically.

B.2.1. Average Lorentzian Distribution $L_{s,\epsilon}$ for the time-evolved $|s\rangle|\epsilon\rangle$ state

To derive the average Lorentzian behavior of Eq. B.8, we begin by calculating the average equilibrium state distribution for the time-evolving state of Eq. B.7. The average equilibrium behavior is given by the long-time average of the density operator

$$\langle\hat{\rho}_{s,\epsilon}\rangle_{t\to\infty} = \big\langle|\Psi_{s,\epsilon}(t)\rangle\langle\Psi_{s,\epsilon}(t)|\big\rangle_{t\to\infty} = \sum_{\xi,\xi'} c_{\xi}^{(s,\epsilon)} c_{\xi'}^{(s,\epsilon)^*} \big\langle e^{-i(E_\xi - E_{\xi'})t}\big\rangle_{t\to\infty} |\xi\rangle\langle\xi'|, \quad \text{(B.11)}$$

where the time-averages are $\langle x\rangle_{t\to\infty} \equiv \lim_{t\to\infty}(1/t)\int_0^t d\tau x(\tau)$ and the coefficients are given by Eq. B.3 with $c_{\xi}^{(s,\epsilon)} = \langle\xi|s\rangle|\epsilon\rangle = \ c_{s,\epsilon}^{(\xi)^*}$. The energy eigenvalues are non-degenerate since there are no symmetries in the random matrix model, so the cross terms average to zero and

$$\langle\hat{\rho}_{s,\epsilon}\rangle_{t\to\infty} = \sum_{\xi} |c_{\xi}^{(s,\epsilon)}|^2 |\xi\rangle\langle\xi| = \sum_{\xi} |g_{s,\epsilon}^{(\xi)}|^2 L_\xi(E_0)|\xi\rangle\langle\xi|, \quad \text{(B.12)}$$

where the last equality has replaced the $|c_{\xi}^{(s,\epsilon)}|^2$ with the expressions from Eq. B.3, with the initial state energy $E_0 = E_s + E_\epsilon$.

We are interested in the distribution of the time-average density operator of Eq. B.12 in the $\{|s\rangle|\epsilon\rangle\}$ basis, where the diagonal elements are $\langle s'|\langle\epsilon'|\langle\hat{\rho}_{s,\epsilon}\rangle_{t\to\infty}|\epsilon'\rangle|s'\rangle$. Using the form of the eigenstates in Eqs. B.2 and B.3 the diagonal elements of the density operator in the zero-order basis are

$$\langle s'|\langle\epsilon'|\langle\hat{\rho}_{s,\epsilon}\rangle_{t\to\infty}|\epsilon'\rangle|s'\rangle \approx \sum_{\xi} |g_{s,\epsilon}^{(\xi)}|^2 |g_{s',\epsilon'}^{(\xi)}|^2 L_\xi(E_0) L_\xi(E_{s'} + E_{\epsilon'}). \quad \text{(B.13)}$$

We assume that the Gaussian variates are statistically independent from the Lorentzian factors so we can simply approximate them with their mean values $\langle|g_{s,\epsilon}^{(\xi)}|^2\rangle = \langle|g_{s',\epsilon'}^{(\xi)}|^2\rangle = 1$ for all values of the indices $\xi, s, \epsilon, s', \epsilon'$. With this approximation

$$\langle s'|\langle\epsilon'|\langle\hat{\rho}_{s,\epsilon}\rangle_{t\to\infty}|\epsilon'\rangle|s'\rangle \approx \sum_{\xi} L_{\xi}(E_0)L_{\xi}(E_{s'}+E_{\epsilon'}). \tag{B.14}$$

We will now make two approximations to greatly simplify this sum, resulting ultimately in a single Lorentzian factor. The first approximation uses a single density of states $\rho(E_\xi) = \rho(E_0)$ evaluated at the initial state energy $E_0 = E_s + E_\epsilon$ instead of the variable eigenstate energy E_ξ. This approximation is reasonable since most of the sum comes from eigenstates with eigenenergies $E_\xi \approx E_0$ where the Lorentzians are near their maxima in Eq. B.4. The second approximation is to replace the sum by an integral over all energies, which is reasonable since the discrete energy level spacings are small. With these approximations Eq. B.14 becomes

$$\begin{aligned}&\langle s'|\langle\epsilon'|\langle\hat{\rho}_{s,\epsilon}\rangle_{t\to\infty}|\epsilon'\rangle|s'\rangle \\ &\approx \frac{1}{\pi^2\rho}\int_{-\infty}^{\infty} dE_\xi \frac{\pi k^2\rho}{(E_0+\Delta E_0-E_\xi)^2+(\pi k^2\rho)^2}\frac{\pi k^2\rho}{(E_\xi-E_{s'}-E_{\epsilon'}-\Delta E_0)^2+(\pi k^2\rho)^2},\end{aligned} \tag{B.15}$$

where $\rho = \rho(E_0)$. There is an additional factor of the density of states $\rho(E_0)$ in the integrand of Eq. B.15 in comparison to the summands in Eq. B.14 since there are ρdE_ξ summands within each interval dE_ξ of the integration. The integral gives the convolution of two Lorentzians. We evaluated the integral using *Mathematica*, the result is a Lorentzian with twice the half-width at half-max and a central energy at $E_{s'} + E_{\epsilon'} = E_0$,

$$\langle s'|\langle\epsilon'|\langle\hat{\rho}_{s,\epsilon}\rangle_{t\to\infty}|\epsilon'\rangle|s'\rangle \approx \frac{1}{\pi}\frac{2\pi k^2}{(E_s+E_{\epsilon'}-E_0)^2+(2\pi k^2\rho)^2}. \tag{B.16}$$

The relation Eq. B.16 gives the average Lorentzian in Eq. B.9 and Fig. B.3 at the start of this section and in Eq. 4.27 and Fig. 4.2. It is a Lorentzian centered at the

initial state energy $E_0 = E_s + E_\epsilon$, with twice the width of the eigenstates, obtained through the convolution of Lorentzians in Eq. B.15. This result was also obtained by Deutsch [21, 22] in a similar model. We will now consider the fluctuations about this Lorentzian average, to determine the factors $\tilde{g}_{s',\epsilon'}$ in Eq. B.8. This will go beyond Deutsch's work and is a critical component of our modeling and results, where the factors $\tilde{g}_{s',\epsilon'}$ play a significant role.

B.2.2. Fluctuations $\tilde{g}_{s',\epsilon'}$ in the coefficients of the time-evolved $|s\rangle|\epsilon\rangle$ state

Now we would like to consider the time-dependent state Eq. B.7 as undergoing fluctuations about its equilibrium Lorentzian average from Eq. B.16, where the fluctuations are given by the factors $\tilde{g}_{s',\epsilon'}$ in Eq. B.8. We expect that the average squared fluctuation is unity, $\langle|\tilde{g}_{s',\epsilon'}|^2\rangle = 1$, so that the $|c_{s',\epsilon'}(t)|^2$ follow the Lorentzian on average. We also expect that the real and imaginary parts of $\tilde{g}_{s',\epsilon'}$ should contribute equally on average. This implies that the fluctuation term can be expressed as

$$\tilde{g}_{s',\epsilon'} = \frac{g_{s',\epsilon'} + i g'_{s',\epsilon'}}{\sqrt{2}}, \tag{B.17}$$

where the real and imaginary components $g_{s',\epsilon'}$ and $g'_{s',\epsilon'}$ each have the average squared values $\langle g^2_{s,\epsilon}\rangle = \langle {g'_{s,\epsilon}}^2\rangle = 1$, so that $\langle|\tilde{g}_{s',\epsilon'}|^2\rangle = 1$.

We examine the real and imaginary components $g_{s',\epsilon'}$ and $g'_{s',\epsilon'}$ separately, in comparison with the exact coefficients $c_{s',\epsilon'}(t)$ of Eq. B.7. By comparison of Eqs. B.7, B.8, and B.17, we have the following relations for $g_{s',\epsilon'}$ and $g'_{s',\epsilon'}$,

$$g_{s',\epsilon'} = \mathrm{Re}\left(\frac{\tilde{g}_{s',\epsilon'}}{1/\sqrt{2}}\right) = \mathrm{Re}\left(\frac{c_{s',\epsilon'}(t)}{\sqrt{L_f^{(s,\epsilon)}(E_{s'} + E_{\epsilon'})/2}}\right) \tag{B.18}$$

and

$$g'_{s',\epsilon'} = \mathrm{Im}\left(\frac{\tilde{g}_{s',\epsilon'}}{1/\sqrt{2}}\right) = \mathrm{Im}\left(\frac{c_{s',\epsilon'}(t)}{\sqrt{L_f^{(s,\epsilon)}(E_{s'}+E_{\epsilon'})/2}}\right). \tag{B.19}$$

Fig. B.4 shows the distributions of the $g_{s',\epsilon'}$ and $g'_{s',\epsilon'}$ taken as the right hand sides of Eqs. B.18 and B.19, at an instant in time t after the $|s\rangle|\epsilon\rangle$ initial state has evolved to equilibrium (the results are similar for other t). The $g_{s,\epsilon}$ and $g'_{s,\epsilon}$ each follow standard Gaussian distributions, indicating that they are each distributed as random Gaussian variates as in Eq. B.6. This is also consistent with the quartile distributions observed previously in Fig. B.3; the squared complex fluctuation term $|\tilde{g}_{s',\epsilon'}|^2 = (g_{s,\epsilon}^2 + {g'_{s,\epsilon}}^2)/2$ has the distribution of a sum of two squared random standard Gaussian variates, which gives coefficients that follows the two degree of freedom χ^2 distribution scaled by $L_f^{(s,\epsilon)}/2$, with the quartiles shown in Fig. B.3. Thus, taking $\tilde{g}_{s',\epsilon'}$ as the sum Eq. B.17 with $g_{s,\epsilon}$ and $g'_{s,\epsilon}$ as random Gaussian variates is giving an entirely consistent description of our results in Figs. B.3 and B.4.

This completes our analysis of the time-evolved $|s\rangle|\epsilon\rangle$ state in Eq. B.8, where the coefficients $c_{s',\epsilon'}(t)$ are given in terms of the the Lorentzian averages $\sqrt{L_f^{(s,\epsilon)}}$ determined by the analysis of the last section and the complex Gaussian variate fluctuation terms $\tilde{g}_{s',\epsilon'}$ we have just discussed.

B.3. Time evolution of a Lorentzian initial state

Now we consider the time evolution of Lorentzian initial states, as in Fig. 4.1 and Eqs. 4.21-4.23 and 4.26-4.28. Our goal here is to systematically characterize the equilibration behavior of the Lorentzian initial states, similar to what we did in Section B.2 for the $|s\rangle|\epsilon\rangle$ initial states.

We consider the initial Lorentzian state from Eqs. 4.21-4.23, repeated here as

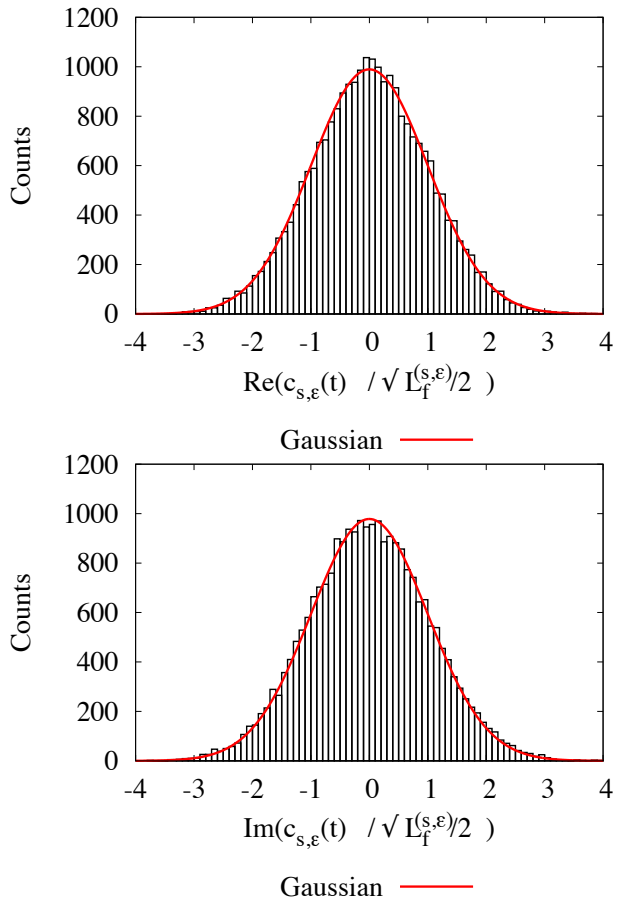

FIGURE B.4. Histogram counts of coefficient variations for a time-evolved $|s\rangle|\epsilon\rangle$ initial state. The real and imaginary parts the variations in Eqs. B.18 and B.19 each follow a Gaussian distribution.

$$|\Psi_L^0\rangle = \sum_\epsilon \tilde{g}_{s,\epsilon}\sqrt{L_0}|s\rangle|\epsilon\rangle, \tag{B.20}$$

where the $\tilde{g}_{s,\epsilon}$ are random complex Gaussian variates as in Eq. B.17 and L_0 is the initial state Lorentzian

$$L_0(E_s + E_\epsilon) = \frac{1}{\pi}\frac{\gamma_0/\rho_0}{(E_s + E_\epsilon - E_0)^2 + \gamma_0^2}, \tag{B.21}$$

where γ_0 is the half-width at half-max, E_0 is the central Lorentzian energy, and $\rho_0(E_0)$ is the density of system-environment states with the system in its initial state $|s\rangle$ at the initial state energy $E_0 = E_s + E_\epsilon$. Our goal is to show that this evolves into the final equilibrium state Lorentzian from Eqs. 4.26-4.28, repeated here as

$$|\Psi_L^f(t)\rangle = \sum_{s,\epsilon} \tilde{g}_{s,\epsilon}\sqrt{L_f}|s\rangle|\epsilon\rangle, \tag{B.22}$$

with the final state Lorentzian

$$L_f(E_s + E_\epsilon) = \frac{1}{\pi}\frac{\gamma_f/\rho_f}{(E_s + E_\epsilon - E_0)^2 + \gamma_f^2}, \tag{B.23}$$

with half-width at half-max

$$\gamma_f = \gamma_0 + 2\pi k^2 \rho_f, \tag{B.24}$$

where $\rho_f = \rho(E_0)$ is the total density of system-environment zero-order states (when all system levels are accessible at equilibrium).

Fig. B.5 shows an initial Lorentzian state of Eq. B.20 on the left and a time-evolved version of the same state as in Eq. B.22 on the right. The state is the same as in Fig. 4.1. The final state Lorentzian L_f is similar to the initial state

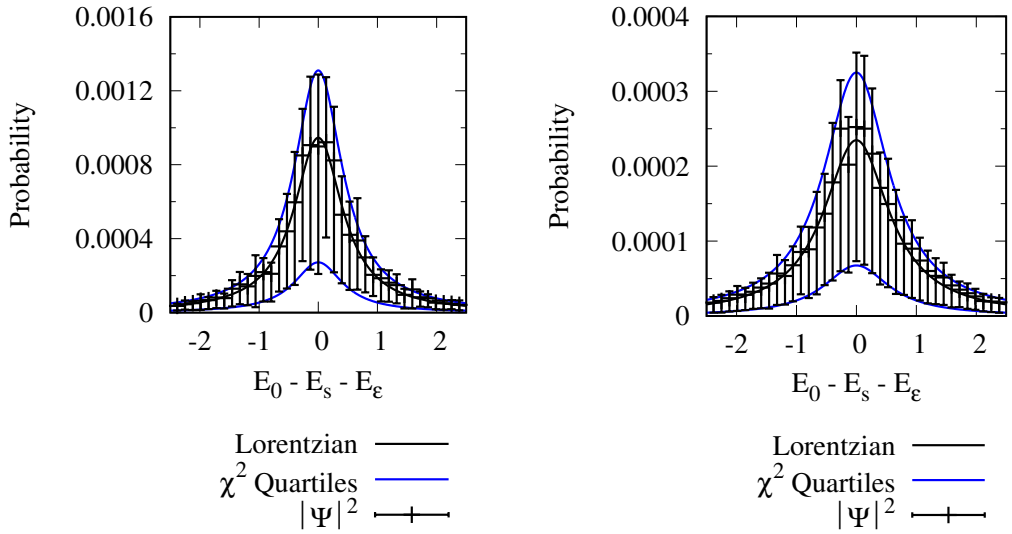

FIGURE B.5. Average squared coefficients $\langle |c_{s',\epsilon'}(t)|^2 \rangle$ for a time-evolved Lorentzian initial state of Eq. B.20 follows a Lorentzian distribution with increased width (the state is the same as in Fig. 4.1). Error bars show the first and third quartiles of the distribution of the individual $|c_{s',\epsilon'}(t)|^2$ in each data point. The quartiles of the coefficient distributions are in good agreement with the quartiles of the two degree of freedom χ^2 distribution scaled by half the Lorentzian weight, shown in blue.

Lorentzian L_0 except the width γ_f is increased by twice the approximate widths of the eigenstates $2\pi k^2 \rho_f$. To rationalize this behavior, we will begin by analyzing the average equilibrium behavior of the time-evolving initial Lorentzian state, then analyze the fluctuations about the average to determine the $\tilde{g}_{s,\epsilon}$. The fluctuations will follow the same type of random Gaussian structure as we had for the time-evolved $|s\rangle|\epsilon\rangle$ states, giving the blue χ^2 quartiles in the figure.

B.3.1. Average final Lorentzian distribution for the time-evolved Lorentzian initial state

To determine the average final state Lorentzian in Eq. B.22, we will calculate the average equilibrium behavior of the time-evolving Lorentzian initial state of Eq. B.20,

analogous to what we did with the average time-evolving $|s\rangle|\epsilon\rangle$ initial state in Section B.2.1. To begin, express the initial state density operator as

$$\hat{\rho}_L^0 = \hat{\rho}_L^{0,\text{diag}} + \hat{\rho}_L^{0,\text{coh}}, \tag{B.25}$$

where $\hat{\rho}_L^{0,\text{diag}}$ gives the diagonal component with trace of unity,

$$\hat{\rho}_L^{0,\text{diag}} = \sum_{s,\epsilon} |\tilde{g}_{s,\epsilon}|^2 L_0(E_s + E_\epsilon)|s\rangle|\epsilon\rangle\langle\epsilon|\langle s|, \tag{B.26}$$

and $\hat{\rho}_L^{0,\text{coh}}$ gives the coherences between the $|s\rangle|\epsilon\rangle$ states with trace of zero,

$$\hat{\rho}_L^{0,\text{coh}} = \sum_{s,\epsilon\neq s',\epsilon'} \tilde{g}_{s,\epsilon}\tilde{g}_{s',\epsilon'}\sqrt{L_0(E_s + E_\epsilon)L_0(E_{s'} + E_{\epsilon'})}|s\rangle|\epsilon\rangle\langle\epsilon'|\langle s'|. \tag{B.27}$$

First consider the diagonal component $\hat{\rho}_L^{0,\text{diag}}$. Its time average is

$$\langle\hat{\rho}_L^{0,\text{diag}}\rangle_{t\to\infty} = \sum_{s,\epsilon} |\tilde{g}_{s,\epsilon}|^2 L_0(E_s + E_\epsilon)\langle\hat{\rho}_{s,\epsilon}\rangle_{t\to\infty}, \tag{B.28}$$

where $\langle\hat{\rho}_{s,\epsilon}\rangle_{t\to\infty}$ is the time-average of a single $|s\rangle|\epsilon\rangle$ initial state. Using the result for $\langle\hat{\rho}_{s,\epsilon}\rangle_{t\to\infty}$ from Eq. B.16, then approximating the sum as a convolution integral analogous to Eq. B.15 this gives

$$\langle s'|\langle\epsilon'|\langle\hat{\rho}_L^{0,\text{diag}}\rangle_{t\to\infty}|\epsilon'\rangle|s'\rangle \approx L_f(E_{s'} + E_{\epsilon'}), \tag{B.29}$$

where $L_f(E_{s'} + E_{\epsilon'})$ is the final Lorentzian in Eq. B.22. Thus, we have arrived at the final Lorentzian distribution by considering the time-averaged diagonal component

of the density operator. We now consider the coherence component of the density operator in Eq. B.25.

The coherence component $\langle\hat{\rho}_L^{0,\mathrm{coh}}\rangle_{t\to\infty}$ of the time-averaged density operator has trace zero, so it has no contribution to the total probability of the time-averaged state and only serves to give fluctuations about the diagonal component $\hat{\langle}\rho_L^{0,\mathrm{diag}}\rangle_{t\to\infty}$, with zero average fluctuation per basis state. Based on the average behavior, we will simply approximate time-average of the coherence term as zero

$$\langle s'|\langle\epsilon'|\langle\hat{\rho}_L^{0,\mathrm{coh}}\rangle_{t\to\infty}|\epsilon'\rangle|s'\rangle \approx 0. \tag{B.30}$$

We will find that this approximation works very well to model our results. Similarly, Deutsch treated $\langle\hat{\rho}_L^{0,\mathrm{coh}}\rangle_{t\to\infty}$ as negligible when calculating operator expectation values, in Eq. 5.7 of Ref. [22].

From the analysis of this section, the average equilibrium distribution for the initial Lorentzian state of Eq. B.20 is

$$\langle s'|\langle\epsilon'|\langle\hat{\rho}_L^{0}\rangle_{t\to\infty}|\epsilon'\rangle|s'\rangle \approx L_f(E_{s'} + E_{\epsilon'}). \tag{B.31}$$

This gives the final average Lorentzian in the time-evolved state of Eq. B.22 and Fig. B.5. We will now consider the fluctuations about the Lorentzian average, to devise the fluctuation terms $\tilde{g}_{s,\epsilon}$ in the final expression for equilibrium Lorentzian state of Eq. B.22.

B.3.2. Fluctuations in the coefficients of the time-evolved Lorentzian state

In this section we analyze the fluctuation terms $\tilde{g}_{s,\epsilon}$ in the expression for the final Lorentzian state of Eq. B.22. Following the same reasoning as in Section B.2.2,

we assume that the fluctuations $\tilde{g}_{s,\epsilon}$ can be expressed in the form of Eq. B.17. We analyze the real and imaginary components $g_{s,\epsilon}$ and $g'_{s,\epsilon}$ using relations analogous using Eqs. B.18 and B.19 but with the final state Lorentzian of Eq. B.23,

$$g_{s,\epsilon} = \mathrm{Re}\left(\frac{\tilde{g}_{s,\epsilon}}{1/\sqrt{2}}\right) = \mathrm{Re}\left(\frac{c_{s,\epsilon}(t)}{\sqrt{L_f(E_s + E_\epsilon))/2}}\right) \tag{B.32}$$

and

$$g'_{s,\epsilon} = \mathrm{Im}\left(\frac{\tilde{g}_{s,\epsilon}}{1/\sqrt{2}}\right) = \mathrm{Im}\left(\frac{c_{s,\epsilon}(t)}{\sqrt{L_f(E_s + E_\epsilon)}}\right), \tag{B.33}$$

where $c_{s,\epsilon}(t)$ are the exact time-dependent coefficients of the $|s\rangle|\epsilon\rangle$ basis states taken at an instant in time t at equilibrium (the results are similar for other t at equilibrium).

Fig. B.6 shows the distribution of the $g_{s,\epsilon}$ and $g'_{s,\epsilon}$, taken as the right hand sides of Eqs. B.32 and B.33. The distributions follow the standard Gaussian distribution, indicating that both $g_{s,\epsilon}$ and $g'_{s,\epsilon}$ behave as standard Gaussian variates, analogous to what we saw with the coefficients of the time-evolved $|s\rangle|\epsilon\rangle$ state in Section B.2.2.

In total, we have seen in this section how the time-evolution of an initial Lorentzian state of Eq. B.20 gives the final Lorentzian state of Eq. B.22, with random complex Gaussian variate fluctuations $\tilde{g}_{s,\epsilon}$ about the final Lorentzian L_f.

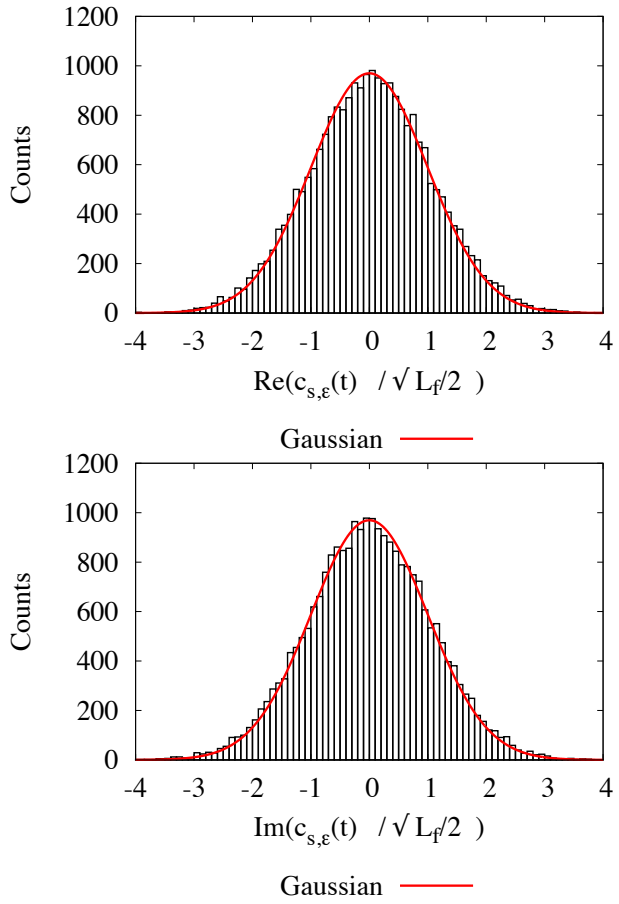

FIGURE B.6. Histogram counts of coefficient variations for a time-evolved Lorentzian initial state. The real and imaginary parts the variations in Eqs. B.32 and B.33 each follow a Gaussian distribution.

APPENDIX C

ENTROPY OF THE LORENTZIAN

This Appendix includes unpublished material co-authored by Michael E. Kellman [3]. Michael Kellman and I both contributed to developing the theory and writing in this Appendix.

In this Appendix we derive the entropy Eq. 4.29 for a state with random variations about a Lorentzian, following the work on Lorentzian states in Section 4.5 and Appendix B.

Each of the Lorentzian states of Section 4.5 has squared coefficients of the approximate form

$$p_\alpha = |c_\alpha|^2 \approx |\tilde{g}_\alpha|^2 L_\alpha = |\tilde{g}_\alpha|^2 \frac{1}{\pi} \frac{\gamma/\rho}{\Delta E_\alpha^2 + \gamma^2}, \tag{C.1}$$

where $\Delta E_\alpha = E_0 - E_\alpha$ is the energy difference between the basis state $|\alpha\rangle = |s\rangle|\epsilon\rangle$ and the initial state energy E_0, $\tilde{g}_\alpha$ is a complex Gaussian variate as in Eq. 4.23, and γ is the half-width at half-max of the Lorentzian. Using these coefficient distributions we will calculate the entropy from Eq. 4.5

$$S^Q_{univ} = -\sum_\alpha p_\alpha \ln p_\alpha. \tag{C.2}$$

Using Eq. C.1 the entropy is

$$S^Q_{univ} \approx -\sum_\alpha |\tilde{g}_\alpha|^2 L_\alpha \ln\left(|\tilde{g}_\alpha|^2 L_\alpha\right) = -\sum_\alpha |g_\alpha|^2 L_\alpha \ln\left(L_\alpha\right) - \sum_\alpha L_\alpha |g_\alpha|^2 \ln\left(|g_\alpha|^2\right) \tag{C.3}$$

The g_α are statistically independent from the L_α by assumption. This suggests replacing the individual $|g_\alpha|^2$ in the first sum on the right of Eq. C.3 with their average value $\langle |g_\alpha|^2 \rangle = 1$,

$$\sum_\alpha |g_\alpha|^2 L_\alpha \ln(L_\alpha) \approx \sum_\alpha L_\alpha \ln(L_\alpha), \tag{C.4}$$

leaving just the entropy of the perfect Lorentzian. For the second sum on the right of Eq. C.3 the statistical independence of the g_α suggests replacing the $|g_\alpha|^2 \ln(|g_\alpha|^2)$ with the average value

$$\sum_\alpha L_\alpha |g_\alpha|^2 \ln\left(|g_\alpha|^2\right) \approx \langle |g_\alpha|^2 \ln\left(|g_\alpha|^2\right)\rangle \sum_\alpha L_\alpha = \langle |g_\alpha|^2 \ln\left(|g_\alpha|^2\right)\rangle \tag{C.5}$$

where the last equality uses the normalization of the Lorentzian $\sum_\alpha L_\alpha = 1$. In total, Eq. C.3 is then approximated as

$$S^Q_{univ} \approx -\sum_\alpha L_\alpha \ln(L_\alpha) - \langle |g_\alpha|^2 \ln\left(|g_\alpha|^2\right)\rangle \tag{C.6}$$

The first term is the entropy of a Lorentzian, while the second term gives the deviation from the perfect Lorentzian entropy due to the random variations in the state.

Now we will evaluate the terms in Eq. C.6. The Lorentzian sum in the first term can be approximated as the integral

$$-\sum_\alpha L_\alpha \ln(L_\alpha) \approx -\int_{-\infty}^{\infty} d(\Delta E_\alpha) L_\alpha(\Delta E_\alpha) \rho(E_0) \ln(L_\alpha(\Delta E_\alpha)) \tag{C.7}$$

In the integral approximation, the density of states ρ is factored into the integrand to account for having approximately $\rho d(\Delta E_\alpha)$ states in the sum that are within

each differential interval $d(\Delta E_\alpha)$ of integration. To simplify the integral, we have approximated the density of states as the constant value at the central energy of the Lorentzian $\rho = \rho(E_0)$, where the majority of probability in the Lorentzian is located.

To evaluate the integral Eq. C.7 we first split it into two separate integrals by factoring $\rho(E_0)/\rho(E_0)$ into the logarithm then separating out a term $-\ln \rho(E_0)$,

$$
\begin{aligned}
&- \int_{-\infty}^{\infty} d(\Delta E_\alpha) L_\alpha(\Delta E_\alpha) \rho(E_0) \ln \left(L_\alpha(\Delta E_\alpha) \right) \\
&= - \int_{-\infty}^{\infty} d(\Delta E_\alpha) L_\alpha(\Delta E_\alpha) \rho(E_0) \ln \left(L_\alpha(\Delta E_\alpha) \rho(E_0) \right) + \int_{-\infty}^{\infty} d(\Delta E_\alpha) L_\alpha \rho(E_0) \ln \rho(E_0)
\end{aligned}
\tag{C.8}
$$

The first integral on the right of Eq. C has the well known solution $\ln(4\pi\gamma)$ for the entropy of a continuous Lorentzian distribution, while the second integral is simply $\ln \rho(E_0)$, since $\rho(E_0)$ is a constant and $\int_{-\infty}^{\infty} d(\Delta E_\alpha) \rho(E_0) L_\alpha(\Delta E_\alpha) = 1$ by the normalization of the Lorentzian. Then in total we have

$$
- \sum_\alpha L_\alpha \ln \left(L_\alpha \right) \approx \ln(4\pi\gamma\rho(E_0)) \tag{C.9}
$$

The final term in Eq. C.6 for the average $\langle |g_\alpha|^2 \ln \left(|g_\alpha|^2 \right) \rangle$ is calculated through integration over all the values of g' and g'' with the Gaussian variate probability density $p(g) = (2\pi)^{-1/2} \exp(-g^2/2)$,

$$
\langle |g_\alpha|^2 \ln \left(|g_\alpha|^2 \right) \rangle = \int_{-\infty}^{\infty} dg' \int_{-\infty}^{\infty} dg'' p(g') p(g'') \frac{g'^2 + g''^2}{2} \ln \frac{g'^2 + g''^2}{2} = g_0 \tag{C.10}
$$

where

$$g_0 = 1 - \gamma_{EM} \tag{C.11}$$

where $\gamma_{EM} = 0.577\ 215...$ is the Euler-Mascheroni constant.

Putting Eqs. C.9 and C.10 into Eq. C.6 gives the approximate entropy Eq. 4.29 for the Lorentzian states,

$$S \approx \ln(4\pi\gamma\rho(E_0)) - g_0. \tag{C.12}$$

APPENDIX D

SINGLE BATH TEMPERATURES IN THE TOTAL SYSTEM WITH TWO BATHS

This appendix includes previously unpublished material co-authored by Michael E. Kellman [5]. Michael Kellman and I both contributed to developing the theory. I wrote this appendix.

This appendix develops the single bath temperatures in the total system with two baths from Chapter VI and Ref. [5]. The next section gives an overview of the definition for the temperature and discusses its calculated behavior. The final section presents the details of the calculation.

D.1. Temperature

In this section we define and discuss the single bath temperatures we use to analyze temperature equilibration in Chapter VI. We begin by considering the standard notion of temperature, based on a total isolated system, in our setup the total system $\mathcal{E}_1\mathcal{S}\mathcal{E}_2$. We then specialize to defining a temperature the single finite baths $\mathcal{E}_1$ and $\mathcal{E}_2$.

Temperature is usually defined with respect to an isolated total system through the fundamental relation

$$\frac{1}{T} = \frac{\partial S}{\partial E}, \tag{D.1}$$

where E is the energy and $S = k \ln W$ is the microcanonical Boltzmann entropy, where W is the number of states in the microcanonical ensemble. For our total system $\mathcal{E}_1\mathcal{S}\mathcal{E}_2$, this temperature can be evaluated exactly by thinking of the two

oscillator baths as a single larger bath and using the equilibrium temperature for a single oscillator bath interacting with a system from Eqs. 5.23 and 5.13. However, this temperature is for the total system, whereas we would like to have separate temperatures for the two baths, with potential for the bath temperatures to vary during equilibration or at equilibrium. For this, we need a new notion of temperature that applies to a single bath in our model.

We define the single bath temperatures using the relation Eq. D.1 applied to the separate baths $\mathcal{E}_1$ and $\mathcal{E}_2$, for example

$$\frac{1}{T_{\mathcal{E}_1}} = \frac{\partial S_{\mathcal{E}_1}}{\partial E_{\mathcal{E}_1}}, \tag{D.2}$$

where the bath entropy is

$$S_{\mathcal{E}_1} = -\sum_{\epsilon_1} p_{\epsilon_1} \ln p_{\epsilon_1} \tag{D.3}$$

and the average bath energy is

$$E_{\mathcal{E}_1} = \sum_{\epsilon_1} p_{\epsilon_1} E_{\epsilon_1}. \tag{D.4}$$

Both $S_{\mathcal{E}_1}$ and $E_{\mathcal{E}_1}$ are defined in relation to the probabilities p_{ϵ_1} of the $\mathcal{E}_1$ microstates $|\epsilon_1\rangle$ with energies E_{ϵ_1} (similar relations hold for the bath $\mathcal{E}_2$ with microstates $|\epsilon_2\rangle$ and probabilities p_{ϵ_2}). To evaluate these expressions, we will derive the p_{ϵ_1} from the fundamental microcanonical ensemble description of the total system $\mathcal{E}_1\mathcal{S}\mathcal{E}_2$. This gives relations for $S_{\mathcal{E}_1}$ and $E_{\mathcal{E}_1}$ based on standard microcanonical reasoning. We use these relations to evaluate the temperature in Eq. D.2, leading ultimately to a temperature-energy relationship $T_{\mathcal{E}} = T_{\mathcal{E}}(E_{\mathcal{E}})$ that we use to calculate the temperature in our simulations.

To define the single bath microstate probabilities we begin by considering the fundamental statistical mechanical description of the total $\mathcal{E}_1\mathcal{S}\mathcal{E}_2$ system in terms of the microcanonical ensemble at total energy E. In the microcanonical ensemble, each of the $\mathcal{E}_1\mathcal{S}\mathcal{E}_2$ microstate trios $|\epsilon_1\rangle|s\rangle|\epsilon_2\rangle$ in the microcanonical energy shell $E-\delta E/2 \leq E_{\epsilon_1} + E_s + E_{\epsilon_2} \leq E + \delta E/2$ are treated as having equal probabilities $p_{\epsilon_1,s,\epsilon_2} = 1/W$, where W is the total number of states in the energy shell. The probabilities p_{ϵ_1} for the single bath microstates $|\epsilon_1\rangle$ come from adding up probabilities for all of the $\mathcal{E}_1\mathcal{S}\mathcal{E}_2$ microstates containing $|\epsilon_1\rangle$,

$$p_{\epsilon_1} = \sum_s \sum_{\epsilon_2} p_{\epsilon_1,s,\epsilon_2} \tag{D.5}$$

(a similar relation holds for the $\mathcal{E}_2$ microstate probabilities p_{ϵ_2}). We calculate the p_{ϵ_1} and p_{ϵ_2} following the method detailed in the next section; in short, we use a continuous density of $\mathcal{E}_2$ states to approximate the discrete sum in Eq. D.5, leading to continuous approximations for $S_{\mathcal{E}_1}$ and $E_{\mathcal{E}_1}$ from Eqs. D.3 and D.4. We use these approximate expressions to numerically calculate the temperature $T_{\mathcal{E}_1}$ in Eq. D.2. The details of the calculatoin can be found in the next section; in the remainder of this section we will discuss the behavior of the resulting temperature-energy relationship $T_{\mathcal{E}_1}(E_{\mathcal{E}_1})$.

Fig. D.1 shows the behavior of the single bath temperature $T_{\mathcal{E}_1}$ of Eq. D.2 with $\eta_1 = \eta_2 = 4$ oscillators per bath (the same curve also applies to the temperature $T_{\mathcal{E}_2}$ of the second bath). $T_{\mathcal{E}_1}$ is compared with the average energy per bath oscillator $\langle E_{osc}\rangle + 1/2 = E_{\mathcal{E}_1}/\eta_1 + 1/2$ (the factor of $1/2$ is an arbitrary added constant that will be explained shortly). To begin analyzing the temperature behavior, we will first present some technical notes on the low-energy behavior of $T_{\mathcal{E}_1}$, then move to an analysis at higher energies as we used in our simulations, where we will compare $T_{\mathcal{E}_1}$ to a more standard type of temperature behavior for an infinite bath. Our temperature

$T_{\mathcal{E}_1}$ begins at a non-zero temperature in the figure, where the bath energy is greater than zero. This is related to the continuous approximation we use, which treats $S_{\mathcal{E}_1}$ as zero in a region around $\langle E_{osc}\rangle = 0$, where the states are highly discrete and our continuous approximation fails, see the next section for details. Another technical note is that there is a discontinuity in the temperature when $\langle E_{osc}\rangle + 1/2 = 0.625$ in the figure, when the total energy is $E = 1$. The discontinuity comes from the discontinuous change in the total density of states when the excited system state with energy $E_s = 1$ becomes accessible. It might be interesting to study discontinuities like this in future studies of thermodynamics of finite systems, but for our purposes here we will focus on higher energies where the temperature is more regular. We now turn to an analysis of the temperature at modest and high energies, in comparison with the standard temperature behavior for an infinite bath.

To rationalize the behavior we see in the figure, we will follow a similar route as in our previous work [4] and compare our curve for $T_{\mathcal{E}_1}$ with a more standard type of type of temperature-energy curve from Einstein's 1907 [56] model for the heat capacity of a solid in an infinite fixed-temperature bath. With the infinite bath, the average number of energy quanta in an oscillator $\langle n_{osc}\rangle$ is related to the temperature by

$$\langle n_{osc}\rangle = \frac{1}{e^{1/T} - 1}. \tag{D.6}$$

We work in units where the energy level spacing of the oscillator is $\hbar\omega = 1$, so that $\langle n_{osc}\rangle = \langle E_{osc}\rangle$. The total energy in the oscillator includes the contribution from energy quanta plus the zero-point energy $\langle E^{tot}_{osc}\rangle = \langle E_{osc}\rangle + 1/2$, shown along the vertical axis in Fig. D.1. The energy starts at the zero-point value of 1/2 at temperature $T = 0$, then quickly approaches the equipartition relation $T = \langle E_{osc}\rangle +$

1/2 at higher energy. This is the standard behavior with an infinite bath that we will compare with our results for the finite bath temperature $T_{\mathcal{E}_1}$.

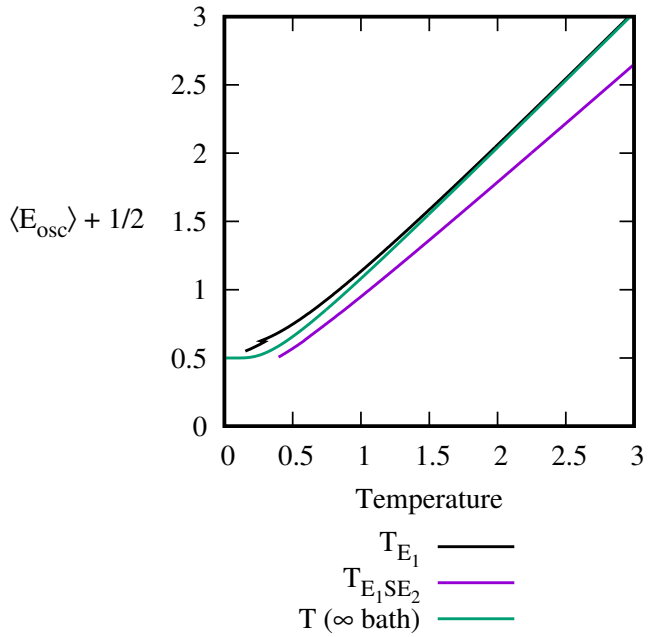

FIGURE D.1. Temperature for a single bath $T_{\mathcal{E}_1}$ in a universe with two baths, from Eq. D.2, approaches the standard temperature-energy relation for an infinite bath from Eq. D.6. In contrast, the temperature for the total system $T_{\mathcal{E}_1\mathcal{S}\mathcal{E}_2}$ for the total system is higher, as discussed in the text.

Now we would like to analyze the behavior of our single bath temperature $T_{\mathcal{E}_1}$ at modest and high energies, in comparison with the infinite bath temperature. For a direct comparison with the infinite bath result, we have plotted $T_{\mathcal{E}_1}$ against $\langle E_{osc}\rangle+1/2$ in the figure, where $\langle E_{osc}\rangle = E_{\mathcal{E}_1}/\eta_1$ is the average energy per oscillator. With the single bath, the factor of 1/2 is an arbitrary added constant needed for a direct comparison with the infinite bath. The 1/2 does not exactly equal the average zero-point energy, which depends on the variable frequencies of the bath oscillators, see Ref. [4] for details.

Consider the behavior of $T_{\mathcal{E}_1}$ at higher energy, where our continuous approximation is working well. In this region, $T_{\mathcal{E}_1}$ approaches the standard infinite bath result, where $T_{\mathcal{E}_1} \approx \langle E_{osc} \rangle + 1/2$ at high energy. Thus, at high energy, we have a very normal type of temperature behavior for the single bath temperature $T_{\mathcal{E}_1}$ from Eq. D.2. The high-energy region is the region we use in our simulations, where we have $T_{\mathcal{E}} \gtrsim 1$.

As a final note, we compare $T_{\mathcal{E}_1}$ with the temperature $T_{\mathcal{E}_1\mathcal{S}\mathcal{E}_2}$ of the total system. The total system temperature $T_{\mathcal{E}_1\mathcal{S}\mathcal{E}_2}$ is shown by the purple line in Fig. D.1, and behaves much differently than both $T_{\mathcal{E}_1}$ and the infinite bath temperature. We compared this type of temperature with the infinite bath temperature in detail in Ref. [4], where we showed there is a direct connection between the difference in the temperature curves and the number of oscillators in the bath. The temperature $T_{\mathcal{E}_1\mathcal{S}\mathcal{E}_2}$ converges to the infinite bath curve as the number of bath oscillators $\eta \to \infty$, as needed in a reasonable temperature definition, with deviations at small η corresponding to finite-size effects. It's interesting to note that in comparison with $T_{\mathcal{E}_1\mathcal{S}\mathcal{E}_2}$, the single bath temperature $T_{\mathcal{E}_1}$ is much closer to the infinite bath temperature despite the finite size of the single bath. The difference is related to energy fluctuations in the single bath—the total system has a fixed energy, whereas $\mathcal{E}_1$ alone has an average energy with significant fluctuations. Evidently, by the analysis of the figure, these energy fluctuations give a temperature $T_{\mathcal{E}_1}$ that is much closer to the standard temperature with an infinite bath.

In summary, we used the standard definition of Eqs. D.1 and D.2 to develop temperatures $T_{\mathcal{E}_1}$ and $T_{\mathcal{E}_2}$ for the single baths within the $\mathcal{E}_1\mathcal{S}\mathcal{E}_2$ equilibrium state. The temperatures vary from the temperature of the total system $T_{\mathcal{E}_1\mathcal{S}\mathcal{E}_2}$ due to finite size effects and energy fluctuations in the bath. The final relations $T_{\mathcal{E}_1}(E_{\mathcal{E}_1})$ and

$T_{\mathcal{E}_2}(E_{\mathcal{E}_2})$ show approximately standard behavior at modest and high energies as used in our simulations, with temperature-energy curves close to the standard curves for an infinite bath.

D.2. Numerical calculation of the single bath temperature

In this section we describe our method of numerically calculating the single bath temperature $T_{\mathcal{E}_1}$ from Eq. D.2 (similar expressions hold throughout for the second bath $\mathcal{E}_2$ with temperature $T_{\mathcal{E}_2}$). To calculate $T_{\mathcal{E}_1}$ using Eq. D.2, we need expressions for the single bath entropy $S_{\mathcal{E}_1}$ and average energy $E_{\mathcal{E}_1}$ from Eqs. D.3 and D.4, which are both defined in relation to the single bath microstate probabilities p_{ϵ_1} of Eq. D.5. Our approach is to approximate the p_{ϵ_1} using a density of states function that gives a continuous "count" of the number of microcanonical states contributing to p_{ϵ_1}. This leads to tractable continuous expressions $S_{\mathcal{E}_1}$ and $E_{\mathcal{E}_1}$ that we use to numerically evaluate the single bath temperature of Eq. D.2 as a converged finite difference.

To begin, consider the expression for p_{ϵ_1} in Eq. D.5. The rightmost sum $\sum_{\epsilon_2}$ counts the number of $\mathcal{E}_2$ states that pair with the $\mathcal{E}_1$ microstate $|\epsilon_1\rangle$ and the $\mathcal{S}$ microstate $|s\rangle$ in the microcanonical energy shell $E - \delta E/2 \leq E_{\epsilon_1} + E_s + E_{\epsilon_2} \leq E + \delta E/2$, where E is the total energy and δE is the width of the energy shell. For given $|\epsilon_1\rangle$ and $|s\rangle$, the number of $\mathcal{E}_2$ states $|\epsilon_2\rangle$ in the shell can be approximated as $\rho_{\mathcal{E}_2}(E_{\epsilon_2})\delta E$, where

$$\rho_{\mathcal{E}_2}(E_{\epsilon_2}) = \begin{cases} \Gamma(\eta_2 + E_{\epsilon_2})/\Gamma(\eta_2)\Gamma(E_{\epsilon_2}+1) & E_{\epsilon_2} \geq 0 \\ 0 & E_{\epsilon_2} < 0 \end{cases} \tag{D.7}$$

is the density of $\mathcal{E}_2$ states [4] at the central $\mathcal{E}_2$ energy $E_{\epsilon_2} = E - E_s - E_{\epsilon_1}$, with Γ the Gamma function. The sum $\sum_{\epsilon_2}$ in Eq. D.5 simply counts the number of $|\epsilon_2\rangle$ states, which we approximate as $\rho_{\mathcal{E}_2}(E - E_s - E_{\epsilon_1})\delta E$ (where $E_{\epsilon_2} = E - E_s - E_{\epsilon_1}$), giving

$$p_{\epsilon_1} \approx \sum_s \rho_{\mathcal{E}_2}(E - E_{\epsilon_1} - E_s)\delta E p_{\epsilon_1,s,\epsilon_2}. \tag{D.8}$$

Next, we consider the microcanonical probability term $p_{\epsilon_1,s,\epsilon_2} = 1/W$, where W is the total number $\mathcal{E}_1\mathcal{S}\mathcal{E}_2$ states in the energy shell. We approximate $W \approx \rho_{\mathcal{E}_1\mathcal{S}\mathcal{E}_2}(E)\delta E$ using the total density of states at the microcanonical energy E,

$$\rho_{\mathcal{E}_1\mathcal{S}\mathcal{E}_2}(E) = \sum_s \int_0^{E-E_s} dE_{\epsilon_1} \rho_{\mathcal{E}_1}(E_{\epsilon_1})\rho_{\mathcal{E}_2}(E - E_s - E_{\epsilon_1}). \tag{D.9}$$

Putting $p_{\epsilon_1,s,\epsilon_2} \approx 1/\rho_{\mathcal{E}_1\mathcal{S}\mathcal{E}_2}(E)\delta E$ into Eq. D.8 gives our final expression for p_{ϵ_1} in terms of the continuous density of states functions

$$p_{\epsilon_1} \approx \frac{\sum_s \rho_{\mathcal{E}_2}(E - E_{\epsilon_1} - E_s)}{\rho_{\mathcal{E}_1\mathcal{S}\mathcal{E}_2}(E)}, \tag{D.10}$$

with a similar expression for the $\mathcal{E}_2$ microstate probabilities p_{ϵ_2}.

With the tractable continuous approximation Eq. D.10 for p_{ϵ_1}, we are now ready to evaluate the single bath entropy and energy of Eqs. D.3 and D.4. Putting Eq. D.10 into Eqs. D.3 and D.4 gives

$$S_{\mathcal{E}_1} \approx -\sum_{\epsilon_1} \left(\frac{\sum_s \rho_{\mathcal{E}_2}(E - E_{\epsilon_1} - E_s)}{\rho_{\mathcal{E}_1\mathcal{S}\mathcal{E}_2}(E)}\right) \ln\left(\frac{\sum_s \rho_{\mathcal{E}_2}(E - E_{\epsilon_1} - E_s)}{\rho_{\mathcal{E}_1\mathcal{S}\mathcal{E}_2}(E)}\right) \tag{D.11}$$

and

$$E_{\mathcal{E}_1} \approx \sum_{\epsilon_1} \left(\frac{\sum_s \rho_{\mathcal{E}_2}(E - E_{\epsilon_1} - E_s)}{\rho_{\mathcal{E}_1 \mathcal{S} \mathcal{E}_2}(E)} \right) E_{\epsilon_1}. \tag{D.12}$$

To further simplify these expressions, we approximate $\sum_{\epsilon_1}$ as an integral, giving the final relations we use to evaluate the single bath energies and entropies in our temperature definition

$$S_{\mathcal{E}_1} \approx - \int_0^E dE_{\epsilon_1} \rho_{\mathcal{E}_1}(E_{\epsilon_1}) \left(\frac{\sum_s \rho_{\mathcal{E}_2}(E - E_{\epsilon_1} - E_s)}{\rho_{\mathcal{E}_1 \mathcal{S} \mathcal{E}_2}(E)} \right) \ln \left(\frac{\sum_s \rho_{\mathcal{E}_2}(E - E_{\epsilon_1} - E_s)}{\rho_{\mathcal{E}_1 \mathcal{S} \mathcal{E}_2}(E)} \right) \tag{D.13}$$

and

$$E_{\mathcal{E}_1} \approx \int_0^E dE_{\epsilon_1} \rho_{\mathcal{E}_1}(E_{\epsilon_1}) \left(\frac{\sum_s \rho_{\mathcal{E}_2}(E - E_{\epsilon_1} - E_s)}{\rho_{\mathcal{E}_1 \mathcal{S} \mathcal{E}_2}(E)} \right) E_{\epsilon_1}, \tag{D.14}$$

with similar final expressions for $S_{\mathcal{E}_2}$ and $E_{\mathcal{E}_2}$. The integrands of Eqs. D.13 and D.14 have additional factors of $\rho_{\mathcal{E}_1}(E_{\epsilon_1})$ in comparison to the summands from Eqs. D.11 and D.12 to account for the fact that there are $\rho_{\mathcal{E}_1}(E_{\epsilon_1}) dE_{\epsilon_1}$ summands in each energy interval dE_{ϵ_1} of integration. The continuous approximation for $S_{\mathcal{E}_1}$ in Eq. D.13 fails at very small total energies E, where the approximate $S_{\mathcal{E}_1}$ can become negative, whereas the true entropy is strictly non-negative. We simply take $S_{\mathcal{E}_1} = 0$ in this region and do not evaluate temperatures until $S_{\mathcal{E}_1} > 0$. This is the reason we use a non-zero minimum energy $\langle E_{osc} \rangle$ in the temperature curve of Fig. D.1.

We are now ready to evaluate the single bath temperature $T_{\mathcal{E}_1}$ of Eq. D.2 using the tractable expressions for $S_{\mathcal{E}_1}$ and $E_{\mathcal{E}_1}$ in Eqs. D.13 and D.14. The temperature $T_{\mathcal{E}_1}$ is calculated numerically in *Mathematica* using a finite difference

$$\frac{1}{T_{\mathcal{E}_1}} \approx \frac{\Delta S_{\mathcal{E}_1}}{\Delta E_{\mathcal{E}_1}}, \tag{D.15}$$

where $\Delta S_{\mathcal{E}_1}$ and $\Delta E_{\mathcal{E}_1}$ are taken as the differences in $S_{\mathcal{E}_1}$ and $E_{\mathcal{E}_1}$ between two microcanonical states with total $\mathcal{E}_1\mathcal{S}\mathcal{E}_2$ energies E and $E + \Delta E$. We find converged results with $\Delta E = 10^{-6}$, so that the finite difference is an essentially exact approximation to the true derivative of Eq. D.2. The relation Eq. D.15, with $S_{\mathcal{E}_1}$ and $E_{\mathcal{E}_1}$ from Eqs. D.13 and D.14, is the final expression we use for $T_{\mathcal{E}_1}$ in Fig. D.1 and in the results of Chapter VI, with a similar expression for temperature of the second bath $T_{\mathcal{E}_2}$.

REFERENCES CITED

[1] G. L. Barnes, P. C. Lotshaw, and M. E. Kellman, ArXiv e-prints (2018), arXiv:1511.06176v3 [quant-ph] .

[2] P. C. Lotshaw and M. E. Kellman, J. Phys. Chem. A **123**, 831 (2019).

[3] P. C. Lotshaw and M. E. Kellman, Manuscript in preparation (2020).

[4] P. C. Lotshaw and M. E. Kellman, Phys. Rev. E **100**, 042105 (2019).

[5] P. C. Lotshaw and M. E. Kellman, Manuscript in preparation (2020).

[6] G. L. Barnes and M. E. Kellman, J. Chem. Phys. **139**, 21410893 (2013).

[7] H. Tasaki, Phys. Rev. Lett. **80**, 1373 (1998).

[8] J. Gemmer, M. Michel, and G. Mahler, *Quantum Thermodynamics: Emergence of Thermodynamic Behavior Within Composite Quantum Systems (Second Edition)*, Lecture Notes in Physics (Springer, 2009).

[9] J. von Neumann, Z. Phys. **57**, 30 (1929).

[10] J. von Neumann, Eur. Phys. J. H **35**, 201 (2010), translated by Roderich Tumulka.

[11] S. Goldstein, J. L. Lebowitz, R. Tumulka, and N. Zanghì, Eur. Phys. J. H **35**, 173 (2010).

[12] S. Popescu, A. J. Short, and A. Winter, Nature Phys. **2**, 754 (2006).

[13] N. Linden, S. Popescu, A. J. Short, and A. Winter, Phys. Rev. E **79**, 061103 (2009).

[14] S. Goldstein, J. L. Lebowitz, R. Tumulka, and N. Zanghì, Phys. Rev. Lett. **96**, 050403 (2006).

[15] S. Goldstein, J. L. Lebowitz, C. Mastrodonato, R. Tumulka, and N. Zanghì, Phys. Rev. E **81**, 011109 (2010).

[16] S. Goldstein, T. Hara, and H. Tasaki, New J. Phys. **17**, 045002 (2015).

[17] P. Reimann, Phys. Rev. Lett. **101**, 190403 (2008).

[18] P. Reimann, Nature Comm. **7**, 10821 (2016).

[19] M. Rigol, V. Dunjko, and M. Olshanni, Nature **452**, 854 (2008).

[20] J. M. Deutsch, Rep. Prog. Phys. **91**, 082001 (2018).

[21] J. M. Deutsch, Phys. Rev. A **43**, 2046 (1991).

[22] J. M. Deutsch, "A closed quantum system giving ergodicity," https://deutsch.physics.ucsc.edu/pdf/quantumstat.pdf, accessed 3-17-2020.

[23] L. D'Alessio, Y. Kafri, A. Polkovnikov, and M. Rigol, Adv. Phys. **65**, 239 (2016).

[24] A. M. Kaufman, M. E. Tai, A. Lukin, M. Rispoli, R. Schittko, P. M. Preiss, and M. Greiner, Science **353**, 794 (2016).

[25] C. Nation and D. Porras, New J. Phys. **20**, 103003 (2018).

[26] D. M. Leitner, Adv. Phys. **64**, 445 (2015).

[27] D. M. Leitner, Entropy **20**, 673 (2018).

[28] M. Esposito, K. Lindenberg, and C. V. den Broeck, New J. Phys. **12**, 013013 (2010).

[29] A. Polkovnikov, Ann. Phys. **326**, 486 (2011).

[30] X. Han and B. Wu, Phys. Rev. E **91**, 062106 (2015).

[31] S. Kak, Int. J. Theo. Phys. **46**, 860 (2007).

[32] D. Reeb and M. M. Wolf, New J. Phys. **16**, 103011 (2014).

[33] D. Z. Xu, S. Li, X. F. Liu, and C. P. Sun, Phys. Rev. E **90**, 062125 (2019).

[34] D. E. Logan and P. G. Wolynes, J. Chem. Phys. **93**, 4994 (1990).

[35] L. Silvestri, K. Jacobs, V. Dunjko, and M. Olshanni, Phys. Rev. E **89**, 042131 (2014).

[36] M. Esposito and P. Gaspard, Phys. Rev. E **68**, 066113 (2003).

[37] P. Borowski, J. Gemmer, and G. Mahler, Eur. Phys. J. B **35**, 255 (2003).

[38] J. B. Pérez and J. C. Arce, J. Chem. Phys. **148**, 214302 (2018).

[39] J. L. Lebowitz, Phys. A **194**, 1 (1993).

[40] J. L. Lebowitz, Phys. Today **46**, 32 (1993).

[41] E. T. Jaynes, Phys. Rev. **106**, 620 (1957).

[42] A. Einstein, B. Podolsky, and N. Rosen, Phys. Rev. **47**, 777 (1935).

[43] J. S. Bell, Physics **1**, 195 (1964).

[44] F. Brandão, M. Horodecki, N. Ng, J. Oppenheim, and S. Wehner, Proc. Natl. Acad. Sci. USA **112**, 3275 (2015).

[45] M. N. Bera, A. Riera, M. Lewenstein, and A. Winter, Nat. Comm. **8**, 2180 (2017).

[46] A. Stotland, A. A. Pomeransky, E. Bachmat, and D. Cohen, Europhys. Lett. **67**, 700 (2004).

[47] A. Einstein, *"On Boltzmann's Principle and Some Immediate Consequences Thereof" Translation by B. Duplantier and E. Parks in "Einstein, 1905-2005"*, Progress in mathematical physics v. 47 Poincare Seminar (7th : 2005 : Institut Henri Poincare)" (Boston : Birkhuser Verlag, 2006).

[48] E. Schrödinger, *Statistical Thermodynamics* (Dover, 1989) p. 40.

[49] R. Kubo, *Statistical Mechanics An Advanced Course with Problems and Solutions*, 7th ed. (Elsevier Science Publishers, 1988) pp. 10-11.

[50] J. J. Prentis, A. E. Andrus, and T. J. Stasevich, Am. J. Phys. **67** (1999), 10.1119/1.19314.

[51] M. A. Nielsen and I. L. Chuang, *Quantum Computation and Quantum Information* (Cambridge, 2000) p. 506.

[52] R. Bigwood and M. Gruebele, Chem. Phys. Lett. **235**, 604 (1995).

[53] M. Gruebele, Theor. Chem. Acc. **109**, 53 (2003).

[54] L. D. Landau and E. M. Lifshitz, *Statistical Physics Part 1*, 3rd ed., Course on Theoretical Physics (Pergamon Press, 1980) pp. 195-196.

[55] "Digamma function," http://mathworld.wolfram.com/DigammaFunction.html, accessed 4-30-2019.

[56] A. Einstein, *"Planck's Theory of Radiation and the Theory of Specific Heat"*, The collected papers of Albert Einstein, Vol. 2 (Princeton University Press, 1989).

[57] M. E. Kellman, Ann. Rev. Phys. Chem. **46**, 395 (1995).

[58] V. Tyng and M. E. Kellman, Acc. Chem. Res. **40**, 243 (2007).

[59] M. Gruebele, Proc. Natl. Acad. Sci. USA **95**, 5965 (1998).

[60] X. Cheng and J. A. Cina, J. Chem. Phys. **141**, 034113 (2014).

[61] P. A. Kovac and J. A. Cina, J. Chem. Phys. **147**, 224112 (2017).

[62] A. Chakraborty and M. E. Kellman, J. Chem. Phys. **129**, 171104 (2008).

[63] G. L. Barnes and M. E. Kellman, J. Chem. Phys. **133**, 101105 (2010).

[64] G. L. Barnes and M. E. Kellman, J. Chem. Phys. **134**, 074108 (2011).

[65] L. D. Landau and E. M. Lifshitz, *Statistical Physics Part 1*, 3rd ed., Course on Theoretical Physics (Pergamon Press, 1980) pp. 23-29.

[66] R. Kosloff, J. Phys. Chem. **92**, 2087 (1988).

[67] C. Leforestier, R. H. Bisseling, C. Cerjan, M. D. Feit, R. Friesner, A. Guldberg, A. Hammerich, G. Jolicard, W. Karrlein, H. D. Meyer, N. Lipkin, O. Roncero, and R. Kosloff, J. Comput. Phys. **94**, 59 (1991).

[68] M. O. Scully, K. R. Chapin, K. E. Dorfman, M. B. Kim, and A. Svidzinsky, Proc. Natl. Acad. Sci. USA **108**, 15097 (2011)